

KNMI Radar Methods

H.R.A. Wessels

KNMI Technical Report, TR-293,
December 2006

Preface

Herman R.A. Wessels has worked as a (senior) scientist at KNMI from 1962 until his retirement in January 2003. During these forty years he has been active in a broad meteorological field ranging from synoptical meteorology, climatology, visibility and fog, ice growth, deep convection, lightning to weather radar. In the field of weather radar, Herman has been deeply involved in the transition from analog display to digital data processing and all related issues, like suppression of (anomalous propagation) clutter, geographical (re)projection, compositing of national and foreign radar data, and determination of radar echotops.

Before his retirement Herman Wessels has compiled a set of documents describing the state-of-the-art of the KNMI radar methods at that time. This Technical Report which is based on these documents contains valuable (historical) information on the KNMI radar systems operational during the 90's. In addition, knowledge on radar meteorology and algorithms can be found in the documents. Finally, I would like to stress that the technical information in this report should be used with care as it may be outdated by now.

Iwan Holleman,
December 1, 2006.

Contents

1	Introduction	9
1.1	General glossary	10
1.2	KNMI glossary	10
2	Radar beam properties	11
2.1	Introduction	11
2.2	Antenna patterns	11
2.3	Radome influence	13
2.4	Propagation and reflection effects	14
2.5	Radar horizon	15
2.6	Obstacle effects	15
2.7	Occultation files and diagrams	16
2.8	Occultation correction	17
2.9	References	18
3	Radar calibration	21
3.1	Introduction	21
3.2	Checking elevation accuracy	21
3.3	Weather signals	23
3.4	The radar equation	23
3.5	Averaging and noise sampling	24
3.6	Output levels in PIF files	26
3.7	Calibration before 1996	26
3.8	Annex: Precipitation echo fluctuations	27
4	Clutter cancellation in KNMI weather radars	31
4.1	Introduction	31
4.2	Method	31
4.3	History	32
4.4	Clutter preprocessing	33
4.5	DVIP emulation (old DVIP)	35

4.6	Clutter postprocessing: selection of clutter flags	35
4.7	Clutter postprocessing: smoothing in polar pseudoCAPPI image	36
4.8	Output	39
4.9	Reference	39
4.10	Annex: Improved clutter postprocessing	40
4.10.1	Suspected clutter flags embedded in rain areas	40
4.10.2	Sea clutter	40
4.10.3	Horizontal echo fluctuations	41
4.10.4	Postprocessing tests	42
4.10.5	Future developments	43
4.10.6	References to Annex	43
5	Scan schedule and data collection	45
5.1	Introduction	45
5.2	Scan settings	45
5.3	Product definitions	47
5.3.1	Reflectivity	47
5.3.2	Velocity	48
5.4	File header labels	48
5.5	Use of labels in rainbow raw data and product files	51
6	PseudoCAPPI and composite pictures	53
6.1	Introduction	53
6.2	KNMI pseudoCAPPI	53
6.3	Compositing considerations	55
6.4	Compositing history	56
6.5	Present compositing method	57
6.6	Clutter removal	59
6.7	Nodata information	59
6.8	Filtering	60
6.9	References	60
6.10	Annex	60
7	Navigation of radar pictures and topographic overlays	63
7.1	Introduction	63
7.2	History	63
7.3	Checking position, range, azimuth and elevation	65
7.4	Conversion from lat/lon to polar stereographic projection	66
7.5	Conversion from polar radar projection to lat/lon	68
7.6	Navigation information for radar users	69
7.7	User display of radar images	70

7.8	Ellipsoid radar navigation on the MWS	71
7.9	Future MWS navigation (Smartwindows)	73
7.10	Reference	74
7.11	Annex A: Navigation of foreign radar data into the KNMI 256x256 picture	74
7.12	Annex B: Navigation of foreign radar composite pictures on KNMI MWS	77
7.12.1	German composite PAAM21	78
7.12.2	French composite PAAM22	79
7.12.3	UK composite PAAL21	80
7.12.4	UK COST-73 composite PAAL31	80
7.13	Annex C: Combining the Netherlands picture with foreign composites on MWS	82
8	Echo top measurements	83
8.1	Introduction	83
8.2	Error sources	83
8.3	History	84
8.4	Refraction correction	86
8.5	Vertical echo profile (attenuation correction)	88
8.6	Corrections for the shape of the radar beam	88
8.7	Selecting cloud tops for annotation in PPI displays	90
8.8	CRIS-processing: quality limits and no-data regions	91
8.9	CRIS-processing: merging procedure	92
8.10	CRIS processing: navigation, scaling and classification	93
8.11	Interpretation of echo top images	94
8.12	References	94
9	Miscellaneous information	97
9.1	Technical information KNMI weather radars	97
9.2	Weather radar product sheet	98
9.3	KNMI radar chronology	99
9.4	External availability of data	99
9.5	Description of weather radar data at 0.5 dB resolution	100
9.5.1	Radar De Bilt	100
9.5.2	Output levels	101
9.5.3	KNMI pseudoCAPPI	101
9.5.4	Reprojection	102
9.5.5	PIF file structure	103
9.6	Specification: coding of 200x200 archive (V)ERAS files	104

A Fortran program: rad2obst.f	105
B Fortran program: utlzon5a.f	107
C Fortran program: rad7comp.f	113
D Fortran program: rad8tops.f	123

Chapter 1

Introduction

Weather radar has been used by KNMI since 1959. In the following years radar products have become essential tools for weather forecasting and hydrology. Although weather radar applications have been extensively treated in textbooks, the actual operational use depends on factory specifications of the installed instruments and local modifications. The algorithms and methods applied at KNMI during the last 15 years are documented in the following chapters. The system components to be described include:

- The antenna, as it is used for transmission and reception.
- The antenna control by the radar processor.
- The signal receiver and preprocessor with clutter control.
- The radar computer creating specific single-radar products.
- A central computer combining and distributing radar products.
- Remote display systems.

Although most of the chapters discuss methods used at the radar site installation, the chapters on compositing, navigation and echo tops also refer to the central computer (CRIS). This documentation is restricted to the products that are currently (2001) operational: PPI and ETH.

1.1 General glossary

AD	Analog to Digital (conversion)
CAPPI	Constant Altitude PPI (=Plan Position Indicator)
COST	COoperation in Science and Technology (in Europe)
DEC	Digital Electronics Corporation
DSP	Digital Signal Processor
DVIP	Digital Video Integrator and Processor
EEC	Enterprise Electronics Corporation, Enterprise Al.
EGA	Enhanced Graphics Adapter
FAT	Factory Acceptance Test
ETZ	Echo Top height (Gematronik Product: Z= radar reflectivity)
KLu	Koninklijke Luchtmacht
MDS	Minimum Detectable Signal
NOB	Nederlands Omroep Bedrijf
NOVA	computer once produced by Data General
PPI	Plan Position Indicator
PRF	Pulse Repetition Frequency
PSTN	Polar STereographic North
RADAR	RAdio Detection And Ranging
RHI	Range Height Indicator
RVP6	Radar Video Processor (nr.6)
STC	Sensitivity Time (=range) Control
TR	Transmit Receive (switch)
VAX	computer once produced by DEC
VCS	Video Computer Systems Nachrichtentechnik GmbH
VMS	Virtual Memory System

1.2 KNMI glossary

APL	Automatische Productie Lijn
BARC	Bliksem APL Radar Computer
CRIS	Centraal Radar Inwin Systeem
ERAS	EGA Radar Animatie Scherm
ETH	Echo Top Height (presentation = KNMI version)
MWS	Meteorological Work Station
PIF	Processed Image File
RDD	Radar Data Display
RDDC	Radar Data Distribution Computer

Chapter 2

Radar beam properties

2.1 Introduction

The radar antenna consists of a parabolic dish with an microwave feed in its focal point. On transmission the radiation is concentrated in a narrow beam. On reception the echo energy is sampled from the same restricted volume as well.

Unfortunately the radar beam may be disturbed by a protecting radome or by a reflecting ground surface. More seriously, the beam may be obstructed completely by man-made or natural obstacles. The useful range of radar for nowcasting as well as the accuracy of precipitation estimates depends strongly on these disturbances.

In a densely populated area like The Netherlands “radar horizon pollution” is an increasing threat to radar meteorology applications. The radar position at Schiphol was abandoned for Den Helder in favour of a better coverage to the northwest. In retrospect, KNMI escaped Schiphol just in time to avoid a high rise airport expansion. The future horizon of the radar on top of the central office at De Bilt is by no means secured. The new location in Den Helder is regularly threatened by plans to install tall wind generators. This chapter tries to provide quantitative information on the degree of distortion caused by these effects.

2.2 Antenna patterns

The one way (transmission only) antenna beam pattern should theoretically approximate the Fraunhofer diffraction pattern known from optics. The important features are the main beam (Airy disc) and concentric side lobes. Deviations may occur due to a feed offset, the presence of feed supports or

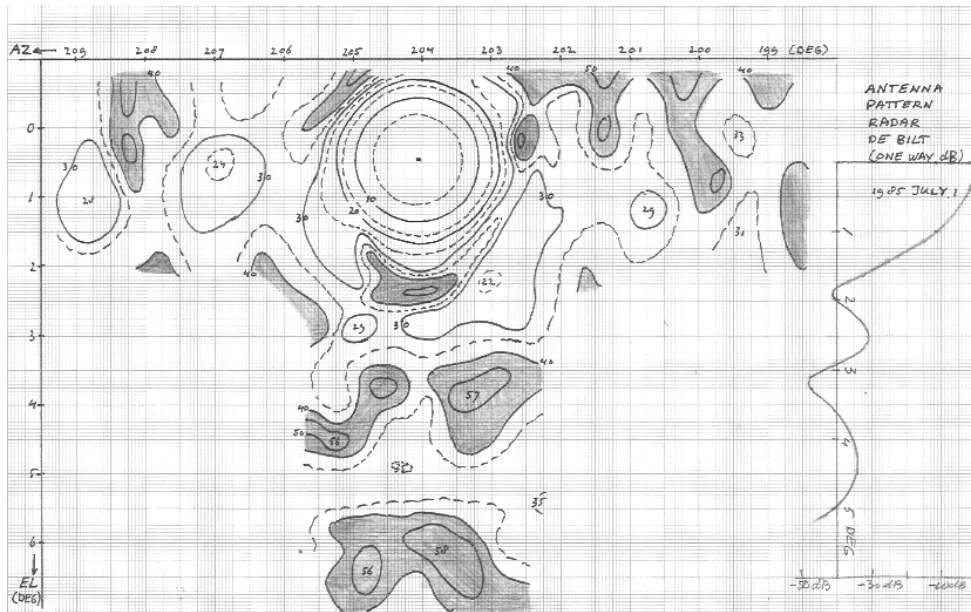


Figure 2.1: Result of antenna pattern measurements (see text).

special concentric side lobe reducing shields. The near field pattern is also strongly influenced by the radome and other constructions like railings on the radar tower. The far field pattern may show the effects of surrounding ground obstacles.

Factory specifications are based on measurements (sometimes without radome) on special towers and are usually not representative for the operational site. It is strongly advised to perform a beam pattern measurement on the radar site and to repeat such measurements to check e.g. radome deterioration.

A microwave transmitter feedhorn (horizontal polarization!) can be mounted on a nearby mast and the scanning radar will record the power as a function of azimuth for various elevations. The complete beam pattern can be reconstructed by combining these records. An example is shown in Figure 2.1. An alternative is to record the radar signal during such multi-dimensional scans with a nearby receiver. This possibility exists at the Den Helder “collimation tower”.

As the measurements are usually relative to the power at the beam axis, it is difficult to use them in measuring the antenna gain. The width of the beam might give a clue whether changes are necessary. A more direct application for KNMI is the beamwidth/sidelobe correction used for the echo top measurements. The correction parameters are derived from simulations

with the measured beam pattern (Section 8.6 of the Echo Top Chapter).

The relevant part of the beam regarding errors of echo tops lies below the axis. As an example the average pattern over a 2 deg azimuth sector is drawn as an insert in Figure 2.1.

A numerical approximation of the normalised (two-way) pattern, up to the second side lobe, is:

$$F = \exp[-b_0x^2] + \exp[-b_1(x - a_1)^2 - 0.23d_1] + \exp[-b_2(x - a_2)^2 - 0.23d_2] \quad (2.1)$$

where x is the off-axis angle in deg. The side lobes are found at a_1 resp. a_2 deg and their two-way peak values are d_1 resp. d_2 dB below the peak of the main lobe. In the example of Figure 2.1 we have $a_1=2.63$, $d_1=63$, $a_2=4.5$ and $d_2=67$. These parameters can be read directly from the graph. The factors $b_0\dots b_2$ determine the width of the main and side lobes: $b_0=5$, $b_1=16$ and $b_2=5$ were found by fitting our example. The measurements in Den Helder on Sep. 7, 1999 can be fitted with $a_1=2.0$, $d_1=58$, $a_2=3.0$, $d_2=63$, $b_0=6.5$, $b_1=7.8$ and $b_2=4$.

The actual echo top correction procedure is described in Section 8.6 of the Echo Top Chapter.

2.3 Radome influence

Radome specifications are usually based on the laboratory-measured absorption of the cover material. It has been demonstrated that the type of panel construction can have an additional negative influence on the beam pattern (Manz et al., 1999).

In particular, for horizontal polarization, a radome with vertical panels has high sidelobes in azimuth direction. KNMI used such a radome at Schiphol. Measurements without and with radome have been compared in 1988/1989 for azimuthal distribution.

Without radome we had $a_1=2.3$ deg and $d_1=70$ dB. With radome 2.0 and 48 respectively. Moreover, the dip between the lobes rose from 90 dB to 50 dB.

Radomes with both vertical and horizontal joints have increased sidelobes in both elevation and azimuth directions. The best performance have space-frame (quasi random panels) radomes. We used one in De Bilt before 1997: In 1985 the measurement gave $a_1=2.1$ deg, $d_1=62$ dB (dip 73 dB).

Dirt on the radome will only slightly increase losses. However, during rain a dirty radome may absorb some 2 dB more than a clean one. Rain

itself increases the radome attenuation. Germann (1999) reports a two-way reduction up to 5.4 dB in moderate rain.

The negative effect of a lower axial gain is a reduction of the accuracy of precipitation measurements. The negative effect of stronger side lobes is mainly an increase of fixed ground clutter.

2.4 Propagation and reflection effects

If we want to observe precipitation at large range, we have to use a low elevation beam. In the Netherlands the radars are positioned at a height around 50 m, so the radar horizon is at an elevation of about -0.1 deg below horizontal. Because the beam width is 1.0 deg, most of the beam is used if the lowest elevation is 0.3 deg. See also Smith (1995). This has (and can again) been checked by maximizing the return of distant low-altitude precipitation.

There are two reasons for non-precipitation radar returns in the 0.3 deg beam:

- In anomalous propagation conditions (see general literature) part of the beam is trapped in a duct, where the power reduction with range is according to an inverse linear rather than the usual inverse squared law. Although this only applies to a part of the beam, the effective antenna gain is increased and scattering cross-sections below 0 dBZ may be detected.
- If the lowest beam is reflected at a flat conducting surface like the sea, interference of the main and reflected beams deform the circular beam pattern into a series of vertically stacked flat sub-beams of which the lowest has a 3 dB larger sensitivity (one way) than the original axial gain (Ma Zhenhua, 1985, p.108).

The targets that become visible in these narrowed beams are:

- land surface echoes, luckily removed by clutter cancellation.
- the sea surface, for which clutter cancellation is less effective.
- (low) clouds, with too small drops to be detected normally.
- refractive index fluctuations, normally smaller than 0 dBZ.
- possibly insects, etc.

In operational practice these confusing echoes occur only over the sea surface. Additional tools to check their non-precipitation character are the radar echo top picture and satellite images for both visible and infrared radiation.

2.5 Radar horizon

The radar is intentionally located on a high position, to avoid nearby obstacles like hills or buildings. In principle a nearby “ring” of obstacles is advantageous to avoid ground clutter, but this reduces the operating range of the radar. In the project COST-73 the radar range has been defined as the range up to where the lowest usable beam axis would detect precipitation echoes not higher than 1.5 km above the local terrain (Newsome, 1992, p.41-50). Due to the curvature of the earth the lowest possible beam will touch the earth surface at a range D_h ,

$$D_h = \sqrt{2H_r R} \quad (2.2)$$

where H_r is the height of the antenna and $R = 1.33 \cdot 6367$ km, the earth radius corrected for near-surface microwave propagation. For Den Helder $H_r=51$ m, so $D_h=30$ km, at least where the radar has a clear view on the sea. For most of the country the horizon consists of trees and buildings, so it is better to increase the height of the earth surface H with about 5 m. It is important to note that nearby obstacles up to 50 m height remain below the radar beam, while a 40 m high row of dunes at 30 km range will rise the lowest beam with 0.08 deg and reduce the radar range with nearly 10%. An 40 m high isolated building with a width of 40 m would hardly have an effect at 30 km range, because 0.08 deg is small for a 1 deg radar beam.

From a radar at height H_r above m.s.l., an obstacle at range D and height H will be seen at elevation

$$E = \arcsin \left(\frac{(R + H_r)^2 + D^2 - (R + H)^2}{2D(R + H_r)} \right) \quad (2.3)$$

This follows from the cosine rule in the triangle: radar, target and the “radar earth” centre. An explicit formula for the connecting line between radar and m.s.l. horizon is

$$H = \frac{\sqrt{2H_r R} - D}{\sin(\arctan((\sqrt{2H_r R} - D)/R))} - R \quad (2.4)$$

expressing the height H as a function of range D .

2.6 Obstacle effects

Even before the radar of Den Helder became operational, KNMI was confronted with plans for a high apartment building. In recent years various

proposals for tall wind generators had to be contested. At first, quantitative evidence of the effect was lacking, which weakened our opposition. The result was the admission - officially for a trial period - of a tall generator at 700 m range with the generator housing just on the axis of the lowest radar beam. This had the minor advantage that the damage could at last be established quantitatively: a 4 dB reduction of the measured echoes. This would make an occultation correction (see later) necessary, unless the radar of De Bilt provides a sufficient data replacement. The measurement of 4 dB was obtained by comparing the obstructed 1 deg sector with the neighbouring unobstructed sectors. In several situations with widespread homogeneous (warm front) rain the average result was 3.5 dB (between 2 and 5 dB).

It was established that the effect of the windmill could be explained by the fractional intercepted area of the beam. A 10% reduction of the beam cross-section area was responsible for a 1 dB two way signal reduction. This is about the acceptance level. As a more general tool the authorities concerned have received - on their request - a table that could be used to check building plans in an early stage. For a certain range the table specifies:

- up to which height buildings are not disturbing
- the allowable width of taller buildings to respect the above 1 dB.

An additional condition is that the angular separation of obstacles is preferably not smaller than 2 deg. A better alternative might be to align the obstacles as seen from the radar.

Table 2.1 is generated by a computer program (see Appendix A) with the following functionality: The radar height H_r has to be entered, As a result a table is built showing the results of Equation 2.3 as a function of H and D . Table 2.2 shows, as a function of (classes of) D , the obstacle height for $E=-0.2$ deg. Also shown is - for higher obstacles - the obstacle width for 10% beam filling.

2.7 Occultation files and diagrams

Experience shows that an obstacle inventory is an essential tool:

- to decide on a new radar location,
- to obtain quantitative arguments against new-planned obstructions,
- to decide on occultation corrections.

The radar horizons of De Bilt and Den Helder have been measured with an optical theodolite, The results have been stored in the files OCCNL50 resp. OCCNL41. The COST-73 program COSTDSP.F can be used to make a horizon sketch. This sketch can be used for visual inspections. It is recommended to check the horizon every year. If relevant changes are found, the theodolite measurements should be up-dated. A separate documentation set is available, containing:

- An instruction for these theodolite measurements (in Dutch),
- An instruction for the use of the theodolite,
- The COST-73 files and software.

2.8 Occultation correction

Occultation corrections in mountainous regions are rather complicated. Therefore Gematronik radars have the facility to edit masks indicating the lowest usable elevation for any pixel. In a flat country the only relevant obstacles are buildings or masts that obstruct certain azimuth sectors. Editing a mask file would be unnecessarily complicated.

KNMI has therefore arranged that certain azimuths are not used, but filled with interpolated polar pixel values from adjacent azimuths. For any occultation zone three parameters are sufficient:

- the first azimuth to ignore, e.g. 145 deg
- the number of degrees (max. 5), e.g. 3 to ignore 145 - 147 deg
- the elevation below which interpolation is required, e.g. 2.0 deg

The clutter flags are interpolated accordingly, as described in the Chapter 4.

For De Bilt two occultation zones are necessary now. The worst is 4 deg wide: a tall office building at about 1 km. The front side of the building is nearly perpendicular to the radar beam and the building serves as a rather effective mirror for microwaves. If thunderstorms move away north-easterly over the Emsland (D), in the south-west mirrored echoes (about 25 dB weaker) move southwesterly over the southern North Sea. Of course these mirror images disappeared after the occultation zone had been set.

2.9 References

Ma Zhenhua, 1985, The effects of earth partial specular reflection on the quantitative rainfall-rate measurements by radar. *Advances in Atm.Sciences*, Springer Verlag, Berlin, 104-111.

D.H.Newsome(Ed.), 1992, *Weather Radar Networking*, Cost 73 Project/ Final report. EUR 13648 EN, 254pp.

P.L.Smith, 1995, On the minimum useful elevation angle for weather radar surveillance radar scans. Prepr. 27 Conf. Radar Meteor., Oct. 9-13, Vail Co. (AMS, Boston)

A.Manz, J.Handwerker, M.Löffler-Mang, R.Hannesen, H.Gysi, 1999, Radome influence on weather radar systems with emphasis on rain effects. 29th Int.Conf. on Radar Meteorology, Montreal, Can.

U.Germann, 1999, Radome attenuation - a serious limiting factor for quantitative rain measurements? *Meteor. Zeitschr.*, 8, p.85-90.

Table 2.1: Den Helder: Elevation (.01deg) of target height h (km) seen from radar at 51 m as a function of distance from radar in km.

h	1	2	3	4	5	6	7	8	9	10	11	12	13	14	15	16	17	18	19	20
63	74	37	24	17	13	10	8	7	5	4	3	2	2	1	0	0	-1	-2	-2	-3
62	61	30	20	14	11	8	7	5	4	3	2	1	1	0	-1	-1	-2	-2	-3	-3
61	56	28	18	13	10	7	6	4	3	2	2	1	0	0	-1	-2	-2	-3	-3	-4
60	51	25	16	12	9	7	5	4	3	2	1	0	0	-1	-1	-2	-2	-3	-3	-4
59	43	21	14	10	7	5	4	3	2	1	0	0	-1	-1	-2	-2	-3	-3	-4	-4
58	38	19	12	8	6	4	3	2	1	1	0	-1	-1	-2	-2	-3	-3	-4	-4	-4
57	33	16	10	7	5	4	3	2	1	0	0	-1	-2	-2	-3	-3	-3	-4	-4	-5
56	28	13	8	6	4	3	2	1	0	0	-1	-1	-2	-2	-3	-3	-4	-4	-5	-5
55	23	11	7	4	3	2	1	0	0	-1	-1	-2	-2	-3	-3	-4	-4	-4	-5	-5
54	18	8	5	3	2	1	0	0	-1	-1	-2	-2	-3	-3	-4	-4	-4	-5	-5	-6
53	10	4	2	1	0	0	-1	-1	-2	-2	-3	-3	-3	-4	-4	-4	-5	-5	-6	-6
52	5	2	1	0	-1	-1	-2	-2	-3	-3	-3	-3	-4	-4	-4	-5	-5	-5	-6	-6
51	0	-1	-1	-1	-2	-2	-2	-3	-3	-3	-4	-4	-4	-4	-5	-5	-5	-6	-6	-6
50	-5	-3	-3	-3	-3	-3	-3	-3	-4	-4	-4	-4	-5	-5	-5	-5	-6	-6	-6	-7
49	-11	-6	-4	-4	-4	-4	-4	-4	-4	-4	-4	-5	-5	-5	-5	-6	-6	-6	-7	-7
48	-18	-10	-7	-6	-5	-5	-5	-5	-5	-5	-5	-5	-6	-6	-6	-6	-7	-7	-7	-7
47	-23	-12	-9	-7	-6	-6	-6	-6	-6	-6	-6	-6	-6	-6	-6	-7	-7	-7	-7	-8
46	-29	-15	-10	-8	-7	-7	-6	-6	-6	-6	-6	-6	-6	-7	-7	-7	-7	-7	-8	-8
45	-34	-17	-12	-10	-8	-7	-7	-7	-7	-7	-7	-7	-7	-7	-7	-7	-7	-8	-8	-8
44	-39	-20	-14	-11	-9	-8	-8	-7	-7	-7	-7	-7	-7	-7	-7	-8	-8	-8	-8	-8
43	-44	-22	-15	-12	-10	-9	-8	-8	-8	-8	-7	-7	-8	-8	-8	-8	-8	-8	-8	-9
42	-52	-26	-18	-14	-12	-10	-9	-9	-9	-8	-8	-8	-8	-8	-8	-8	-8	-9	-9	-9
41	-57	-29	-20	-15	-13	-11	-10	-10	-9	-9	-9	-9	-9	-9	-9	-9	-9	-9	-9	-9
40	-62	-31	-21	-17	-14	-12	-11	-10	-10	-9	-9	-9	-9	-9	-9	-9	-9	-9	-9	-9
39	-67	-34	-23	-18	-15	-13	-12	-11	-10	-10	-9	-9	-9	-9	-9	-9	-9	-9	-10	-10
38	-72	-37	-25	-19	-16	-14	-13	-12	-11	-10	-10	-10	-10	-10	-10	-10	-10	-10	-10	-10
37	-80	-40	-27	-21	-18	-15	-14	-13	-12	-11	-11	-10	-10	-10	-10	-10	-10	-10	-10	-10
36	-85	-43	-29	-22	-19	-16	-14	-13	-12	-12	-11	-11	-11	-11	-10	-10	-10	-10	-11	-11
35	-90	-46	-31	-24	-20	-17	-15	-14	-13	-12	-12	-11	-11	-11	-11	-11	-11	-11	-11	-11
34	-95	-48	-33	-25	-21	-18	-16	-14	-13	-13	-12	-12	-11	-11	-11	-11	-11	-11	-11	-11
33	-99	-51	-34	-26	-22	-19	-17	-15	-14	-13	-13	-12	-12	-12	-11	-11	-11	-11	-11	-11
32	-99	-53	-36	-28	-23	-19	-17	-16	-15	-14	-13	-13	-12	-12	-12	-12	-12	-12	-12	-12
31	-99	-57	-39	-29	-24	-21	-18	-17	-15	-14	-14	-13	-13	-12	-12	-12	-12	-12	-12	-12
30	-99	-60	-40	-31	-25	-22	-19	-17	-16	-15	-14	-14	-13	-13	-13	-13	-13	-13	-13	-13
29	-99	-62	-42	-32	-26	-22	-20	-18	-17	-16	-15	-14	-14	-13	-13	-13	-13	-13	-13	-13
28	-99	-65	-44	-33	-27	-23	-21	-19	-17	-16	-15	-15	-14	-14	-13	-13	-13	-13	-13	-13
27	-99	-67	-45	-35	-28	-24	-21	-19	-18	-17	-16	-15	-14	-14	-14	-13	-13	-13	-13	-13
26	-99	-71	-48	-37	-30	-25	-22	-20	-19	-17	-16	-16	-15	-15	-14	-14	-14	-14	-14	-14
25	-99	-74	-50	-38	-31	-26	-23	-21	-19	-18	-17	-16	-15	-15	-15	-14	-14	-14	-14	-14
24	-99	-76	-51	-39	-32	-27	-24	-21	-20	-18	-17	-16	-16	-15	-15	-15	-14	-14	-14	-14
23	-99	-79	-53	-40	-33	-28	-25	-22	-20	-19	-18	-17	-16	-16	-15	-15	-15	-14	-14	-14
22	-99	-81	-55	-42	-34	-29	-25	-23	-21	-19	-18	-17	-17	-16	-16	-15	-15	-15	-15	-14
21	-99	-84	-57	-43	-35	-30	-26	-23	-21	-20	-19	-18	-17	-16	-16	-15	-15	-15	-15	-15
20	-99	-90	-61	-46	-38	-32	-28	-25	-23	-21	-20	-19	-18	-17	-17	-16	-16	-16	-16	-15
19	-99	-93	-63	-47	-39	-33	-29	-26	-23	-22	-20	-19	-18	-18	-17	-17	-16	-16	-16	-16
18	-99	-96	-64	-49	-40	-34	-29	-26	-24	-22	-21	-20	-19	-18	-17	-17	-17	-16	-16	-16
17	-99	-98	-66	-50	-41	-34	-30	-27	-25	-23	-21	-20	-19	-18	-18	-17	-17	-17	-17	-16
16	-99	-99	-68	-52	-42	-36	-31	-28	-25	-23	-22	-21	-20	-19	-18	-18	-17	-17	-17	-17
15	-99	-99	-70	-53	-43	-37	-32	-29	-26	-24	-22	-21	-20	-19	-19	-18	-18	-17	-17	-17
14	-99	-99	-72	-54	-44	-37	-33	-29	-27	-24	-23	-22	-21	-20	-19	-18	-18	-18	-17	-17
13	-99	-99	-74	-56	-45	-38	-33	-30	-27	-25	-23	-22	-21	-20	-19	-19	-18	-18	-18	-17
12	-99	-99	-75	-57	-46	-39	-34	-30	-28	-26	-24	-22	-21	-20	-20	-19	-19	-18	-18	-18
11	-99	-99	-77	-58	-47	-40	-35	-31	-28	-26	-24	-23	-22	-21	-20	-19	-19	-18	-18	-18
10	-99	-99	-80	-60	-49	-41	-36	-32	-29	-27	-25	-24	-22	-21	-21	-20	-19	-19	-19	-18
9	-99	-99	-81	-62	-50	-42	-37	-33	-30	-27	-25	-24	-23	-22	-21	-20	-20	-19	-19	-18
8	-99	-99	-83	-63	-51	-43	-37	-33	-30	-28	-26	-24	-23	-22	-21	-21	-20	-19	-19	-19

Table 2.2: Allowed maximum width (m) for obstacles lower than the indicated height (200...20 m) for a radar at 51.5 m, i.e., for Den Helder.

distance (m)	max.height	200m	170m	140m	110m	80m	50m	20m
0- 300	50	0.1	0.1	0.1	0.1	9.0	0.2	999.9
300- 600	49	0.5	0.5	0.5	0.5	9.0	1.6	999.9
600- 800	48	1.0	1.0	1.0	1.0	9.0	3.2	999.9
800- 1200	47	1.2	1.2	1.2	1.2	9.0	3.9	999.9
1200- 1400	46	1.8	1.8	1.8	1.8	9.0	6.6	999.9
1400- 1700	45	2.1	2.1	2.1	2.1	9.0	7.3	999.9
1700- 1900	44	2.5	2.5	2.5	2.5	9.0	9.0	999.9
1900- 2300	43	2.7	2.7	2.7	2.7	9.0	9.7	999.9
2300- 2700	42	3.3	3.3	3.3	3.3	9.0	12.5	999.9
2700- 2900	41	3.8	3.8	3.8	3.8	9.0	15.3	999.9
2900- 3200	40	4.1	4.1	4.1	4.1	9.0	16.0	999.9
3200- 3400	39	4.5	4.5	4.5	4.5	9.0	17.7	999.9
3400- 3800	38	4.8	4.8	4.8	4.8	9.0	18.4	999.9
3800- 4100	37	5.3	5.3	5.3	5.3	9.0	21.2	999.9
4100- 4400	36	5.8	5.8	5.8	5.8	9.0	22.9	999.9
4400- 4800	35	6.2	6.2	6.2	6.2	9.0	24.7	999.9
4800- 5100	34	6.7	6.7	6.7	6.7	9.0	27.5	999.9
5100- 5400	33	7.1	7.1	7.1	7.1	9.0	29.3	999.9
5400- 5700	32	7.5	7.5	7.5	7.5	9.0	31.0	999.9
5700- 6400	31	7.9	7.9	7.9	8.2	9.0	32.8	999.9
6400- 6800	30	8.9	8.9	8.9	10.2	9.0	39.2	999.9
6800- 7100	29	9.4	9.4	9.4	11.3	9.0	42.2	999.9
7100- 7400	28	9.9	9.9	9.9	12.2	9.0	44.0	999.9
7400- 7700	27	10.3	10.3	10.3	13.1	9.0	45.7	999.9
7700- 8200	26	10.7	10.7	10.7	14.0	9.0	47.5	999.9
8200- 8600	25	11.4	11.4	11.6	15.6	9.0	51.7	999.9
8600- 8900	24	11.9	11.9	12.6	17.0	9.0	54.7	999.9
8900- 9300	23	12.3	12.3	13.4	18.0	9.0	56.4	999.9
9300- 9700	22	12.9	12.9	14.5	19.4	9.0	59.4	999.9
9700-10200	21	13.4	13.4	15.6	20.8	9.0	62.4	999.9
10200-10600	20	14.1	14.1	17.1	22.7	9.0	66.7	999.9
10600-10900	19	14.7	14.7	18.3	24.3	9.0	69.8	999.9
10900-11300	18	15.1	15.4	19.2	25.4	9.0	71.5	786.3
11300-11700	17	15.6	16.5	20.4	27.0	9.0	74.5	633.5
11700-12100	16	16.2	17.5	21.7	28.6	9.0	77.6	543.0
12100-12700	15	16.7	18.6	23.0	30.2	9.0	80.6	483.7
12700-13100	14	17.5	20.4	25.2	32.9	9.0	86.4	456.4
13100-13400	13	18.1	21.5	26.5	34.7	9.0	89.4	424.7
13400-13900	12	18.8	22.4	27.6	35.9	9.0	91.1	394.9
13900-14400	11	20.1	23.9	29.4	38.2	9.0	95.6	382.2
14400-15200	10	21.5	25.5	31.3	40.6	9.0	100.0	372.7
15200-15600	9	23.8	28.2	34.6	44.8	9.0	108.7	380.4
15600-16100	8	24.9	29.5	36.1	46.7	9.0	111.8	369.8
16100-16600	7	26.4	31.2	38.2	49.2	9.0	116.3	365.6
16600-17200	6	27.9	33.0	40.3	51.8	9.0	120.9	362.6
17200-17700	5	29.8	35.2	42.9	55.1	9.0	126.9	364.8
17700-18400	4	31.4	37.0	45.1	57.7	9.0	131.5	363.5
18400-19200	3	33.7	39.7	48.4	61.8	9.0	139.1	370.8
19200-19800	2	36.5	43.0	52.3	66.6	9.0	148.3	382.3
19800-20400	1	38.6	45.4	55.2	70.2	9.0	154.5	386.1
20400-21200	0	40.8	47.9	58.1	73.8	9.0	160.7	390.3
21200-22300	-1	43.8	51.4	62.3	79.0	9.0	170.2	402.2
22300-23200	-2	48.2	56.6	68.4	86.6	9.0	184.6	425.4

Chapter 3

Radar calibration

3.1 Introduction

Radar calibration is necessary for any quantitative use such as hydrology or specific warnings. First the pointing accuracy will be discussed (Section 3.2). The following Sections treat the intensity measurements. The procedure follows the RVP6 manual. For comparison and for quantitative use of the archive files, procedures of the earlier EEC radars will be mentioned. Doppler measurements are outside the scope of this documentation.

3.2 Checking elevation accuracy

Although precision leveling and north adjustment are carried out during installation, there is always uncertainty about the precise direction of the main lobe axis with respect to the antenna surface. There is also a need to regularly check the accuracy of the angle decoders. It should be remembered that an error of 0.1 deg in elevation causes about 0.5 km error in radar tops at 250 km range! Checking the elevation (as well as the azimuth) is easily done with the sun. The continuous radio transmission of the sun produces a signal at all ranges as the antenna is pointed within about 0.3 deg to the sun.

- The transmitter should be working, to ensure that the receiver is kept tuned.
- The signal is about 15 dBZ, but is attenuated at short range by the STC range correction. Only beyond the 150 km range the solar signal exceeds the lowest presentation level of 7 dBZ.

- In a PPI image the sun sometimes shows up as a spoke near the edge of the picture. As the lowest elevation scan is repeated every 5 minutes and the solar elevation change between these scans is about 0.8 deg, the probability of solar disturbance is about 50% for each sunset or sunrise (tolerance 0.2 deg). In reality the probability is less, because obstacles may reduce the sensitivity of the 0.3 deg elevation scan.
- In an ETH picture the sun may leave its trace during more than an hour, because elevations up to 12 deg are affected. Again the trace is a spoke near the edge of the picture. If elevations above 3 deg are involved, the present MWS presentation shows the sun's trace with the "no data" color.

During maintenance the position of the sun can be measured by moving the antenna horizontally or vertically over the sun and measuring the azimuth respectively elevation limits where the sun exceeds "noise". The average of these limits is considered to represent the centre of the sun's disk. For both horizontal and vertical transitions the time should be recorded with an accuracy of about 15 sec. An inferior alternative is to wait till the sun passes the scan cone during fixed elevation PPI scanning, but the maximum of a signal is difficult to establish with a 20 sec passing interval.

Given the radar position at a given time, we need the real position of the sun for comparison. A Fortran program (see Appendix B) is available that presents this at 10 min. intervals after entering the geographical position and the date (including year). The position at observation time can be obtained by linear interpolation. It should be noted that the radar position of the sun for elevations below 2 deg is not available with "astronomical" precision. An average refraction correction is used in the program. A better way to check such low elevations is to find the elevation that gives the maximum signal for very distant precipitation. The optimum elevation is about 0.3 deg above the lowest usable elevation according to an occultation diagram (see Section 2.7). This should be repeated for a number of cases.

A regular check of the elevation accuracy can also be obtained from the ETH pictures. For a series of successive pictures before sunset or after sunrise the length of the sun's "spokes" at certain product times can be recorded. A Fortran simulation has been used that compared expected results with observed "spokes". The accuracy depends on the specification of the radar's time schedule, which has been changed on some occasions. The above program can be used to perform a graphical check: plot the length of the spoke against the angle between the radar elevation and the solar altitude. If a correction seems necessary, adjustments should be applied during maintenance and their effect should again be checked by low sun sightings.

The azimuth can be calibrated in the same way. Note that it might be considered to offset the radar counterclockwise to correct for the radar data collection lagging behind some 0.3 deg during scanning. (See Section 4.5).

3.3 Weather signals

The purpose of weather radar calibration is to obtain precipitation intensity estimates via accurate measurements of the total scattering cross-section Z of the precipitation particles per unit volume. The dimension of Z is mm^6/m^3 . During radar processing the measured echo power values are normalised for range, so there is a fixed range-independent relation between Z and the rainfall intensity R (mm/h). This relation is approximate and may be different for snow or non-common raindrop spectra. A frequently used approximation is

$$Z = 200R^{1.6} \quad (3.1)$$

Precipitation echoes are commonly measured in logarithmic units dBZ. The reference value is $Z=1$, in contrast with the signal power measurement reference 1 mW for dBm. Therefore the echo, expressed in base-10 logarithmic units, and with applying Equation 3.1 is

$$\text{dBZ} = 10 \log Z = 16 \log R + 23 \quad (3.2)$$

Examples are 7 dBZ for 0.1 mm/h and 23 dBZ for 1 mm/h. Note that throughout this report \log is used for base-10 logarithm and \ln for natural logarithm (base- e).

3.4 The radar equation

The signal received not only depends on the scatterers, but also on radar characteristics. The instrument properties are accounted for in the “radar equation”. The radar equation relates dBZ at 1 km distance with signal I :

$$\text{dBZ} = 10 \log I + 10 \log C \quad (3.3)$$

with

$$C = \frac{2.69 \times 10^{16} \lambda^2 L_t L_r}{P_t T B^2 G^2} \quad (3.4)$$

with peak power P_t , wavelength λ , pulse length T , beamwidth B and antenna gain G . For a different range r the value of C has to be multiplied by r^2 . Because the transmitted power is not measured outside the radome but at

the waveguide near the transmitter, a transmission loss L_t has to be included, accounting for waveguide and radome losses. Equally, the receiver is normally calibrated at the receiver input, so a receiver loss L_r is included.

NOTE: In the RVP-6 manual L_r is not part of the radar equation, because I is taken at the antenna feed. Gematronik, however, uses Equation 3.4.

The actual measurement of the receiver output signal is done with an AD-counter. The calibration graph allows the weather signal I (mW) at the receiver input (near the point where test signals can be inserted) to be read from AD counts

$$S \cdot AD = 10 \log(I + I_n + I_0) - 10 \log I_* \quad (3.5)$$

where S = slope (dB/ADunits), I_n = noise, I_0 = noise corrected roll-off for weak signals ($10 \log I_0$ is comparable with MDS = minimum detectable signal), I_* = zero-AD roll-off for the logarithmic part of the receiver characteristic (see RVP-6 manual). S , I_0 , and I_* are updated daily by an autocalibration routine, so they can be used to solve I from Equation 3.5 so that finally dBZ values can be produced with Equation 3.3. C is computed in the Rainbow-DAC from values entered manually. (see table). Rather than C an auxiliary quantity dBZ_0 , the calibration reflectivity, is used:

$$\text{dBZ}_0 \equiv 10 \log I_0 + 10 \log C \quad (3.6)$$

which is updated after daily autocalibration. Some typical values of radar parameters and calibration values are listed in Table 3.1.

In March 1998 the AD converter of Den Helder has been changed to start near 25 counts as advised in the Manual. In the daily autocalibration report I_* (as above) is about 12 dB lower than would follow from the accompanying dBm/AD table. The dBm in the table is based on signal generator output rather than AD input. The signal generator loss has to be added as well as a generator offset of 0.95 dB.

NOTE: It is important to regularly update the values in the table. Values that are likely to change are the log amplifier (S and I_0) and the radome (L_t , L_r and G). We noted e.g. a sharp rise in I_0 for Den Helder after the Site Acceptance Test (SAT).

NOTE: An extra requirement is brought about by the clutter recognition: the “linearity” of the AD conversion has to be corrected.

3.5 Averaging and noise sampling

During radar operation Equation 3.5 converts AD samples to signal values $(I + I_n + I_0)/I_*$. These signals are subsequently averaged in time and/or range.

Table 3.1: Typical values of radar parameters and calibration values.

long pulse only	De Bilt	Den Helder
λ (cm)	5.293	5.163
P_t (kW)	268	264.43
Radome	0.35	0.35
Waveguide, etc	0.84	0.63
$10 \log L_t$ (dB)	1.19	0.98
Radome	0.35	0.35
Waveguide, etc	2.70	1.99
$10 \log L_r$ (dB)	3.05	2.34
T (μs)	2.023	2.037
B (deg)	0.94	0.906
$10 \log G$ (dB)	45.425	45.74
Cables	2.76	2.46
Coupler	9.64	9.47
Sig.generator loss (dB)	12.40	11.93
Recent test results		
S (dB/AD-units)	0.458	0.473
$10 \log I_0$ (dBm)	-111.78	-108.527
Calibration		
$10 \log C$ (dB)	64.02	63.51
dBZ ₀ at LP (dBZ)	-46.867	-44.499
$10 \log I^*$ (dBm)	-120.990	-120.137

Every hour noise samples are obtained from a far range where $I = 0$. The quantities obtained represent average values of $(I_n + I_0)/I_*$ and I_n/I_* , necessary to separate the weather signal in $I + I_n + I_0$. They are made available as AD units and named LLM and LLSD respectively. The calculation procedure with the average values is as follows, starting from a combination

of Equations 3.3 and 3.6

$$\begin{aligned}
\text{dBZ} &= \text{dBZ}_0 + 10 \log(I/I_*) - 10 \log(I_0/I_*) & (3.7) \\
&= \text{dBZ}_0 + 10 \log[(I + I_0 + I_n)/I_* - (I_0 + I_n)/I_*] \\
&\quad - 10 \log[(I_0 + I_n) - I_n/I_*] \\
&= \text{dBZ}_0 + 10 \log[10^{AD \cdot S/10} - 10^{LLM \cdot S/10}] \\
&\quad - 10 \log[10^{LLM \cdot S/10} - 10^{LLSD \cdot S/10}]
\end{aligned}$$

As examples we take values for De Bilt on 19.3.1998 (Den Helder on 17.2.1999): LogLinMean = 24.16 (25.4566), LogLinSD = 15.55 (15.41), and $S=0.456$ (0.470). Then the last term in Equation 3.7 is $10 \log(I_0/I_*) = 8.76$ dB (10.17 dB). However, from calibrations on the same day we have $10 \log I_0 - 10 \log I_* = 10.25$ dB (11.61 dB).

NOTE: This difference of 1.5 dB is still unexplained. The exact procedure of the RAINBOW Software is therefore still not understood (despite repeated request for clarification).

3.6 Output levels in PIF files

The echo power of calibrated weather radars is converted to units of Z, a property of distributed scatterers (dimension mm^6/m^3) In the radar output file the data are converted to 8 bit integers (0-255). The scale and offset of the conversion follow from:

$$\text{dBZ} = (\text{value} - 64)/2 \quad (3.8)$$

A rainfall intensity of 0.1 mm/h is represented by the value 78, 1 mm/h by 110, etc. To avoid integer cut-off it may be better to use 63 rather than 64 in Equation 3.8.

The lowest value presented is 61, a Gematronik parameter “tophat”, indicating the lowest measurable intensity of about 0.03 mm/h. A data value 0 is used to indicate that no measurement is available, i.e. beyond 320 km from the radar.

3.7 Calibration before 1996

This section is mainly of interest for users of archived radar data. The original EEC radars had a local PPI screen output with scaled intensity levels controlled by discrete logic. The lowest presentation level was just

above noise (0.1 mm/h at 128 km). The other levels were optionally STC corrected: 1, 3, 10, 30 and 100 mm/h. STC correction was applied only between 5 and 128 km range. The STC corrected signals (those above a preset STC comparator level) were increased with 28 dB prior to being tested with digital comparators set at the aforementioned intensity levels. Besides, the signals from the AD converter were used by a “NOVA” computer to create remote display files. As an example we refer to measurements with the radar at De Bilt: $P_t=263$ kW, $G=43$ dB, $MDS=10 \log I_0=-106$ dBm.

From the radar parameters follows that the receiver should expect -86.4 dBm from 1mm/h at 128 km and -54.4 dBm for 100 mm/h. The test signal was introduced via a coupler loss of 30.5 dB in the common waveguide near the TR switch, so $10 \log L_r$ and $10 \log L_t$ were both 2 dB (including 1 dB for the radome). The test signal was lowered with 2.5 dB to correct for the log-amplification of fluctuating signals (See Annex). The test signal was retarded so as to appear on the screen at a range of 128 km.

The AD scale start was fixed at -112 dBm, sufficiently below the MDS. This equals $10 \log I_*$ from the previous sections. For Schiphol we took -113 dBm to make all other settings of both radars equal. Taking into account this reference the comparators for 1...100 mm/h were set. By tuning the video offset and gain, test signals corresponding with 1 and 100 mm/h were made to just trigger their respective comparators. The rather objective triggering criterion was: half of the 128 km ring on the screen should light up. Because the gain was tuned as well the resulting AD slope was $S=0.50$.

The lowest presentation level was set just above the MDS (which could vary between calibrations) The NOVA translates the so calibrated AD output to 6 levels, 0.1, 0.3, 1, 3, 10 and 30 mm/h fixed in a parameter file (1.5, 9, ..dB above a Noise threshold $NS= 8$ dB).

Prior to 1988 NS was set at 14.5 dB, so intensities were underestimated, probably to imitate the console levels. In those years only a few remote displays were used. From Nov. 1989 the console was abandoned. The calibration continued as described, but the output at 1 resp. 100 mm/h was checked numerically at the computer.

3.8 Annex: Precipitation echo fluctuations

The radar echo power from a volume of random isotropic scatterers (phase of targets independent and between 0 and 2π) is the sum of the individual contributions. If monitored over a time much longer than required for mutual displacements to exceed a quarter wavelength, the distribution of the phase vector components (X and Y) is Gaussian around the value 0 with standard

deviation σ , e.g.

$$\frac{1}{\sigma\sqrt{2\pi}} \exp(-X^2/2\sigma^2) \quad (3.9)$$

The amplitude A can then be shown to vary as a two-dimensional Rayleigh distribution (Marshall and Hirschfeld, 1953, Canadian J. of Physics, **31**, pp. 962-995):

$$f(A) = \frac{2A}{\langle A^2 \rangle} \exp(-A^2 / \langle A^2 \rangle). \quad (3.10)$$

Here the symbol $\langle \rangle$ is used for a time-averaged value and $\langle A^2 \rangle = 2\sigma^2$.
 The mode of A , following from $df(A)/dA = 0$, is $\frac{\sqrt{\langle A^2 \rangle / 2}}$,
 the average value $\int Af(A)dA$ is $\frac{\sqrt{\pi \langle A^2 \rangle / 4}}$,
 and the standard deviation is $\frac{\sqrt{(1 - \pi/4) \langle A^2 \rangle}}$.
 Also the median, from $\int f(A)dA = 0.5$, is $\frac{\sqrt{\ln 2 \langle A^2 \rangle}}$.

The intensity $I = A^2$ follows an exponential distribution

$$f(I) = \frac{1}{\langle I \rangle} \exp(-I / \langle I \rangle) \quad (3.11)$$

with $\langle I \rangle = \langle A^2 \rangle$. In most radars a logarithmic amplifier is used. A logarithmic amplifier (log with base 10) transforms the power A in

$$W = s \log(cA^2) \quad (3.12)$$

Since $d(A^2)/dW = \exp(W/s') / (s'c)$, W is a Gumbel variable:

$$f(W) = \frac{1}{s'c \langle A^2 \rangle} \exp[W/s' - \exp(W/s') / (c \langle A^2 \rangle)] \quad (3.13)$$

where $s' = s / \ln 10$.

The most probable value of W is $s \log(c \langle A^2 \rangle)$,
 the average (with Euler's const.) is $s \log(c \langle A^2 \rangle) - s0.5772 / \ln 10$,
 and the standard deviation is $s' \pi / \sqrt{6}$.
 The numerical value of the latter is $0.5572s$,
 independent of $\langle A^2 \rangle$.

The standard unit for W is dB, so $s = 10$. The value of c decides whether the scale is dBZ or dBm. Then the bias of the average value caused by the logarithmic amplifier is -2.507 dB and the standard deviation of W is 5.57 dB.

Finally it may be useful to numerically simulate precipitation echo fluctuations. The variable A can be simulated by transforming a random signal

RND, uniformly distributed between 0 and 1. We have to find a value A , so that $\exp(-(A/\sqrt{\langle A^2 \rangle})^2)$ varies as RND. This is satisfied for

$$A = \sqrt{-\langle A^2 \rangle \ln \text{RND}} \quad (3.14)$$

or after logarithmic amplification,

$$W = s \log(-c \langle A^2 \rangle \ln \text{RND}) \quad (3.15)$$

Chapter 4

Clutter cancellation in KNMI weather radars

4.1 Introduction

In 1993 a clutter detection system was added to our existing radars. The method is described in the next section. The following sections document the successive implementations of the clutter detection system.

4.2 Method

The method was designed and tested by means of several high resolution radar pictures, acquired at De Bilt on several occasions in early 1992. The data consisted of 600 kHz samples of the log-amplifier output, providing a polar resolution of 250 m by 0.07 deg. This is the original resolution of radar data, before they are smoothed by the preprocessor. The cases included situations with rain or snow and situations with anomalous propagation clutter. The procedure, that finally was chosen, involves 3 steps that subsequently improve the accuracy of the decision to mark an output pixel of 2 km by 1 deg as “cluttered”.

Firstly, with a 1 deg wide beam rotating at 3 r.p.m., it is possible to obtain a sufficient number of samples to study echo fluctuations in range bins of 250 m (compatible with the pulse length). The beamwidth of 1 deg makes it probable that the samples may be attributed to the “same” echo. The slow rotation rate ensures a sufficient dwell time to obtain more or less independent samples. So the variance obtained can be used to judge, with limited certainty, a possible non-Rayleigh character of the echo.

Secondly, due to e.g. screening effects, clutter occurs independently in adjacent range bins, so we have 4 independent tests on non-Rayleigh behaviour. The 4 tests together enable a more accurate decision for the 1 km/1 deg pixels of the preprocessor output.

Thirdly, clutter and precipitation echoes occur separately over areas of a scale of 10 km or so, at least in non-mountainous regions. So post-processing by means of spatial statistics can be used. The final result offers - on average - a 98% certainty of detecting clutter while only 2% of rain areas may falsely be removed. Different from other clutter methods, clutter pixels are not corrected with a certain number of dB's, but removed from the image.

4.3 History

Automatic clutter cancellation was the last step in the automation of the distribution of radar pictures. The reasons for automation were - apart from the evident savings on personnel cost - the improvement of the quality of the display of radar information to its users. Here quality refers to accuracy, resolution, timeliness and availability on many remote locations.

In the 1980's the radars at De Bilt and Schiphol were EEC WSR-81 radars. By May 1988 the national facsimile distribution of hand made radar sketches had completely been replaced by the automatic remote computer display of composite pictures from two-elevation pseudoCAPPIs, i.e., a range-dependent combination of reflectivity data from more elevations (see chapter 6 for details).

However, the manual top measurements had to be continued. This was the main reason, that in 1989 the site computers, the processing software and the control interface were replaced. The DVIP (= Digital Video Integrator and Processor) preprocessor remained in function. From Nov. 1989 both new computers were operational, producing four-elevation pseudoCAPPI's with automatic top measurements. The operational use still demanded a manual correction of ground clutter before the pictures could be distributed.

The automatic clutter detection system required a new preprocessor, that not only could produce 1 km/1 deg polar intensity values, but also clutter flags resulting from a statistical analysis of the unaveraged sub-pixel intensities. The new preprocessor was built around a TMS320C40 DSP, then recently available. The clutter detection also required changes in the main radar computer software, because the final decision regarding the presence of ground clutter is based on the horizontal distribution of clutter flags in surrounding pixels.

This clutter detection system, introduced in late 1993, operated success-

fully from mid 1994. Anomalous propagation clutter over land was removed almost completely. In summer months nighttime thunderstorms may propagate above a surface inversion. Then the thunderstorm echoes that are hidden in extended clutter areas, are perfectly singled out by the present method. However, the system is only partly (40%) effective in removing sea clutter, because echoes from breaking waves have fluctuation characteristics resembling rain echoes. Since the Schiphol location was replaced by a coastal site (Den Helder, 1996), the occurrence of sea clutter increased substantially.

A few years later, KNMI purchased new Doppler radars (Gematronik METEOR 360 AC) that became operational in 1996/1997. It was decided that the clutter detection system should be continued. This involved modifications to the RVP6 preprocessor and specific additions to the Rainbow software. To avoid a redesign of the algorithms, the procedures were almost exactly copied from the earlier implementation. So, the AD-sample rate of 600 kHz, the Pulse Repetition Frequency of 250 kHz, the antenna speed of 18 deg/s and the output resolution of 1 km/1 deg were maintained. Initial problems were caused by a mismatch of the clutter and intensity pictures. Only after this was solved in early 1998, the original quality was reached.

Before 1999, in a small percentage of warm front situations, too much rain (up to 20%) was wrongly removed. This was fixed in 1999 by improved postprocessing criteria.

4.4 Clutter preprocessing

After transmission of a pulse (at 0.004 sec intervals) the receiver output of the log. amplifier is sampled by an AD converter with 600 kHz. So the samples originate from range bins of 250 m. Clutter analysis depends on measuring signal fluctuations between echoes of successive pulses measured in a certain range bin.

NOTE: This requires a very good synchronization of the AD conversion to the pulse transmission time (within 10 nsec).

NOTE: Another hardware requirement is the absence of fluctuations in the transmitted power of the successive pulses.

The resolution of the AD converter is in units of about 0.5 dB. As the computations are carried out on 1 deg sectors, the program is checking the azimuth read-out and restarts calculations at 1 deg transitions. For every 1 deg sector about 15 ($=N_d$) radials are available, each containing 4 sample values $P(r, a)$ per km range interval up to a range of 320 km (for the old radar 384 km). In the following computations the original log amplifier output has to be used, i.e. without the distance correction. For every value $a = 1 \dots N_d$

a running average over N_g radials is computed for all rang bins r , as follows

$$P_g(r, a) = \frac{1}{N_g} \sum_{i=a-N_g+1}^{a+N_g-1} P(r, i) \quad (4.1)$$

N_g , an odd integer, is a parameter. We presently use $N_g = 5$. For the old radar N_g was fixed at 5 and the computation could not use data of the next 1 deg sector, so it used instead $a = -1, 0, \dots, (N_d - 2)$ where the last samples of the previous sector are numbered 0, -1, -2, etc. The variance of the signal with respect to the running average is

$$\text{Var} = \frac{1}{N_d} \sum_{i=1}^{N_d} [Pg(r, i) - P(r, i)]^2 \quad (4.2)$$

For every range bin r (we have 4 such range bins in 1 km), the value Var is compared with tabulated values $V_{min}(P)$ and $V_{max}(P)$. Values outside these limits correspond to non-Rayleigh fluctuations. The base P of the tables V_{min} and V_{max} is the average signal of the N_d samples, found from

$$P(r) = \frac{1}{N_d} \sum_{i=1}^{N_d} P(r, i) \quad (4.3)$$

The use of a table allows the correction of the variance estimates for “non-linear” behaviour of the log-amplifier. Even a very good log-amplifier will deviate some 0.5 dB from the design curve and all amplifiers will fail to discriminate dB values for weak signals.

NOTE: In operational practice the log-amplifier has to be checked regularly and -if necessary- new tables for V_{min} and V_{max} have to be loaded into the preprocessor.

The above procedure is applied for all range bins at 250 m intervals. The clutter detection for a 1 km/1 deg sample is based on 4 tests of values Var: if at least C_{nr} of these tests conclude to clutter, a clutter flag is set for that particular polar pixel. C_{nr} is an external parameter to allow changes in the range sampling (e.g. to 125 m intervals). With 4 samples the optimal value is 2.

NOTE: It seems probable that more accurate clutter flags can be computed with faster AD-conversion. A larger PRF or a slower antenna scan rate would certainly produce more reliable clutter flags, but also negative side effects: second trip echoes, slower update. Data with slower scan rate were indeed acquired in 1992, parallel to the test files mentioned in Section 4.2,

and a better performance of the clutter cancellation on those data could be demonstrated.

NOTE: It is also possible to combine range bins over 2 km range and demand that e.g. 3 out of 8 tests suggest clutter. However, this would also require retuning the postprocessing algorithms.

4.5 DVIP emulation (old DVIP)

Another task of the preprocessor is the production of average intensity values. The integration starts in the radial direction by taking the average of 4 range bins. In the old DVIP and the old preprocessor this average was integrated over the azimuth by means of a recursive filter:

$$\bar{P}(i) = (1 - A) \cdot P(i) + A \cdot \bar{P}(i - 1) \quad (4.4)$$

with $A = 0.25$. The actual value of $\bar{P}(i)$ is output at the 1 deg transition. In the old radar the north was set at 359.3 deg to correct for the lag involved in applying Equation 4.4 (see Section 3.2). In the new radar the RVP6 calculates the exact average of the linearized power output. Therefore the 2.5 dB (Rayleigh) correction for logarithmic averaging is no longer necessary.

4.6 Clutter postprocessing: selection of clutter flags

The data from the preprocessor have a range resolution of 1 km, but in the main processor this resolution is reduced to 2 km. Per range bin we then have 2 intensity values and 2 clutter flags. The 2 intensity values are logarithmically averaged, but for every range-bin 2 intensity flags are retained that indicate if one or both of the (STC-corrected) 1 km intensities exceeds a threshold value (parameter with default value of about 1 dBZ). Clutter flags are only used if the corresponding 1 km intensity flag is set. Both flag counts can have values, 0...2.

In the polar image an occultation correction may be performed: If intensity data for obstructed azimuths are replaced by interpolating between data from nearby unobstructed azimuths, the clutter flags and the intensity flags are replaced as well. For a maximum of 5 adjacent occulted radials the flags are copied from the nearest usable radial. If the number of occulted radials is odd, the centre radial is filled with the average flag count, rounded upward respectively downward for odd respectively even range count (2 km steps).

Polar PPI-pictures at 4 elevations are combined into a low-altitude pseudoCAPPI image. Also a polar clutter map is constructed that contains per 2 km range bin counts for intensity as well as clutter flags. These counts can have the value 0, 1 or 2. These data are copied from the elevations that contribute more than a minimum weight percentage (parameter) to the intensity of the final picture. Flag counts from 2 elevations are averaged and eventually rounded upward.

NOTE: in the new radars the critical weight percentage is fixed at 49, so only one elevation is used. This simplification was based on experience with the old radar, but might be reconsidered.

If the radome is wetted by rain, nearby ground returns increase because of decreased side-lobe reduction. Even the 3 deg elevation used at close range for the pseudoCAPPI picture shows ground echoes added up to the nearby rain. The resulting signal is more stable than a rain echo and is indeed recognised as clutter. Therefore clutter flags up to a certain range (parameter, e.g. 25 km) are ignored for those azimuths where the echo at a predefined range (parameter, e.g. 15 km) exceeds a predefined value (parameter, just above the echo strength in dry weather).

4.7 Clutter postprocessing: smoothing in polar pseudoCAPPI image

Four parameters determine the spatial scale of the smoothing. Each pixel is surrounded by an outer area. The radial size of that area is D_2 (2 km pixels) and the tangential size A_2 (degrees). Within that outer area is a centered inner area $D_1 \times A_1$. Over both these areas together the sum N of the intensity flags is counted. For those 1 km-pixels that qualify for N , the sum T of the clutter flags is counted. The maximum value for N and T is N_s , the sum of the 1 km pixels in both areas together. The central pixel is part of both the outer and the inner areas. In the following the central pixel receives additional weight in the decision equations, the smoothing weight factors approximate a bell-shaped area around the central pixel. The counts are performed over the inner and outer area together.

If the value of the clutter flags of the central pixel is I ($= 0, 1$ or 2), the following coefficients are used:

$$C_0 = 0.60 - 0.10 \cdot I \quad (4.5)$$

$$C_2 = -0.20 - 0.10 \cdot I \quad (4.6)$$

$$C_3 = 0.01 - 0.03 \cdot I \quad (4.7)$$

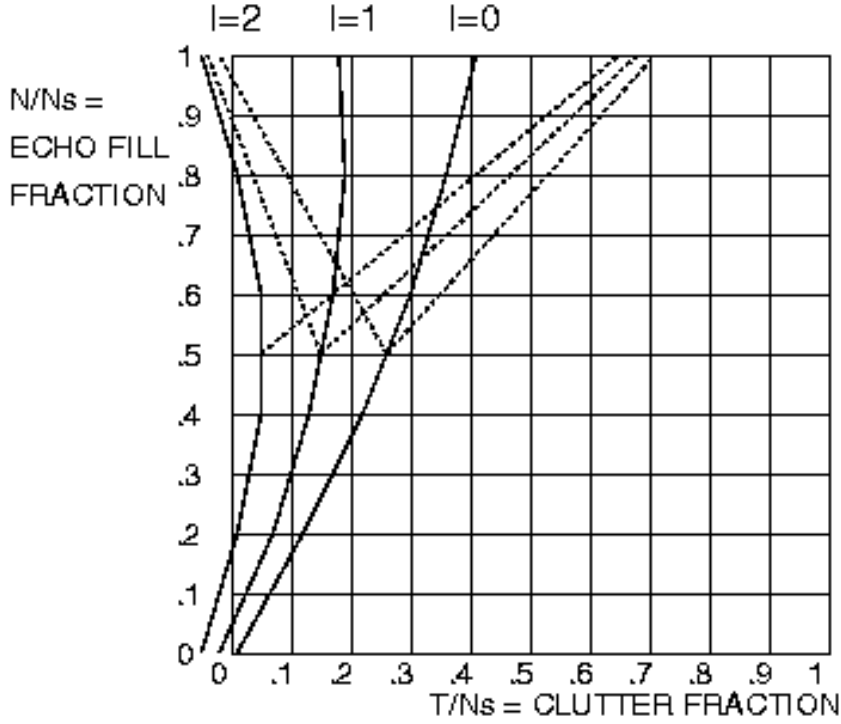


Figure 4.1: Illustrating the old and new clutter detection criteria. Pixels positioned by N/N_s and T/N_s (depending on surrounding pixels) to the right of the full curves are considered clutter. The value of I is the number of clutter flags of the central pixel. The dotted/dashed curves are attempted modifications of the criteria: dashed for warm fronts (higher threshold for T) and dotted for sea clutter.

If the central pixel is at range R (2 km units) we also have

$$C_d = \min(1.40/R, 0.40) \cdot (1 + 2.00 \cdot I) \quad (4.8)$$

The output clutter flag for the central (2 km) pixel is set if $I > 0$ and

$$T/N_s > (C_0 + C_d) \cdot N/N_s + C_2 \cdot (N/N_s)^2 + C_3 + C_4 \quad (4.9)$$

where the value of C_4 is explained later in this section. The rationale behind these equations is, that pixels with $I = 2$ are almost automatically classified as cluttered, independent of the properties of the surrounding pixels. On the other hand, pixels with $I = 0$ can also acquire a clutter flag, especially if they are embedded in a massive echo (N/N_s close to 1) with at least 40%

clutterflags according to T/N_s . Pixels in massive echoes with $I = 2$ are accepted as cluttered regardless of their surroundings.

An important condition is that isolated ($N = 1$ or 2) pixels with $I = 0$ should not be considered as clutter. So the first term of C_3 should not be negative. Note that all 9 real numbers in the above equations are external parameters, so they can easily be optimized. Experience shows that increasing this first term of C_3 with 0.01 results in 10% less clutter flags.

In 1999 the equation for T/N_s was modified depending on the texture of the surrounding echo-area, expressed by the standard deviation σ of the horizontal variations -corrected for the mean gradient -over an area $D_3 \times A_3$ (2 km,deg). If the echoes were typically from warm front rain, i.e. $\sigma < 7$ (0.5 dB units, parameter), a term

$$C_4 = -C_h(I) \cdot \frac{N/N_s - F_s}{1 - F_s} \quad (4.10)$$

was added to the r.h.s. of the above condition if $N/N_s > F_s$. The parameter F_s is typically 0.5 and parameter $C_h = -0.3, -0.5, -0.7$ for $I=0,1,2$ respectively. The reason for this addition was to prevent the removal of echoes from steadily falling snow flakes. (see Section 4.10).

An attempt was also made, to recognise sea-clutter by choosing $\sigma \geq 13$ (parameter) and using $C_h = 0.45, 0.20$ and 0.00 for $I=0,1,2$. This sometimes increases the number of clutter flags in showers. For this case the parameters C_h have therefore been reduced to 0.00.

The calculation of the standard deviation proceeds as follows. First the average gradient of the echo values (in units of 0.5 dB) is determined by two-dimensional least squares fitting. Take $i_3 = (D_3 - 1)/2$, $j_3 = (A_3 - 1)/2$ and the number of pixels $N_3 = A_3 \times D_3$ Compute for $i = -i_3 \dots i_3$ and $j = -j_3 \dots j_3$ the sums

$$S_i = \sum i \cdot I(R + i, A + j) \quad (4.11)$$

$$S_j = \sum j \cdot I(R + i, A + j) \quad (4.12)$$

$$S_{ii} = \sum i^2 \quad (4.13)$$

$$S_{jj} = \sum j^2 \quad (4.14)$$

$$S = \sum I(R + i, A + j) \quad (4.15)$$

The regression plane is then determined by the coefficients: $\alpha = S_i/S_{ii}$, $\beta = S_j/S_{jj}$, and $\gamma = S/N_3$. Finally, again over the area $-i_3 \dots i_3$ by $-j_3 \dots j_3$

$$S_z = \sum [I(R + i, A + j) - \alpha \cdot i - \beta \cdot j - \gamma] \quad (4.16)$$

$$S_{zz} = \sum [I(R + i, A + j) - \alpha \cdot i - \beta \cdot j - \gamma]^2 \quad (4.17)$$

The standard deviation is then

$$\sigma = \sqrt{(S_{zz} - S_z^2/N_3)/(N_3 - 1)} \quad (4.18)$$

The input and output of the smoothing process is logged in a file. For each picture, apart from the time stamp, 4 numbers are saved. First the total number of intensity flags and clutter flags (up to 2 per pixel) of the original pseudoCAPPI image. Also for the output polar image - only for ranges larger than a certain parameter: the number of pixels above the threshold intensity from Section 4.6, and the number of clutter flags (up to 1 per pixel). The logfile is closed every month and the monthly files are kept on the Radar Site Computer.

4.8 Output

The polar pseudoCAPPI intensity and clutter map are both transferred to a rectangular picture and finally to a rectangular picture in polar stereographic projection. In the old radars this process was done in one step by using a look-up table defining the azimuth and range that should fill a certain output pixel.

In the new radars the polar to rectangular conversion of intensity values was originally performed by two-dimensional interpolation. It proved necessary to define a lower limit of the intensity scale near 0 dBZ (rather than the original -31.5 dBZ) to avoid unrealistic interpolation results both in the pseudoCAPPI composition and the coordinate conversions. Finally it was decided to replace interpolation for the coordinate conversion by resampling the value of the nearest pixel of the originating grid. By doing so the clutter flags accompany the proper intensity values during the conversion to a rectangular pixel.

The intensity and clutter maps are produced separately. In the clutter mask clutter gets the value 0, a non-clutter pixel is 255. The actual clutter removal is carried out in the compositing and distribution computer (CRIS), so it remains possible to distribute pictures with clutter as well as cleaned pictures.

4.9 Reference

Wessels, H.R.A., J.H.Beekhuis, 1994, Stepwise procedure for suppression of anomalous ground clutter. COST-75 Int. Seminar on Advanced Weather Radar Systems, Brussels 20-23 Sep.

4.10 Annex: Improved clutter postprocessing

The experiments that led to the 1994 clutter removal system have been described in the reference above. Here further information will be given about the improvements reached in 1999.

4.10.1 Suspected clutter flags embedded in rain areas

Sometimes “clutter” areas appear in stratiform rain, notably near warm fronts. These areas have a typical size of 20 km. Inspection shows that nearly all pixels in these regions are filled with values $C=1$ or 2, so classification as clutter is hard to avoid. Typical intensities that are removed are between 0.5 and 2 mm/h; therefore these areas appear as “holes” surrounded by unaffected precipitation echoes.

A large area of the Netherlands is covered by two radars and it could be observed that often the “holes” from both radars would partly overlap. Then compositing brings little help.

The holes appear at a range of 50-100 km from the radar, usually near the range where the beam would cross the melting level. It is an interesting question why these echoes don't show the typical (Rayleigh) fluctuation behaviour of rain echoes. It might be that the low fluctuation rate of these echoes is caused by the presence of slowly falling snow flakes.

From the above characteristic properties two possible tools emerge to recognise these echoes: their narrow intensity range, and especially their horizontally uniform echo distribution.

4.10.2 Sea clutter

The evident explanation of the partial absence of clutter flags over sea areas is that scattering at waves causes echo fluctuations comparable to those at an ensemble of precipitation particles. Many studies have been made of radar echoes from the sea surface, including effects of frequency, incidence angle and sea wave characteristics (Nathanson, 1969).

The sea state is very important. In our pictures sea clutter appears with wind speeds above about 5 m/s. Most probably it is connected with breaking waves. According to Iguchi (1989) the backscatter increases some 30 dB if the wind speed increase from 2 to 8 m/s. Of course this is without clutter suppression.

Like anomalous ground clutter over land, echoes from the sea surface are characterised by large horizontal intensity differences. In many sea clutter situations only part of the pixels in a certain area exceed the lowest presentation level of 0.3 mm/h. Large continuous areas of sea clutter are more rare.

Sea clutter is easily recognised by meteorologists, but is disturbing if shown to the general public in TV broadcasts. For hydrological purposes precipitation measurements over the sea usually have little interest.

Typical situations for sea clutter to occur are:

- subsidence inversions,
- dry air advection, usually with easterly wind in the spring,
- cold air advection in autumn and winter.

In the latter two situations dew points are colder than the sea surface and so-called evaporation ducts occur. In such ducts the distance reduction of radar beam intensity is less than the normal inverse square law. This “focusing” increases returns from the surface or other scatterers like refractive index gradients. It can be argued that reflection at the sea surface may cause increased focusing.

4.10.3 Horizontal echo fluctuations

To check whether there are typical differences between various echo categories: warm front rain, showers, land clutter and sea clutter, a number of polar radar pictures was analysed.

For each 2 km/1 deg pixel a surrounding area of 25 pixels was used (10 km/5 deg). The quantity studied was the pixel intensity (dBZ). First the horizontal gradient was removed by two dimensional least squares fitting (see Section 4.7). The remaining standard deviations were computed for all pixels with significant echo over the complete picture.

Sea clutter and land clutter did not show much difference. Typical examples are given in Table 4.1.

Fluctuations above 3 dB (6 units) are rare in warm frontal rain and common for sea clutter, but unfortunately rather frequent in showery rain. The discrimination does not improve if the fluctuations are measured over other areas, e.g. 49 or 9 pixels. On the basis of such studies we consider in Section 4.7 fluctuations smaller than 3.5 dB as “warm front”.

Table 4.1: Exceedance of small-scale horizontal fluctuations expressed in standard deviation (units of 0.5 dB)

date	hr	echo type	98%	95%	90%	80%	50%	20%	10%	05%	02%
19980326	17	warm front	1	1	2	3	3	3	4	6	7
19980116	11	showers	1	5	6	7	10	14	17	19	23
19980509	19	sea clutter	7	9	10	12	17	22	27	30	33

Table 4.2: Warm front rain criteria; percentage classified as clutter with old/new criteria (dH=Den Helder, dB=De Bilt).

date	hr		elevation 0.3 deg	elevation 1 deg
19971221	09	dH	20 / 8	2 / 2
19971221	09	dB	6 / 1	12 / 1
19980116	11	dH	37 / 38	13 / 14
19980326	17	dB	2 / 0.2	23 / 0.1
19980505	16	dH	19 / 6	32 / 12
19980505	16	dB	4 / 2	16 / 0.4

4.10.4 Postprocessing tests

Changes in the postprocessing criteria of Section 4.7 were attempted to reduce the “warm front holes”. We want a higher detection criterion T/N_s , especially if $I=1$ or 2. Situations with low T are excluded, because then estimates of the standard deviation are probably inaccurate.

So we increase C_4 in the r.h.s. of Equation 4.9 linearly, starting at $N/N_s=0.5$, to reach for $N/N_s=1$ a value of 0.3, 0.5 and 0.7 for $I=0, 1$ and 2 respectively. As mentioned in Section 4.7 attempts with better sea clutter removal were hardly successful. The results are listed in Table 4.2.

Considering the results for De Bilt, the “holes” in warm front rain are very well restored by the method proposed. The results for Den Helder seem relatively even better, but are misleading. At the time too many clutter flags were originally set in weak echoes at the outer edges of rain areas. This was caused by a poor tuning of the receiver and preprocessor chain. This problem has since then been fixed.

The results for sea clutter (Table 4.3) are not spectacular. Because we don’t want shower echoes to be removed, it was decided not to use this correction operationally.

Table 4.3: Sea and land clutter; percentage classified as clutter with old/new criteria (dH=Den Helder, dB=De Bilt).

date	hr		elevation 0.3 deg	elevation 1 deg
19980509	19	dH	68 / 84	79 / 81
19980512	10	dH	53 / 64	71 / 83

4.10.5 Future developments

In early 2001 elevation corrections were made in Den Helder, that might reduce focusing by beam reflection at the sea surface. Results for spring season sea clutter are not yet available. Possible further refinements for sea clutter removal could be attempted by using a land-sea mask for the radar of Den Helder and use a different postprocessing over the sea or even use information from satellites. Satellite information on clouds over the sea surface can be very reliable.

4.10.6 References to Annex

- F.E.Nathanson, 1969, Radar design principles, McGraw Hill, New York.
T.Iguchi, 1989, Measurements of sea backscatter at extremely low grazing angles by a C-band Doppler radar. J. of the Communications Res.Lab., 36, nr.149, p.157-169.
M.W.Long, 1975, Radar reflectivity of land and sea. Lexington Books

Chapter 5

Scan schedule and data collection

5.1 Introduction

In this chapter scan and product definitions are presented in tabular form. These settings may change for various reasons. The actual settings of the radars are documented in the INFO pages on the radar computers: info/prod.rd. In the final sections a short description of the meaning and the use of the various file header labels is given.

5.2 Scan settings

In this section the present (2001, Jan) scan schedule is given. The timings are based on net scan times (20 s for 18 deg/s, 14.4 s for 25 deg/s) augmented with 5 s. setting time. The total time of the watchdog is then $4 \cdot 25 + 2 \cdot 19.4 = 2'19''$. The splitting of the volz scan makes the timing of the 4.0 deg elevation scan uncertain. It is possible (fast rotation, short setting time) that the scan can be completed in the first 5 min period without interruption.

```
SCHEDULER:    <rd?.wdg>  in directory $GAMPATH/watchdog.d
SCANS:        <rd?intz>  in directory $GAMPATH/scan.d
               <rd?intv> , <rd?volz> , <rd?volv>
PRODUCTS:    <rd?.pcp>  in directory $GAMPATH/pdf.d
               <cltmap.pcp> etc. under elevations/timings
```

Scan definitions per 15 min:

```
Name:          rd?volz.sca  rd?volv.sca  rd?intz.sca  rd?intv.sca
```

Nr.elev.:	14	7	4 (3x)	2 (3x)
Elev.& start	0.3 02'20"	1.1 12'20"	0.3 *00'00"	0.7 *01'40"
time min+sec	0.8 02'40"	2.5 12'40"	1.1 *00'25"	1.6 *02'00"
	1.3 03'00"	4.0 13'00"	2.0 *00'50"	
* = +0	1.8 03'20"	5.5 13'20"	3.0 *01'15"	
+05'00"	2.3 03'40"	7.0 13'40"		
or +10'00"	2.8 05'00"	8.5 14'00"		
	3.3 05'20"	10.0 14'20"		
	4.0 07'20"			
	5.0 07'40"	at 08h52'		
	6.0 08'00"	replaced by		
	7.5 08'20"	AUTOCAL		
	9.0 08'40"			
	10.5 09'00"			
	12.0 09'10"			
Products:				
	rd?.vil	rd?.vad	rd?.pcp	rd?.hcv
	rd?.eth	rd?.vp2	cltmap.pcp	rd?.uwt
	rd?.etz	rd?.uwt		rd?.ppv
	rd?.caz	rd?.ppv		
	rd?1..4.vcz			
Settings:				
Advanced:	on	on	on	on
Data:	Z	V,W	Z,C	V,W
Dopplerfilter:	off	off	off	off
Range(km):	320	120	320	160
Resol.(km):	1	0.5	1	0.5
Range samples:	4	4	4	4
Free runmode	on	on	on	on
Ant.deg/s:	24	24	18	24
Time sampl.	na	na	na	na
Pulse length	long	short	long	short
Pulse freq:	400	1153/864	250	822/661
Unfolding:	none	3/4	none	3/4
Max.Velocity:	na	45.85	na	35.09
Range norm:	default	default	default	default
STC/AGC AGC	AGC	AGC	AGC	AGC
Cl.thresh.:	-18	-18	-18	-18
Log.thresh:	1	1	1	1
SQI:	0.5	0.5	0.5	0.5
Dop.sp.rem:	off	off	off	off
Log.sp.rem:	off	off	off	off

5.3 Product definitions

5.3.1 Reflectivity

	pcp	clt	vil	eth	etz	vcz
V6 Layer hght(km)	na	na	na	na	na	na
V2 Ly.spacing(km)	na	na	na	na	na	0.125
V4 Max.height(km)	na	na	16	16	16	14
V5 Min.height(km)	na	na	1	na	na	na
A8 Displ.elev(deg)	na	na	na	na	na	na
D8 Max.range(km)	na	na	na	na	320	320
D7 Min.range(km)	na	na	na	na	160	na
P4 Displ.range(km)	400	400	160	320	na	na
D10 Nr.pixels	200	200	160	160	na	na
D11 Dyn.range	-1.5	-1.5	+0.05	na	na	-31.5
(dBz or m/s)	+95.5	+95.5	+65	na	na	+95.5
Projection	PSTN	PSTN	PSTN	PSTN	PSTN	none
Resolution	fullres	fullres	fullres	fullres	Fullres	image
P14 Cnvalue	na	na	3000	na	na	na
P15 Dnvalue	na	na	2.3	na	na	na
P14 Intens.grad.	na	na	na	0.0048	na	na
P15 Intens.exp.	na	na	na	2.8	na	na
P24 Side lobe att.	na	na	na	25	na	na
P25 Noise lev.(dBZ)	na	na	na	7	na	na
V6 Ax/Ay cut	na	na	na	na	na	*1)
V7 Bx/By cut	na	na	na	na	na	*1)
D14 Display time(h)	na	na	na	na	na	na
P24 Bias thrsh.(m/s)	na	na	na	na	na	na
P25 Range aver.(km)	na	na	na	na	na	na
P26 Range.avg.start	na	na	na	na	na	na
P27 Upper gap (deg)	na	na	na	na	na	na
P28 Lower gap (deg)	na	na	na	na	na	na
P29 Gap thr.(m/s)	na	na	na	na	na	na
P30 Azim.grad.thr.	na	na	na	na	na	na
P31 Low p.filt.(deg)	na	na	na	na	na	na
P32 Tan.az.size(deg)	na	na	na	na	na	na
L-Min	na	na	na	na	+5	na
L-Max	na	na	na	na	+95.5	na

*1)actual values with range = [-200, +200]

rdh1.vcz -130/-200 resp. +150/+080, over Schiphol, 400 km long, SW-NE

rdh2.vcz -158/-200 resp. +122/+080, parallel to rdh1.vcz, 20 km to NW

rdh3.vcz -102/-200 resp. +178/+080, parallel to rdh1.vcz, 20 km to SE

rdh4.vcz -154/+080 resp. +126/-200, over Schiphol, NW-SE

17	VCUTZ		12467	12	567890123		.01		1	13
18	VCUTR		12467	12	56789012345		.01		138	13
19	VCUTV		12467	12	567890123		.01		1	13
20	VCUTW		12467	12	567890123		.01		1	13
21	ETopZ		12401		123456789012345				56	12
22	ETopR		12401		123456789012345	45			3568	12
23	EBasZ		12401		1234567890123				56	12
24	EBasR		12401		123456789012345				3568	12
25	VAD	1238			1234567890123					12
26	VVP1	123	249		1234567890123				.0	12
27	VVP2	123	249		1234	67890123		784		12
28	ETH		34		123456789012345	(24-25)			.0	12
29	PCAPPI				1234567890123		.01			12
30	PsCAPZ		15		1234567890123		.01			12
31	PsCAPR		15		123456789012345		.01		38	12
32	PsCAPV		15		1234567890123		.01			12
33	PsCAPW		15		1234567890123		.01			12
34	UWT		5		1234567890123	(24-32)	.01			12
100	Az/Vol	39			12345670129012	(92, W, X, F9)				
101	Elev	9			12345670129012	(92, W, X, F9)				
1001	SRI				123456789012345	36	.01		380	12
1002	PAC				6		.01345678		1	12
1003	RIH		1242				.0134567890		1	12
1004	PAL				6		.01345678		1	12
1005	VIL		45		123456789012345		.01			12
2001	HHW		12458		1234567890123	6				12
2002	WARN				345	(38-47,52-90,92)	(25-29)			12
3001	TRACK				345	(33-52)	(21-24)			12
4001	RDS	123			1234567890123	7	401			12
4002	AZS	123			1234567890123	8	401			12
4003	ELS				1234567890123		401			12
4004	HZS		5		1234567890123	(30)	.01			12
4005	VCS				1234567890123	(31-32)	.01			12
4006	RAS	123			1234567890123	78	401			12
4007	RES				1234567890123		401			12
4008	3DS				1234567890123	79	401			12
4009	LTB				1234567890123	(31-32)	.01			12

Chapter 6

PseudoCAPPI and composite pictures

6.1 Introduction

Data from a single radar are collected at various elevations. These “volume” data are too complicated to distribute and display. Therefore they are combined into a single PPI (plan position indicator) type picture.

The Netherlands is - at least partly - covered by two KNMI radars and several foreign radars. Again we won't expect the user to inspect many single pictures, but rather one combined “composite” picture. An advantage of pseudoCAPPI pictures is that data from nearby a radar are from higher elevations, so local ground clutter is reduced. Data from nearby a radar may exclude overhead showers because the maximum elevation is 12-16 deg (in our case 3 deg for the 5-min. scan). The missing region is metaphorically named “cone of silence”. Our technique of compositing allows the data from nearby a radar to be replaced by a not to distant other radar. Another advantage of compositing is its automatic back-up function if one of the radars is missing.

At KNMI the pseudoCAPPI is created in the radar site computer. Compositing is performed in the CRIS.

6.2 KNMI pseudoCAPPI

The antenna scans around a vertical axis. Four complete scans at elevations 0.3, 1.1, 2.0 and 3.0 deg are combined into a single picture. The height H of a radar beam (above the radar level) depends on the elevation and the range

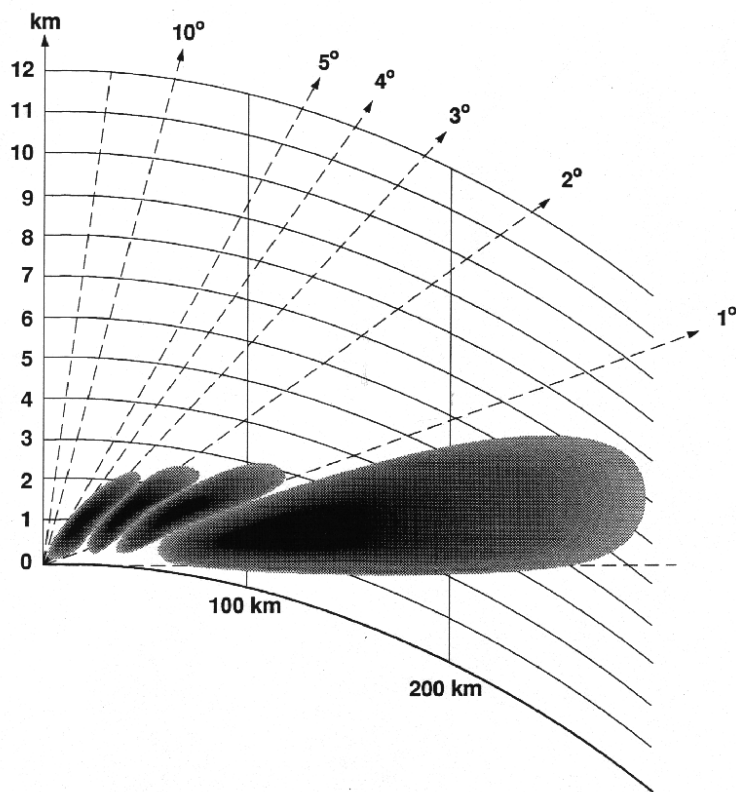


Figure 6.1: The height of the radar beam as a function of range for four elevations.

D (see Figure 6.1):

$$H = D \sin E + \frac{D^2}{2R_a} \quad (6.1)$$

where R_a is the earth radius, multiplied by 1.33, to correct for microwave atmospheric refraction. We take $R_a=1.33 \cdot 6367$ km. In the combined picture we use gradually lower elevations at increasing range. The result is that up to about 100 km the data are measured near 1 km height (CAPPI= constant altitude plan position indicator). At larger range the data come from gradually higher altitude due to the earth's curvature. This pseudoCAPPI picture is built by means of weighted averaging of dBZ values (averaging rainfall would give different results).

Because at short range weak echoes (noise) are reduced to negative dBZ values, that would lead to unrealistically low average results, a minimum value around 0 dBZ is substituted before averaging. In the old radars this was achieved automatically by an echo scaling starting at about 0 dBZ. The

Gematronik radars use a scale starting at -31.5 dBZ, so KNMI had to ask for a tophat-function that corrects echoes below about 0 dBZ.

The elevations are E_1 , E_2 , E_3 and E_4 . For a certain range and azimuth these elevations contain respectively values P_1 , P_2 , P_3 and P_4 (dBZ). For pseudoCAPPI height H (km) the elevation at distance R (km) is:

$$E = \arcsin\left(\frac{H}{D} - \frac{D}{2R_a}\right) \quad (6.2)$$

The pseudoCAPPI dBZ value P is found as follows:

```

IF E>=E4 THEN P=P4
IF E<E4 AND E>=E3 THEN A=(E-E3)/(E4-E3); P=A*P4 +(1-A)*P3
IF E<E3 AND E>=E2 THEN A=(E-E2)/(E3-E2); P=A*P3 +(1-A)*P2
IF E<E2 AND E>=E1 THEN A=(E-E1)/(E2-E1); P=A*P2 +(1-A)*P1
IF E<E1 THEN P=P1

```

In Chapter 4 on “Clutter Cancellation” the parallel procedure for the vertical combination of clutter flags is described. In Annex 6.10 the weight factors that result from both pseudoCAPPI combination and compositing are illustrated as a function of distance for the two KNMI radars.

6.3 Compositing considerations

Compositing can be performed in three stages.

- Firstly the data from all participating radars have to be remapped into the same pixel grid. This is a navigation problem and is treated in the Chapter on Navigation.
- Secondly, the level slicing of the contributing radars has to be converted to a common scale. This may be a problem if foreign radars are involved. It may also be a problem if some radars have a calibration bias. Again some information is given in the Navigation Chapter.
- Thirdly, the level of each target pixel has to be determined from the levels measured by the available radars. This stage will be treated here.

Many countries distribute composite pictures. The level-choice techniques used are very different (Wessels, 1992, Newsome, 1992). Even now, choosing the nearest radar is popular. This leads to discontinuities along fixed boundaries.

A better method is - at least at ranges beyond 25 km from any radar - to choose the maximum echo of all available radars. At ranges within e.g. 25 km from a radar it may be possible to use other data to remove fixed ground clutter and to fill in “holes” above the radar caused by elevation restrictions. However, outside a 120 km radius no radar can be expected to replace with sufficient quality near field data of other radars.

A gradual transition around the 25 km boundary should prevent discontinuities in the composite picture: we use the maximum echo at far range but possibly the minimum echo at short range. If radars are within 2.25 km additional measures are required.

A final point is, that the compositing algorithms should automatically neglect missing radars, e.g. by choosing the maximum available signal.

6.4 Compositing history

In the 1987 radar distribution and compositing computer (RDDC = Radar Data Distribution Computer) only two radar pictures were combined. The output value was read from a chosen 8x8 table with output 0-7 for any two inputs 0-7. At least 10 of such 8x8 tables were required to e.g. guarantee a gradual transition from copying the first to copying the second radar.

Two examples of such tables are shown here: one for (nearly) following radar A, one for choosing the maximum of both radars.

B:	0	1	2	3	4	5	6	7
0	0	1	2	3	4	5	6	
1	0	1	2	3	4	5	6	
2	0	1	2	3	4	5	6	
A: 3	0	1	2	3	4	5	6	
4	0	1	2	3	4	5	6	
5	0	1	2	3	4	5	6	
6	1	2	3	3	4	5	6	
7								

B:	0	1	2	3	4	5	6	7
0	0	1	2	3	4	5	6	
1	1	1	2	3	4	5	6	
2	2	2	2	3	4	5	6	
A: 3	3	3	3	3	4	5	6	
4	4	4	4	4	4	5	6	
5	5	5	5	5	5	5	6	
6	6	6	6	6	6	6	6	
7								

The 8x8 table number was read from a reference map covering all image pixels. The reference map was generated automatically from a few parameters, radar coordinates, ranges, and codes indicating the trigonometrical computations to be performed. Because the conversion is fixed for each pixel, the transmission of the result could - in principle - start while the rest of the input pictures was being received. This was not practised, because the timing was no great problem: The observation of HH (minutes) was finished at HH+3 (4 PPI + 4 RHI). Reception by the RDDC until HH+4: start transmitting product HH+5; available for user HH+6 minutes.

This system ran satisfactorily on the RDDD-PC. In 1992 the radar distribution had to be revised, e.g. to accommodate the use of foreign data. Therefore, in designing the CRIS, the combination of up to 16 radars was anticipated. Also it was anticipated that there would grow interest in a finer intensity slicing than only 6 levels. Evidently the system with tables was not easily expandable, so different algorithms had to be used.

The next major change took place in 1996, when the CRIS was transferred from VAX computers to Alpha servers. The operating system changed from VAX/VMS to OPEN/VMS.

6.5 Present compositing method

The method remains based on: 1) choosing the maximum radar, but 2) replace - if possible - nearby pixels by data from another radar. To avoid checking all radars the second part can be rephrased: replace nearby pixels with the maximum of the data from all other radars (excluding the local radar). A schematic overview of the compositing algorithm is presented in Figure 6.2.

Therefore, during processing of radar pictures two intermediate files are created with the help of all radar input files and $\langle \text{locrad} \rangle$: $\langle \text{max} \rangle$ of all radars and $\langle \text{max-1} \rangle$, i.e. the maximum without the local radar.

The assignment of individual pixels is controlled by a map with values of “mix”, a weight factor with values between 0 and 255. The value of “mix” depends on the pixel location and is read from a prefabricated map.

The merged value is a weighted average of $\langle \text{max} \rangle$ and $\langle \text{max-1} \rangle$:

$$\text{mix} \cdot \langle \text{max} \rangle + \frac{255 - \text{mix}}{255} \langle \text{max-1} \rangle \quad (6.3)$$

The map with $\langle \text{mix} \rangle$ values, i.e. the file $\langle \text{mixfac} \rangle$ is different for different configurations, e.g. with missing radars. So either a series of such files must be available or the file has to be computed at runtime or if the configuration has changed.

To compute $\langle \text{mixfac} \rangle$, the pixel positions of the radars have to be known. With these data an intermediate file $\langle \text{locrad} \rangle$ is built, a map indicating which radar (number) is the nearest radar for each pixel. We call this radar the “local” radar. Note that $\langle \text{locrad} \rangle$ is also necessary to evaluate $\langle \text{max-1} \rangle$

A number of parameters is needed:

R_x the maximum distance between radars that can mutually replace data (default 200 km; Note that 140 km might be better, because Zaventem-De Bilt = 143 km),

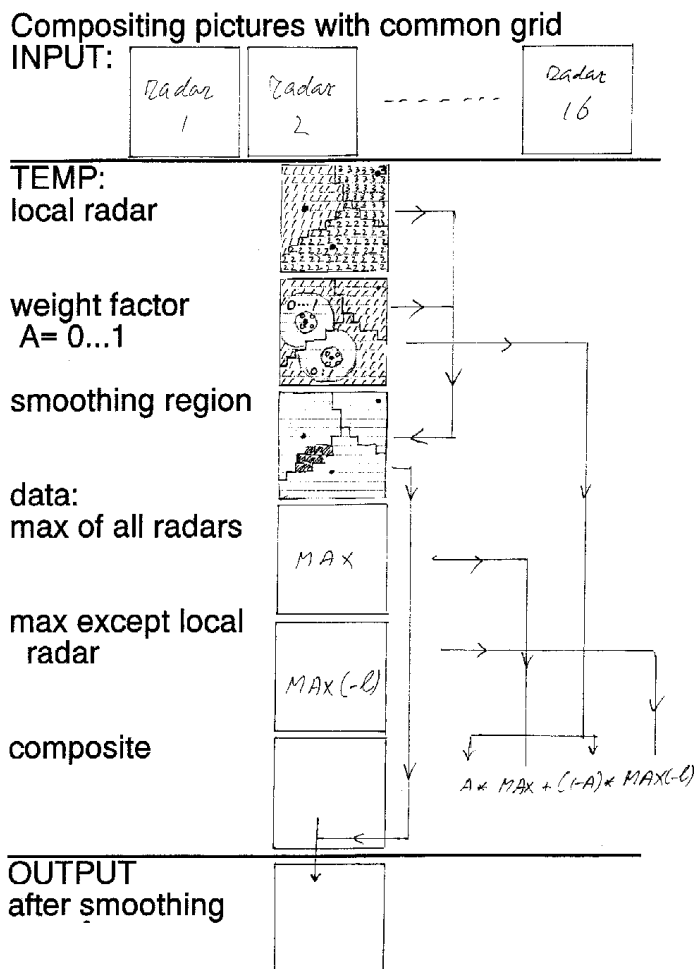


Figure 6.2: A schematic overview of the compositing algorithm.

R_n the distance up to where all pixels of the local radar may be replaced (default 15 km)

N_t number of steps between $\langle \text{mix} \rangle = 0$ and 255 (default 19).

p scale factor km per pixel (default 2.3 km)

As a first step all pixels in $\langle \text{mixfac} \rangle$ become 255. Then for each radar within R_x from another radar all pixels within R_n km become 0. For those radars all pixels with the proper radar number in $\langle \text{locrad} \rangle$ get intermediate values 0 to 255 according to the increasing range from R_n (km) to $R_n + (N_t + 1) \cdot p$.

Because of unavoidable observation or calibration problems the data in the file $\langle \text{max-1} \rangle$ are not necessarily continuous at the boundaries between

the local radars. This problem arises along the line with equal distance to radars at closer distance than $2 \cdot (R_n + (N_t + 1) \cdot p)$. In that situation pixels along the dividing line have a value of “mix” smaller than 255. As the location of this possible discontinuity is known, a smoothing action, e.g. a nine-point-filter, can be applied to a small part along the dividing line, identified in a “loccor.map”, of file <max-1>. The file “loccor.map” contains those pixels that are within <cor_width> pixels (1, default 0) on each side of those parts of the boundaries where the value of <mixfac> is smaller than <cor_mix> (200, default 255).

The nine-point filter counts only the pixels with echo larger than <cor_rad> because including the pixels with value zero would erase echo edges. For the old radar <cor_rad> had default 21, for the new one it should be 76 (no longer necessary because <tophat>=61).

6.6 Clutter removal

In the CRIS the Netherlands radar pictures have their clutter removed before their combination. Compared to the application of a combined (OR'ed) clutter map, the result will display more clutter that passed the filter and remove less rain that was falsely filtered. The best procedure depends on the balance between detection efficiency and false alarms and on user wishes. The new 1999 clutter postprocessing has a much lower rain removal rate. So the sequence of operations might be reconsidered.

If clutter removal is done after merging, we avoid the problem that removed clutter can be restored by foreign radars. Of course any clutter originating solely from the foreign radars will not be removed.

6.7 Nodata information

The 200x200 picture was nearly completely covered by the radars at De Bilt and Schiphol. The 256x256 picture has large areas without radar coverage, especially if one of the radars is missing. It is therefore necessary to automatically display the actual areas outside radar range.

The European (COST-73) convention to mark no data pixels is to use the value 15 or 255 for 4 or 8 bit pictures respectively. If the no data function of the CRIS is active, pixel values 0 in the Gematronik PPI files are changed to 255. The pixels with data have at least the value 61.

During compositing the no data values will be ignored during the computation of <max> and <max-1>. The output picture will contain no data

values for pixels set to no data for all contributing radars. The no data processing of the echo top pictures is treated in the Chapter 8, because very different algorithms are used.

6.8 Filtering

There are two filters available in CRIS:

- a smoothing function, a value is replaced by the average of the surrounding ones in a rectangle with horizontal and vertical dimensions read from configuration parameters.
- a filter applied to remove spurious isolated echoes from output PPI products: all non-border pixels with less than `<number=parameter>` pixels of the 8 surrounding ones larger or equal than a value `<threshold>` are removed (set to 0 or `<tophat>`).

6.9 References

Wessels, H.R.A. 1992, Weather radar coverage and networking procedures, Final COST-73 Seminar, Ljubljana 1991 June 3-5, EUR 13649, p. 133-138.
D.H.Newsome (Ed.), 1992, Weather radar networking, COST-73 Final Report, EUR 13648, p.104-106.

6.10 Annex

Table 6.1 presents the weight factors (in %) for the Netherlands radars as a function of height. The total of the numbers in a vertical column is 100.

For short ranges the lowest beam of the other radar is used, which has broadened considerably at a range of about 10 km. At increasing range the 2.1 deg beam is partly used between 20 and 30 km. The 3.0 deg beam is mainly important if the other radar is missing! The 1.1 deg beam dominates between 30 and 50 km and beyond that the lowest beam is used. Note that the measuring “profile” varies considerably with range, although the average stays around 800 m.

Table 6.1: Weight factors (echopower Z) as a function of range (km) and height (km).

Range					0.5				1.0				1.5							
2	1	1	1	1	2	2	3	4	6	8	10	14	11	9	6	5	4	3	2	2
4	1	1	1	1	2	2	3	4	6	8	10	14	11	9	6	5	4	3	2	2
6	1	1	1	1	2	2	3	4	6	8	10	14	11	9	6	5	4	3	2	2
8	1	1	1	1	2	2	3	4	6	8	10	14	11	9	6	5	4	3	2	2
10	1	1	1	1	2	2	3	4	6	8	10	14	11	9	6	5	4	3	2	2
12	1	1	1	1	2	2	3	4	6	8	10	14	11	9	6	5	4	3	2	2
14	1	1	1	1	2	2	3	4	6	8	10	14	11	9	6	5	4	3	2	2
16	1	1	1	1	2	3	3	4	6	8	10	14	11	9	6	5	4	3	2	2
18	1	1	1	1	2	3	4	5	6	8	11	14	11	8	6	5	4	3	2	2
20	1	1	1	1	2	2	4	6	7	8	10	14	11	8	6	5	3	3	2	1
22	1	1	1	1	2	2	3	5	10	8	10	13	10	8	6	4	3	2	2	1
24	1	1	1	1	2	4	4	5	8	11	10	13	10	8	6	4	3	2	2	1
26	1	1	1	1	2	4	5	5	6	10	12	13	10	7	5	4	3	2	2	1
28	0	1	1	1	2	5	8	5	6	8	13	13	10	7	5	4	3	2	2	1
30	0	1	1	1	2	4	10	8	6	7	9	15	10	7	5	3	3	2	1	1
32	0	1	1	1	2	4	9	14	8	7	8	11	11	7	4	3	2	2	1	1
34	0	0	1	1	2	4	8	18	13	8	7	8	8	6	4	3	2	1	1	1
36	0	0	1	1	2	4	8	16	21	11	8	7	5	4	3	2	1	1	1	1
38	0	0	1	2	2	3	7	13	28	17	9	6	4	2	2	1	1	1	0	0
40	1	1	2	5	3	3	5	10	21	25	12	6	3	1	1	0	0	0	0	0
42	1	1	3	6	5	4	4	7	13	26	15	8	4	2	1	0	0	0	0	0
44	1	2	4	7	7	4	4	5	9	17	19	10	5	3	1	1	0	0	0	0
46	1	2	4	7	9	5	4	4	6	11	20	12	6	3	2	1	1	0	0	0
48	1	2	4	7	11	7	5	4	5	8	14	15	8	4	2	1	1	0	0	0
50	1	2	4	7	12	8	5	4	4	6	9	16	10	5	3	2	1	1	0	0
52	1	2	4	7	12	10	6	4	4	5	7	11	12	7	4	2	1	1	0	0
54	1	2	4	7	11	12	7	5	4	4	5	7	12	8	5	3	2	1	1	0
56	1	2	4	6	10	14	9	6	4	3	4	5	8	9	5	3	2	1	1	0
58	1	2	4	6	10	16	10	6	4	3	3	4	6	9	6	4	2	1	1	1
60	1	2	3	6	9	15	12	8	5	4	3	3	4	6	7	4	3	2	1	1
62	1	2	3	5	8	13	14	9	6	4	3	3	3	4	7	5	3	2	1	1
64	1	2	3	5	8	12	16	10	7	5	3	3	3	3	5	5	3	2	1	1
66	1	2	3	5	7	11	17	12	8	5	4	3	2	3	3	5	4	2	2	1
68	1	2	3	4	7	10	16	13	9	6	4	3	2	2	3	3	4	3	2	1
70	1	2	3	4	6	10	14	15	10	7	5	3	2	2	2	2	3	3	2	1
72	1	2	3	4	6	9	13	17	11	8	5	4	3	2	2	2	2	3	2	1
74	1	2	2	4	5	8	12	17	13	9	6	4	3	2	2	2	2	2	2	1
76	1	2	2	3	5	7	11	16	15	10	7	5	3	2	2	1	1	1	1	1
78	1	2	2	3	5	7	10	14	16	11	8	5	4	3	2	1	1	1	1	1
80	1	1	2	3	4	6	9	13	18	13	9	6	4	3	2	1	1	1	1	0
82	1	1	2	3	4	6	8	11	16	14	10	7	5	3	2	2	1	1	1	0
84	1	1	2	3	4	5	7	10	14	15	11	8	5	4	3	2	1	1	1	1
86	1	1	2	2	3	5	6	9	13	16	12	8	6	4	3	2	2	1	1	1
88	1	1	2	2	3	4	6	8	11	16	13	9	7	5	3	3	2	1	1	1
90	1	1	1	2	3	4	5	7	10	14	14	10	7	5	4	3	2	2	1	1
92	1	1	1	2	3	4	5	7	9	12	15	11	8	6	4	3	2	2	1	1
94	1	1	1	2	2	3	4	6	8	11	15	12	9	7	5	4	3	2	1	1
96	1	1	1	2	2	3	4	5	7	10	13	13	10	7	5	4	3	2	2	1
98	1	1	1	2	2	3	4	5	7	9	12	14	11	8	6	4	3	2	2	1
100	1	1	1	1	2	2	3	4	6	8	10	14	11	9	6	5	4	3	2	2

Chapter 7

Navigation of radar pictures and topographic overlays

7.1 Introduction

Single radar data are collected in a polar coordinate system centered at the radar. The radar output product is a rectangular 256x256 picture in polar stereographic projection. In the next stage the data from two or more radars are combined in a product suitable for distribution. As the two Netherlands radars use the same projection, this stage is straightforward. The combination with foreign radar data is more difficult.

The composite product has to be displayed together with an accurate topographic map. Radar data have to be compared with other observations or warnings have to be issued for certain locations. Because topographic maps are stored as lat/lon data measured on an ellipsoid earth, the radar pixel output too has to be computed for an ellipsoid earth.

In the following sections the creation of the radar pixel output is described and documentation is given on the navigation procedures of various display facilities.

7.2 History

From 1987 until 1989 the polar radar data were digitized in a rectangular picture with 2x2 km pixels. The picture size was 216 (N-S) x 201 (E-W). The radars were at position (101,101). The conversion from polar to rectangular was by plain trigonometry without correction for great circle navigation.

Two radars were combined in a 227x215 composite by overlaying the data (De Bilt 11 S/14 E from Schiphol. The north directions of both radars

were slightly offset to improve the match of the pixels: true north was read as -0.5 for De Bilt and -0.1 for Schiphol (this includes the correction for digitization lag). Pixel values (0-6) were weighted (integer result) between those of the two radars. See Section 6.4 on Compositing. On the PC displays a topographic pixel map (in colour 7) was shown. The projection of the overlay was according to “Postel”, a projection plane touching the earth at a point somewhere between the radars. The production started at H+5, H+20, ... to allow (half-)hourly manual sketches to continue (starting about H+20 and H+50).

The 1989 radar site computers applied a look-up table with 220x220 pixels for the navigation. From then on both radars produced data in the same grid. A subgrid of 200x200 starting at pixel 15/15 was finally used for display.

For each pixel the azimuth and range could be read that were to be used. Of course both radars had their own look-up table. During creation of the tables, the radar azimuth and distance were converted to lat/lon by great-circle formulae. Subsequently the lat/lon was converted to a polar stereographic grid. As both radars had exactly the same grid specification, compositing was relatively easy. (See Chapter 6 on compositing)

The present Gematronik radars follow the same method as their predecessors. The picture was enlarged to 256x256 in 1999/2000 (to avoid hiding data from Den Helder).

Some initial problems had to be overcome.

- There was a mismatch of the rectangular clutter maps with respect to the reflectivity maps. This was solved early 1998.
- The configuration offsets of a 200x200 picture (i_0, j_0 as explained in Section 7.4) had to be $-40, -261$ to fit echoes of topographical features with the existing display maps. The latter, however, were computed for offsets $-40, -259$.

Three factors could contribute:

- a. The radar position is difficult to locate in the radar picture. The location accuracy is about one pixel. A closer look showed that the radar position estimated from known objects was at (from upper left of 0-200 image) 93.6, 55.6 for Den Helder and 107.8, 93.8 for De Bilt. The computed radar positions for $-40, -259$ should be 93.5, 52.9 for Den Helder and 107.8, 91.2 for De Bilt, i.e. 2.7 resp. 2.8 pixels north of the echo centre (i.e. echoes south of map). Therefore in the first years $-40, -261$ was used in the Gematronik configuration to correct the difference. Of historic interest is the computed Schiphol position in the 200*200 grid: 95.0, 84.9 for offsets $-40, -259$.

- b. The echoes from De Bilt could be at the wrong position due to a range error (Section 7.3). This was corrected in 1999, Mar.
- c. In 1998, Apr. it was discovered that the correction term $f(B)$ (Equation 7.4) was partly reversed. Then the radar Lat would be plotted in the map 2.9 (2x1.4) pixels too far south. This explained most of the difference with $-40, -259$ and was corrected 1999, May.
- d. The conversion method may contain a (still hidden) rounding problem, justifying the use of $-40, -260$ since 1999, Mar. (0,212 for the 256x256 picture).

The picture size change from 200x200 to 256x256 illustrated the importance of flexibility and the proper transfer and use of navigation metadata. In the present chain: radar - CRIS - MWS the configuration of the radar fixes the navigation on display. The ad-hoc configuration files on the CRIS are no longer required. The situation with the 200x200 image for PC-displays and external users remains a maintenance problem. A more flexible solution for the data transfer outside the chain radar-CRIS-MWS is required.

7.3 Checking position, range, azimuth and elevation

The range measurement of the radar should be correct. To investigate this the echoes (at 3 deg elevation) of some known buildings have been identified in the polar and rectangular pictures of both De Bilt and Den Helder and used as reference marks (1998). The polar pictures (1 km scale) initially showed all objects at a range some 700 m too large (De Bilt, less in Den Helder). For all azimuths the first pixel is filled with a high value (156 ± 1 decimal for Den Helder, 142 ± 1 for De Bilt). After reprojection this value appears at the pixel closest to the radar position in the rectangular and PSTN pictures. In the rectangular map the pixel position of the radar was estimated by backward ranging from the known object positions. Although the radar range measurement has been corrected in 1998, future checks may be necessary.

The angular measurement (azimuth and elevation) with radar can best be done with the help of solar microwave radiation. See Chapter 3 on Calibration.

Since 2000 ellipsoid navigation is maintained along the chain: radar, CRIS, MWS. An easy check of the final result can be obtained by feeding a transmission pulse triggered test signal into the radar receiver, causing

a “ring” of 2 or 3 pixels inner diameter. The map of the MWS contains motorways and railways and can be used to check whether the radar map position is correctly centered in the “ring”. Note that such a ring is only visible if the other radar is not available.

7.4 Conversion from lat/lon to polar stereographic projection

In the following sections the navigation formulae are documented. Radar data are available in a polar system (azimuth and range). Their conversion to lat/lon is treated in Section 7.5. The transformed radar data as well as data from the topographical data base are available in lon/lat= L, B and are converted to pixel coordinates x, y in the polar stereographic projection plane as follows.

The projection is polar stereographic, parallel to the L_0 (E) meridian. The pixel size is p km at latitude B_0 (N). The pixels are counted (East positive) from the point L_0 E, B_0 N. In that coordinate system the upper left corner of the Netherlands data has an offset of i_0, j_0 (integer pixels) with respect to the origin of a larger grid aligned at L_0 E, B_0 N.

The plotting distance $r(B)$ and the scale $s(B)$ (km projection/km arc length) for projection of a point at latitude B and longitude L on an ellipsoid earth with equatorial radius R and eccentricity e are (projection plane touching at N-pole)

$$r(B) = 2R \cdot f(B) \cdot \tan(45 - B/2) \quad (7.1)$$

$$s(B) = \frac{r(B)}{R \cos B} \sqrt{1 - (e \sin B)^2} \quad (7.2)$$

$$= \frac{2f(B)}{1 + \sin B} \sqrt{1 - (e \sin B)^2} \quad (7.3)$$

where

$$f(B) = \frac{1}{\sqrt{1 - e^2}} \left[\frac{(1 - e) \cdot (1 + e \sin B)}{(1 + e) \cdot (1 - e \sin B)} \right]^{e/2} \quad (7.4)$$

is a small correction for non-sphericity of the earth. With $e = 0$ we have $f = 1$. Both $r(B)$ and $s(B)$ then reduce to the sphere values:

$$r(B) = 2R \tan(45 - B/2) \quad (7.5)$$

$$s(B) = \frac{2}{1 + \sin B} \quad (7.6)$$

Conversion from lat,lon to pixel coordinates is as follows

$$\text{rpix} = \frac{r(B)}{p \cdot s(B_0)} \quad (7.7)$$

$$\text{rpix}_0 = \frac{r(B_0)}{p \cdot s(B_0)} \quad (7.8)$$

$$x = \text{rpix} \cdot \sin(L - L_0) - i_0 \quad (7.9)$$

$$y = \text{rpix} \cdot \cos(L - L_0) - \text{rpix}_0 - j_0 \quad (7.10)$$

For pixel centers 0.5 has to be subtracted from x and y . The CRIS uses navigation on a spherical earth with $B_0=60$ deg Two scale values are used, in column and line direction respectively:

$$\text{cres} = \text{lres} = \frac{10^6 p}{R} \quad (7.11)$$

Although cres and lres are different parameters, they are not allowed to have different values in CRIS. The offsets of the upper left picture corner are:

$$\text{coff} = i_0 \quad (7.12)$$

$$\text{loff} = j_0 + \text{rpix}_0 = j_0 + \frac{10^6 \cos B_0}{\text{lres}} \quad (7.13)$$

where rpix_0 is the pixel count between the North pole and reference latitude B_0 , for which the CRIS uses $B_0=60$ deg, so $\cos B_0 = 0.5$. In this system the Equations 7.7 and 7.8 are replaced by

$$\text{rpix} = \frac{10^6}{\text{cres}} \cdot (1 + \sin B_0) \cdot \tan(45 - B/2) \quad (7.14)$$

$$\text{rpix}_0 = \frac{10^6 \cos B_0}{\text{cres}} \quad (7.15)$$

and x and y follow with equations 7.9 and 7.10.

An alternative formulation for a spherical earth model, using the trigonometric relation $\tan(45 - B/2) = \cos B/(1 + \sin B)$, is

$$\text{rpix} = \frac{R \cos B}{p} \cdot \frac{1 + \sin B_0}{1 + \sin B} \quad (7.16)$$

For e.g. the creation of look-up tables the inverse conversion (lon,lat from x, y) may be needed. The distance of 0.5 pixel has to be added to x and y if pixel centres are to be converted. In the ellipsoid case we first compute Equation 7.8. Then the longitude is

$$L = L_0 + \arctan(x'/y') \quad (7.17)$$

with $x' = x + i_0$ and $y' = y + j_0 + \text{rpix}_0$.

The latitude follows from an intermediate range (km)

$$\text{rplot} = \frac{\sqrt{x'^2 + y'^2}}{p \cdot s(B_0)} \quad (7.18)$$

B is found by iteration, starting at the radar latitude B_r

$$B = 90 - 2 \arctan \left(\frac{\text{rplot}}{2R \cdot f(B_r)} \right) \quad (7.19)$$

$$B = 90 - 2 \arctan \left(\frac{\text{rplot}}{2R \cdot f(B)} \right) \quad (7.20)$$

For more accuracy the latter equation may be repeated one more time. An alternative is to solve B from $r(B) = \text{rplot}$ with (Newton-Raphson). In the CRIS-system Equation 7.17 is used and B follows directly

$$B = 90 - 2 \arctan \left(\frac{10^{-6} \text{cres} \sqrt{x'^2 + y'^2}}{1 + \sin B_0} \right) \quad (7.21)$$

For checking purposes, the image corners of the 256x256 picture are:

0.0/55.296 9.743/54.818

0.0/49.769 8.337/49.373

If, for some reason, the offsets are set back to 0, -211 we have

0.0/55.318 9.750/54.840

0.0/49.790 8.342/49.394

7.5 Conversion from polar radar projection to lat/lon

The data presented at a pixel centre (i, j) , measured from a radar (L_r, B_r) with pixel position (i_r, j_r) , are obtained from measured values of azimuth A and range D (km). Because the grid is aligned at 60N, 0E, the radars are usually not at pixel centers (or boundaries). So, i_r and j_r are float values. The pixels coordinates may be integers, but the conversions must be done to pixel centres (0.5 pixel correction, if necessary).

A repeated on-line computation of (i, j) from (A, D) involving great “circle” navigation on an ellipsoid is rather tedious. Preferably A and D are read from a look-up table. This look-up table is built by performing for all

pixels the reverse computation (i, j) to (A, D) as follows. First we approximate by trigonometry (justified by the orthomorphic properties of the polar stereographic projection):

$$D = \frac{p \cdot s(B_0)}{s(B_r)} \cdot \sqrt{(i - i_r)^2 + (j - j_r)^2} \quad (7.22)$$

$$A = \arctan\left(-\frac{i - i_r}{j - j_r}\right) + (L_r - L_0) \quad (7.23)$$

Then a deformation correction is applied (see reference, p.6):

$$D = \frac{D}{1 + 0.04 \tan(45 - B_r/2) \cdot \cos A} \quad (7.24)$$

$$A = A + 0.00449D \cdot \tan(45 - B_r/2) \cdot \sin A \quad (7.25)$$

These values are stored in the look-up table for each of 256x256 pixels. Without the deformation correction step errors up to 3 km occur already at 250 km range. Such errors are now reduced to less than 0.1 km.

7.6 Navigation information for radar users

The specification of the polar stereographical projection on an ellipsoid earth is controlled by a configuration file of the Gematronik radar computer (Rainbow software). The output data are accompanied by navigation information in the file header.

The configuration file parameters are:

```
x-pixel and y-pixel resolution = 2.5 km (=p)
projection reflon, reflat      = 0.0 E , 60.0 N (=L0,B0)
equatorial and polar earth radii = 6378.388 resp. 6356.912 km
                                (=R resp Rp, so e=0.0819918)
x-size, y-size                 = 256 by 256 (used to be
                                200x200 with i0=-40,j0=260)
x-offset and y-offset         = 0, 212 (= i0,j0)
image ref. (to match offset)  = 0.0, 60.0
```

In the CRIS the 256x256 area is maintained. The data may change for various reasons: compositing with other radars, marking no-data areas (not covered by radar), classification (combine a range of dBZ values in a new class). Other information (lightning positions) may be added. Temporarily a 200x200 section is made for display devices not yet upgraded to 256x256 in 2001.

Unfortunately VCS does not support polar stereographic projection on a spheroid earth. The navigation information in VCS-PIF headers consists of: line and column offset resp. resolution: loff, coff, lres=cres. These numbers are restricted to integer format forbidding scale changes smaller than 2.5% and offset steps smaller than 2.4 km. For a pixel size of $p=2.5$ km the scale follows from $lres=cres=10^6 p/R$, where R is an estimated spherical earth radius. With $R=6378.69$ and $p=2.5$ km we have $cres=lres=391.93$ rounded to 392. In the CRIS computer various Rainbow labels from the radar file header can be transferred automatically to the VCS-pif header:

G2, G3 → coff, loff -0, resp. -1491 for 256x256 picture
 G4, G5 → cres, lres = (int) $(G4 \cdot 10^6 / R_p / R^2) = 391$
 G6, G7 → goff_lon = (int) $(1000 G6) = 0$, goff_lat = 60000

These parameters would produce inaccurate results on the MWS, so hard entries for the navigation is read from a configuration file in CRIS. This was used until 1997 with values found by little trial and much error: coff=-38, loff=-1527, cres=lres=393.

Since mid 2000 the VCS software is still not upgraded to ellipsoid navigation, but is capable of transferring ellipsoid navigation parameters to the PIF header.

7.7 User display of radar images

A file with radar data is dumped in a rectangle on the screen. This transformation is linear and may be specified by parameters: horizontal and vertical offsets and scale factors.

A topographical overlay is drawn on the screen, i.e. vectors from a background map database (lat, lon) have to be positioned on the radar image. The parameters in the data header specify the projection and the conversion from lon/lat to x, y pixels in the projection plane. Finally x, y is converted to screen coordinates with the same transformation as used for the radar data. On PC displays it has been customary to off-line build a topographic pixel overlay that can be merged with the radar pixel data.

NOTE: The navigation information that accompanies the radar data is not used to navigate those radar data but rather the topographic overlay data.

- a. KNMI displays (ERAS etc.) use a fixed map, computed to match the radar data. This overlay is available as a local file in pixel coordinates. The result is accurate, but the use of local files is not flexible.

- b. Some external users have their own navigation system. E.g. the Royal Dutch Air Force (KLu) approximates the echo positions by using the Lat/Lon values of the 4 picture corners. The accuracy at the picture center can then be disappointing due to the special scale properties of the polar stereographic projection.
- c. Up to June 1997 the television presentation (NOB) also used the PIF header data. Like on the MWS this caused a position error of the radar data of about 11 km to the north-northwest. Following justified complaints NOB replaced the header data with better values: $-1536, -41, 392, 391$, reducing the shift to -0.9 ± 0.1 E, -1.5 ± 0.1 S (pixels). The remaining mean error could vanish for float offsets (e.g. $-1534.5, -40.0$)

NOTE: The background maps on the TV-presentation are displayed in Azimuthal Equidistant Projection. So the radar data have to be remapped prior to display.

7.8 Ellipsoid radar navigation on the MWS

The display of PPI and ETH pictures on the MWS involves two steps. Firstly the picture (PIF-) file is dumped on the screen, filling a window (zooming is possible).

Secondly a vector map (composed from topographical data in lat/lon computed for an ellipsoid earth) is drawn over the radar picture. The correct navigation of that map depends on parameters read from the header record of the PIF file.

The MWS uses its own specific navigation facility for combining satellite, radar and model data together with a topographic overlay. The radar reprojection originally was based on a spherical earth with radius 6378.69 km. In the VCS-PIF system this would match with $\text{cres}=391.93$, but floating values are not allowed. The resolution and offset can be set to approximate the correct map position within about 5 km. However, for many years the map was shifted about 11 km south-southeasterly compared to the radar data ($\text{loff}=-1527, \text{coff}=-38, \text{cres}=393$ were used, found by trial and error). If float values had been allowed for the PIF parameters, the error could have been reduced to about 3 km.

Therefore in 1998 the MWS Vs. 3.3 has been prepared to optionally use ellipsoid navigation for radar data. If a flag is set at a certain position (byte 215=FF) in the file header, different navigation data are read from a spare part in the following part of that header. These navigation data

are CRIS-conversions of the Gematronik labels G2..G9, K1 and K2 (see Chapter 5), all multiplied with 1000 to avoid the use of float values. It is important to note that the MWS uses a reference latitude $B_0=60$ deg regardless of the reference latitude in the file header.

The standard PIF header contains the following parameters: *coff*, *loff*, *reflon*, *reflat*, *x-size*, *y-size* and *cres*. The scale *cres* defines the relation between pixelsize p (true at latitude B_0) and earth radius R (see Section 7.4).

In the extended header the first 6 values are used too, but with a 1000 times higher resolution (e.g. *loff*=-1490906 for offset 212 of a 256x256 picture). Instead of *lres* and *cres* we have additional parameters:

- *x-pixel* and *y-pixel* ($p=2500$ m)
- equatorial and polar earth radius R and R_p (6378388 and 6356912).

These new parameters are used to compute a latitude-dependent correction factor for a spheroid compared to a sphere

$$g(B) = \frac{1}{\sqrt{1 - (e \sin B_0)^2}} \cdot \left[\frac{(1 + e \sin B) \cdot (1 - e \sin B_0)}{(1 - e \sin B) \cdot (1 + e \sin B_0)} \right]^{e/2} \quad (7.26)$$

where $e = \sqrt{1 - (R_p/R)^2}$. A typical value of $e=0.0819918$, so $g(B)$ is close to 1. At the start of the navigation process a table for $g(B)$ is prepared in steps of 0.1 deg This saves computing time while keeping location errors below a few meters.

In the present (2000) version of the MWS the conversion of lat/lon (B/L) of the topographical data to screen coordinates is done via intermediate reference systems. As a first step from the PIF header the pixel coordinates of so-called anchor points NP and SP are found, respectively at the north pole and Lat=0 (28 deg in some versions) and Lon= L_0 .

$$\text{NPX} = \text{SPX} = \text{coff} \quad (7.27)$$

$$\text{NPY} = \text{ysize} - \text{loff} \quad (7.28)$$

$$\text{SPY} = \text{NPY} - 10^6/\text{cres}(1 + \sin B_0) \quad (7.29)$$

Secondly the lat/lon values of these scale points are converted to WVS coordinates (units of 0.1 arcsec along the earth):

$$-180 \text{ deg to } 180 \text{ deg} = 0 \text{ to } 1296000$$

$$-90 \text{ deg to } 90 \text{ deg} = 0 \text{ to } 648000$$

The routine that converts lat/lon to polar stereographic uses WVS as input. These data are shifted to reference L_0 and converted to polar stereographic. The latter output is in a special scale PRJ. The scale unit in PRJ is 0.001 arc-sec along the earth surface (at least at B_0) As a result we have the anchor

points in PRJ coordinates as we had them in the first step for radar pixel coordinates.

By combining these results we can define the scale and offset of the conversion from PRJ to pixel coordinates

$$\text{XCONV} = \text{YCONV} = \frac{\text{SPY} - \text{NPY}}{Y_s - Y_n} \quad (7.30)$$

$$\text{XMIN} = \frac{0 - \text{NPX}}{\text{XCONV}} \quad (7.31)$$

$$\text{YMIN} = \frac{0 - \text{NPY}}{\text{YCONV}} \quad (7.32)$$

Finally all points in the data base are converted from lat/lon via WVS to polar stereographic to xx , yy in PRJ and finally to pixel coordinates that match the radar picture.

$$x = (xx - \text{XMIN}) \cdot \text{XCONV} \quad (7.33)$$

$$y = (yy - \text{YMIN}) \cdot \text{YCONV} \quad (7.34)$$

In the function “ForceKnmiRadarProjection(p_prod)” the “res_factor” no longer is $10^6 / \text{nav_lres}$, but reads $R/p \cdot g(0)$, using pixel size p and function “g” for $B=0$. Then the correction for ellipsoid navigation is complete.

An additional problem in the MWS pictures occurs at zooming the radar pixels. The combination of integer rounding of pixel positions on a topographic overlay computed from float values causes “walking around” of radar pixels with respect to the overlay during zooming. This problem has been reduced to an acceptable level in 1997, but might not be completely solved.

7.9 Future MWS navigation (Smartwindows)

In 2000, Aug, formulae were supplied to 3SI for a new “SmartWindows” screen presentation, with parameters UpperLat (top of the screen), LowerLat (bottom of the screen), LonMeridian and OffsetRatio.

We assume that UpperLat and LowerLat are found by extending the picture to the LonMeridian. If e.g. latitudes at the left edge of the picture were meant, computations would be much more complicated.

From the PIF header are read: loff, coff, cres, lres, reflon, reflat, x -size, y -size, and the center: $(0,60) = \text{goff_lon}, \text{goff_lat}$. For correct overlays, i.e. compatibility with lat/lon’s from a topographical data base, use instead of cres and lres the extended PIF header (divide values by 1000): pixel size p , equatorial earth radius R and polar radius R_p . Compute the eccentricity (about 0.081) from $e = \sqrt{1 - (R_p/R)^2}$.

Then (make arctan return degrees and use $B_0=60$):

- LonMeridian = reflon
- $DUM = 10^{-6}$ cres ; for spheroid first guess: $DUM=p/R/g(B_r)$
- UpperLat (deg) = $90 - 2 \arctan(DUM/(1 + \sin B_0) \cdot -loff)$. For spheroid: new approximation $DUM=p/R/g(UpperLat)$ and repeat Upperlat = $90 - 2 \arctan(DUM/(1 + \sin B_0) \cdot -loff)$
- LowerLat (deg) = $90 - 2 \arctan(DUM/(1 + \sin B_0) \cdot (-loff+ysize))$ For spheroid: new approximation $DUM=p/R/g(Lowerlat)$ and repeat LowerLat = $90 - 2 \arctan(DUM/(1 + \sin B_0) \cdot (-loff+ysize))$
- OffsetRatio = $coff/(screensize \text{ in pixels})$ Note that for negative coff the reflon is left off the screen

7.10 Reference

Wessels, H.R.A., 1990, Coordinate conversions for presenting and compositing weather radar data. KNMI, TR-129.

7.11 Annex A: Navigation of foreign radar data into the KNMI 256x256 picture

Pictures from two German and one Belgian radar are available since 1994/1995. The data of two English radars were added in 2001. In the CRIS these data are resampled - every 15 min.- into our picture. Up to 2001, June this was a 4 bit 200*200 picture with BUFR name PANL21. The BUFR-names changed on March 12, 2002; This product became PACM21. The present Netherlands 8 bit 256x256 composite is PACM22 (old PANL21)

The off-line creation of a look-up table $T(256 \times 256)$ to resample pixels from an originating radar $D(i_1, j_1)$ into the user picture frame of another radar $N(i_2, j_2)$ is illustrated by the following pseudocode:

```
for i2=0 to 255
for j2=0 to 255
use (7.17 - 7.20) to compute L, B from i2,j2 (parameters dest.)
use (7.7 - 7.10) to find i1,j1 from L, B (parameters origin)
if values i1,j1 are in the radar data range, then
    store them in look-up table T on position i2,j2
```

```

    else store a 'no pixel' code
next j2
next i2

```

The real-time use of this table to fill a frame for radar N with data from radar D is as follows:

```

for i2=0 to 255
for j2=0 to 255
read i1,j1 from T(i2,j2) or a no-pixel code
if no-pixel store no-data code in N1(i2,j2)
else read pixel-value D(i1,j1), may be additional no data and
    store value or no-data code in N1(i2,j2)
next j2
next i2

```

For other foreign radars the pictures N_2 , N_3 etc. are created. Finally these are merged with the original Netherlands composite (see Chapter 6 on PseudoCAPPI and Composite). The navigation parameters used to find i_1, j_1 from lon/lat are derived in the following.

The files of Emden and Essen (PADL41 & PADL51, april 1995, now renamed into PAAM41 and PAAM51) measure 224×224 . As the first 24 lines and the last 24 columns are outside the PPI picture, the data we need are at $i_1=0-199$ and $j_1=24-223$.

The radar data are from “ground projection of nearest reflectivity to the ground”. The coordinates of the radars are respectively 7.0250 E, 53.3394 N and 6.9678 E, 51.4069 N. The projection is polar stereographic with $L_0=10$ E, $B_0=60$ N, $p=2$ km, and $R=6370$ km (sphere). The radar position is at $i_1=99.5$, $j_1=123.5$, but the DWD mentioned that in the projection grid the radars were at $(x,y$ in km) 204.387 by 3932.773 and 220.148 by 4155.954.

Therefore the other projection parameters are:

$$\text{cres} = 10^6 p/R = 314 \quad (7.35)$$

$$\text{coff} = -i_0 = 201.7 \text{ resp. } 209.6 \quad (7.36)$$

$$\text{loff} = 1842.9 \text{ resp. } -1954.5 \quad (7.37)$$

If the j -index for the look-up table is sought, -24 has to be added to loff, so we use -1978 resp. 1867 . For j_0 subtract loff from $\text{rpix}_0=1592.5$: 386.0 resp. 274.4 . On the spherical earth specified, the picture corners for Emden are:

3.83 E/54.93 N 9.91 E/55.12 N
 4.42 E/51.49 N 9.92 E/51.66 N
 And for Essen:
 3.95 E/52.98 N 9.69 E/53.17 N
 4.50 E/49.49 N 9.72 E/49.76 N

The filesize for Zaventem (B) (PABX40, nov. 1994, new name PAAH40) is 256×256 , centered around the radar. The data are obtained from a single 0.7 deg scan. Data beyond 233 km are not available. Note that the limiting circle centre in the projection is 0.7 pixel south of the projected radar position.

The radar position is given as 4.467 E, 50.90 N (4.4556 E, 50.9053 N might be more accurate). The projection is polar stereographic with $L_0=4.467$ E, $B_0=60$ N, $cres=332$, $coff=128$, $loff=-1868$. The pixel size is given as 2 km, which is not compatible with $cres!$ Evidently 2 km is the pixel size in the southern part of the picture and $p=2.12$ km at B_0 . Finally we have $j_0=361.0$. On the spherical earth specified, the picture corners are:
 0.55 E/53.15 N 8.36 E/53.15 N
 1.02 E/48.55 N 7.89 E/48.55 N

The UK radars Chenies and Ingham (PAUK45 and PAUK49, Jun. 2001, now renamed PAAL45 and PAAL49) have a dimension of 110×110 , using a rather large pixel size: 5 km. The data are acquired at an elevation of 0.5 deg (also 4.0 deg for Chenies), but data from elevations 1.0 to 2.5 are used as infill. The projection was before 2001 based on UK national grid coordinates, but has since been changed to polar stereographic with reference 0, 60 deg for a spherical earth with radius 6371.221 km. The conversion from Lon/Lat to Easting/Northing is still an unused subroutine (pixuk) in a Fortran program (see Appendix C). The radar coordinates are -0.530 W, 51.688 N resp. -0.557 W, 53.335 N. From the corner lat/lon given in the BUFR header we deduce for Chenies and Ingham respectively: $cres=785$ and 785 ; $coff= 62.76$ and 61.14 ; $loff=-766.56$ and -729.63 . On the spherical earth specified, the Chenies picture corners are:

4.68 W/54.14 N 3.53 E/54.19 N
 4.09 W/49.42 N 3.08 E/49.46 N
 And for Ingham:
 4.79 W/55.76 N 3.83 E/55.80 N
 4.16 W/50.99 N 3.33 E/51.03 N

Further details, e.g. about level slicing, are given in Chapter 6 on compositing. Some information also in Annex B

NOTE: these rectangular pictures were originally computed for a spherical earth and probably without correction for great-circle positioning with

the radar. No attempt has been made to correct this. The final step from lon,lat (inaccurate, at least at large distance from the original radar) to the Netherlands picture has been done with spheroid formulae.

NOTE: Testing of x, y pixel values in the 256x256 composite can be done as follows: pixel 72,128 comes from: Zaventem 65,41 Chenies 99,40 Ingham 97,77 pixel 128,128 from Zaventem 131,46 Emden 9,148 Essen 17,36

7.12 Annex B: Navigation of foreign radar composite pictures on KNMI MWS

Composites are presented as separate items on the MWS. As no merging take place, resampling tables do not apply. In the following we present the navigation parameters for both the old spherical model and the extended PIF header for spheroid navigation. Also the level slicing will be treated, because no further compositing is carried out (yet) between foreign composites.

The Netherlands pictures present 6 levels $n=1$ to 6 for $R=0.1$ to 30 mm/h. The conversions are $\text{dBZ} = 8n - 1 = 16 \log R + 23$. The German levels are based on $Z = 256R^{1.42}$. In the winter they use a lowest level of 1 dBZ, but 4 dBZ for Emden.

The assignment of foreign levels in the CRIS is (lower limits NL and foreign levels in dBZ):

Level	NL dBZ	BE dBZ	DE dBZ	FR dBZ	UK dBZ	UK new mm/h	Chenies/Ingham mm/h
1	7	7	7	7	7	2	1
2	15	18	19	16,20	15,18	8	3
3	23	28	24,28	23,26,28	30	10	
4	31	31	32,36	31,33,35	72	28	
5	39	39	37	40,44	39,42,45	116	72
6	47	47,50	46	48,52	49	156	111
(7	55	55	56,60,64	52	194	150)	

At present level 7 is combined with 6. France and the UK use 14 levels, excluding the value 0 and a no-data code (15 or 255).

NOTE: In the BE and DE picture a level had to be skipped to prevent a too large overestimate at the highest levels.

NOTE: The above levels are entered in the configuration file ORG-CENT.TXT in Gematronik values $63+2 \cdot \text{dBZ}$ rather than dBZ. (the actual formula is $64+2 \cdot \text{dBZ}$, but 63 prevents a rounding bias).

7.12.1 German composite PAAM21

The DWD (Deutsche Wetterdienst) specifications are:

- picture 230x230 pixels,
- polar stereographic, reference longitude 10 deg E,
- spherical earth model with radius “about” 6370 km,
- pixel size after projection 4 km,
- picture centre 9E,51N projected to $x=-73.46$, $y=-4208.62$
- levels 1-6, in dBZ: ≥ 7 (winter 1), resp. 19,28,37,46,55
- nearest reflectivity to ground; maximum in overlapping areas.

Evidently x and y are km in the projection plane with reference to the north pole. The offset of the upper left corner is $(-133.365, 937.155)$ pixels. The offset to 60 N is 140.905. On the spherical earth specified, the picture corners are:

1.901E/54.662N	15.887E/54.819N
3.481E/46.860N	14.733E/46.980N

PIF header entries are:		Extra header data for MWS V.3.3:
picture size 230x230		
reflat= 60000		reflat 60000
reflon= 10000		reflon 10000
loff = -937		y-offset -937155
coff = 133		x-offset 133365
lres = 628		y-pixel 4000
cres = 628		x-pixel 4000
		eq.radius 6370000
		pol.radius 6370000

The error in pixels with the integer parameters is at the corners:
 $-0.35/0.07$ $-0.37/0.07$
 $-0.35/0.05$ $-0.37/0.05$

The proposed parameters give minimum errors at the western side which is most important for users in the Netherlands.

7.12.2 French composite PAAM22

Meteo-France send the following specifications:

- picture 512x512 pixels,
- polar stereographic, reference longitude 0 deg E,
- spherical earth model with radius 6371.229 km.
- pixel size 3 km at 45 N
- picture north-west corner at 9.965 W,53.670 N
- presentation in levels 1-15, in mm/h resp. 0.1, 0.36, 0.65, 1.2, 2.1, 3.7, 6.5, 12., 21., 37., 65., 115., 205., 365., while 15 means “no data”.(values based on $Z = 200R^{1.6}$)

In the French model the offsets of the upper left corner can be calculated as: 205.845 resp. -1171.589 . The pixel size has to be scaled to 60N (used in the MWS) as follows $3000(1 + \sin 60)/(1 + \sin 45) = 3279.277$. Then the scale cres/lres is $3279277/6371.299 = 514.701$. On the spherical earth specified, the picture corners are:

9.965 W/53.670 N (.042 W .001 S) 14.645 E/53.061 N (.044 E .000 N)
6.971 W/39.856 N (.023 W .005 S) 10.306 E /39.466 N (.020 W .006 N)

The numbers between brackets are the differences with respect to a projection on the Hayford ellipsoid fitted for the center of the picture (2.018 E/46.989 N).

PIF header entries are:		Extra header data for MWS V.3.3:
picture size 512x512		
reflat= 60000		reflat 60000
reflon= 0		reflon 0
loff = -1171		y-offset -1171590
coff = 206		x-offset 205845
lres = 515		y-pixel 3279
cres = 515		x-pixel 3279
		eq.radius 6370690
		pol.radius 6370690

Note that in the right column, radii smaller than 6371229 are used, to compensate for taking the pixel size smaller than 3279.277. The error in pixels with the integer parameters is at the corners:

0.27/-0.09 -0.02/-0.09
0.27/-0.39 -0.02/-0.39

7.12.3 UK composite PAAL21

The UK Met.Office send the following specifications:

- picture 368 rows of 278 pixels,
- polar stereographic, reference longitude 0 deg E,
- pixel size 5 km, true at 60 N
- picture corners lon(E=+), lat:
-18.9289 61.7647 8.447 62.9527
-11.7376 46.2923 5.1413 46.9651
- presentation in levels 1-15, in mm/h resp. 0.1, 0.3, 0.5, 1.0, 1.5, 2.0, 3.0, 4.0, 6.0, 10.0, 16.0, 24.0, 40.0, 64.0, while 15 means ≥ 127 as well as 'no data'.

It was assumed that the same spherical earth model has been used as for the COST-composite (radius 6371.221 km). In this model the offsets of the upper left corner are calculated as -193.999 resp. 565.693 and the scale cres/lres is $5000000/6371.221 = 784.779$.

```
PIF header entries are:      | Extra header data for MWS V.3.3:
pif_n = 278 (pix.p.line)|
pif_l = 368 (nr.of lines)|
reflat= 60000              |      reflat      60000
reflon= 0                  |      reflon      0
loff  = -565              |      y-offset    -565693
coff  = 194               |      x-offset    193999
lres  = 785               |      y-pixel     5000
cres  = 785               |      x-pixel     5000
                                           |      eq.radius   6371221
                                           |      pol.radius  6371221
```

The error in pixels with the integer parameters is at the corners:
0.06/0.53 -0.02/0.53
0.06/0.43 -0.02/0.43

7.12.4 UK COST-73 composite PAAL31

An earlier version measured 512x512 pixels of 5 km with upper left corner at 27 W 57 N. This picture was received since early 1989 (hourly with 70 min.

retardation). The Netherlands data formed part of this composite since May 1990.

The UK Met.Office send the following specifications:

- picture 256x256 pixels
- polar stereographic, reference longitude 12 deg E,
- pixel size 6 km
- picture corners lon(E=+), lat:

-12.0	54.5	11.804	57.399
-5.161	42.379	11.864	44.277
- presentation in levels 1-15, in mm/h resp. 0.1, 0.3, 0.5, 1.0, 1.5, 2.0, 3.0, 4.0, 6.0, 10.0, 16.0, 24.0, 40.0, 64.0, while 15 means ≥ 127 as well as “no data” (same as UK levels).

After some tests it was concluded that:

- the earth model is spherical (we take a radius 6371.221 km),
- the scale is true at 60 N,
- most importantly, the upper left corner is at $-12.0, 54.5$

In this model the offsets of the upper left corner are calculated as -257.983 resp. 579.440 and the scale cres/lres is $6000000/6371.221 = 941.735$.

PIF header entries are:	Extra header data for MWS V.3.3:
picture size 256x256	
reflat= 60000	reflat 60000
reflon= 12000	reflon 12000
loff = -580	y-offset -579440
coff = 258	x-offset 257983
lres = 941	y-pixel 6000
cres = 942	x-pixel 6000
	eq.radius 6371221
	pol.radius 6371221

The error in pixels with the integer parameters is at the corners:

0.09/-0.11	0.02/-0.11
0.09/0.09	0.02/0.09

7.13 Annex C: Combining the Netherlands picture with foreign composites on MWS

The KNMI 256x256 picture can be combined with the composites B1-B3 to a picture of Western-Europe that lacks data only in three corners. Future updates could profit from (order of priority) Spanish, Danish, Norwegian data. Also e.g. Swiss and Italian data could be added, but with less significance for Netherlands nowcasting. Only very small areas north of the Hebrides and south of the Pyrenees are cut off from the above-mentioned composites. The pixel size (60 N) is 4 km, so, during resampling, some detail above France is lost. Detail lost from the Netherlands composite does not count, because the original stays available and is even recommended for local use.

The picture corners are:

15.000W	59.000N	20.446E	58.089N
9.275W	41.935N	12.801E	41.419N

PIF header entries are:		Extra header data for MWS V.3.3:
picture size 512x512		
reflat= 60000		reflat 60000
reflon= 0		reflon 0
loff = -796		y-offset 799047
coff = 214		x-offset 214104
lres = 628		y-pixel 4000
cres = 628		x-pixel 4000
		eq.radius 6378388
		pol.radius 6356912

The error in pixels with the integer parameters is at the corners:
 0.72/-0.04 -1.24/0.00
 0.45/-0.36 0.86/-0.30

NOTE: The various header parameters mentioned in these ANNEXES are also used in the navigation program in Appendix C.

NOTE: This program contains some extra unused subroutines, e.g. for the transformation to and/or from the English and Netherlands national grids.

NOTE: Testing of x, y pixel values can be done as follows: the pixel 300,256 comes from: NL 138,198 FR 311,112 DE 35,114 and UK 263,276.

Chapter 8

Echo top measurements

8.1 Introduction

Echo tops add valuable information to the traditional near-surface precipitation (PPI) radar pictures. Three-dimensional aspects of the radar echoes are highlighted: deep convection, anvils, cloud screens, split fronts, etc. For aeronautical meteorology the position and height of echo tops can provide important aircraft safety information.

Traditionally, echo top measurements were done by measuring manually the elevation and range of selected echoes. Sometimes the height could be read from a RHI (range height) screen. From about 1980 digital image processing of volume scans (horizontal scans at many elevations) could produce ETZ echo top pictures, i.e. the greatest height above a pixel where the echo strength exceeded a certain threshold value (e.g. 7 dBZ). Measuring echo tops with radar beams of 1 deg up to ranges of 200 km is not an easy task. Maddox et al.(1999) report uncertainties up to 7 km in WSR-88D tops. KNMI has developed a series of corrections and checks. These will be documented in following sections. The KNMI/Gematronik echo top product will be referred to as ETH.

8.2 Error sources

Tops are defined as the highest level where a certain echo power can be observed. At KNMI we take 7 dBZ, but other choices are possible. The quantities measured are an highest elevation E_0 and a distance D . The height H with respect to the observer's height is then

$$H = D \sin E_0 + \frac{D^2 \cos^2 E_0}{2fR} \quad (8.1)$$

where the second term is a correction for earth curvature. To correct for the vertical gradient of the radio refractive index, a fictitious earth radius fR is used in stead of the actual earth radius R . At least five error sources can be identified:

- incorrect elevation reading.
- the radar-elevation has to be corrected for refraction. The commonly used correction with $f=1.33$ is only valid for average conditions and for objects below 5 or 10 km.
- a limited number of elevations is used, causing detection and interpolation problems.
- side lobe echoes sometimes lead to strongly overestimated heights: if the main beam points 1 deg above the radar top, the lower side lobe may still cause an echo from the storm core to be displayed above the actual storm top.
- the 1 degree radar beamwidth also leads to overestimation of tops at moderate ranges, especially with mature showers having a sharp vertical radar reflectivity gradient at their top. The edge of the main beam still shows an echo while the beam axis is above the storm top. It is quite typical in ETZ (or even ETH) pictures that tops become gradually higher at ranges beyond 150 km. This problem has received attention in various publications. Correction methods can be based on simulations with model beams and model storm tops.

As a result, the conventional echo top product is rather inaccurate. The product usually displays artificial effects, e.g. a systematic increase of displayed shower heights for increasing range. In the following is described how these errors can be quantified and/or corrected.

8.3 History

Manual top measurements were performed in the Netherlands since the 1950's. It was then practice to subtract a half-beamwidth from the measured elevation of echo tops. This works well for convective cells of moderate intensity.

Around 1966 these measurements were done regularly (hourly or half-hourly) and a few echo top heights at ranges between 50 and 150 km, were

indicated by writing on the PPI sketches that were distributed by facsimile. For these measurements side-lobe echoes were avoided by attenuating the receiver and so rising the lowest presentation level to 40 dB below the maximum echo core intensity. Moreover the elevation corrections were made dependent on the echo top intensity, so that only strong echoes received the half-beamwidth correction. These corrections were seldom larger than the traditional 0.5 deg (half beamwidth) correction, as is seen in the following example: If the echo core exceeded 1, 3, resp. 10 mm/h, the corrections were -0.3 , -0.4 , resp. -0.5 deg. For intensities above 30 resp. 100 mm/h the elevation of the 1 mm/h contour was used and corrected with -0.2 resp. -0.4 deg.

In 1988 the facsimile distribution was replaced by remote display of computer pictures, but the manual top measurements were continued and their results could be entered as annotation in the computer pictures.

From 1989, Nov., a new radar computer was used that automatically performed top measurements and annotation. During a low-elevation PPI scan the 4 strongest echoes (if possible spread over all azimuths) were located and RHI scans were carried out above these echoes. The use of RHI read-out at 0.5 deg elevation steps minimised digitization errors. Also correction formulae for sidelobe and beamwidth effects were applied (described in Section 8.6). With this method the tops could be underestimated for non-vertical cells. Therefore a shear vector had to be entered manually from time to time, so that the method was not completely automatic. A further source of error, also inherent with the manual method, is the limited number of samples and the possibility that the strongest echoes were not necessarily capped by the highest tops.

As early as 1983/1984 the KNMI radars were capable of producing ETZ pictures, but these were considered inaccurate. Moreover the performance of extensive volume scans led to excessive maintenance of the mechanical parts of the radars. The new radars of 1996 had sufficient scanning capabilities and the necessary corrections to the ETZ software - as specified by KNMI - could be introduced. Because at that time no separate ETZ/ETH presentation was available at the remote displays, the annotation in the PPI pictures was continued, but the tops were now selected from the ETH picture (1996, Section 8.7). The introduction of (composite) ETH pictures on the meteorological work stations (MWS) finally took place in 2000, Oct.

This historical survey is not complete without mentioning the dissatisfaction of many aeronautical meteorologists at Amsterdam Airport with the top measurement results. Sometimes real errors were found and corrected (false electronic elevation readout), but mostly the corrections were blamed to systematically produce top values lower than those expected from sound-

ings or reported by pilots. An explanation might be that cloud tops (with small particles not detected by radar) are higher than echo tops. However, the difference should be small in cases of deep convection.

Another error source is the attenuation of the signal near echo tops caused by precipitation particles in the radar beam. This would affect the echo tops more than the echo cores. Correcting already reduced tops could have an adverse effect. However, KNMI at an early stage changed from 3 cm to 5 cm radars (Schiphol 1968, De Bilt 1978), so that serious attenuation within the 150 km top detection range will have been rare. In the present radars an attenuation correction is applied prior to evaluating the vertical echo profile.

The manual measurements have been evaluated in various ways. A series of 211 measurements from De Bilt were only $0.2 \text{ km} \pm 0.3 \text{ km}$ higher than simultaneous measurements from Schiphol (1980, May). The method was evidently consistent.

In the year between 1981, Oct.- 1982, Sept. the daily maximum top height reports were above 10 km on 22 days and above 12 km on 9 days. For comparison: cloud tops on thunder days in 1957-1960 exceeded these levels on 7 resp. 3 days per year as reported by pilots or - sometimes- radar (KNMI, Onweders, enz.). This small climatology does not suggest an underestimation by the radar method.

The change to automatic top measurements in 1989 may have led to a negative bias caused by the difficulty to find the azimuth of the highest top. The radar operator was instructed to search for the top in a high-elevation sector scan, but the automatic method only used the estimated shear vector, as mentioned earlier. However, because 4 tops were scanned per picture, a representative high top could hardly be overlooked.

From 1996 volume scans were used and converted to top annotations, hence this sampling problem no longer occurred.

8.4 Refraction correction

Refraction of a ray or beam with electromagnetic radiation is caused by the dependence of the propagation velocity on air density and water vapour pressure. The velocity is reduced to c/n , where c is the velocity in vacuum and n the refractive index. Consider a ray starting at height $H = 0$ with elevation E_0 , reaching height H . The slope E with reference to the local earth surface, will than have changed according to (e.g. Battan, 1973)

$$E^2/2 = E_0^2/2 + H/R + n - n_0 \quad (8.2)$$

where R is the earth radius. In the absence of the atmosphere ($n = 1$) we would have found

$$E'^2/2 = E_0^2/2 + H/R \quad (8.3)$$

For small angles $E^2 - E'^2 = 2E'(E - E')$, so the elevation change up to height H is approximated by

$$E - E' = \frac{n - n_0}{E'} \quad (8.4)$$

Because n depends on H , the actual height error follows from integration of Equation 8.4 over the length D of the ray

$$\Delta H = \int_0^D (E - E')dD = \int_0^H \frac{E - E'}{E'}dH = \int_0^H \frac{n - n_0}{E'^2}dH \quad (8.5)$$

The integration is performed numerically with substitution of a height-dependence of n according to the CRPL Exponential Reference Atmosphere (Bean en Dutton, 1968)

$$N \equiv 10^6 \cdot (n - 1) = 344.5 \exp(-0.1558H) \quad (8.6)$$

As an example we mention the height error of a radar-observed radiosonde near the 30 km level: 0.247 km for an elevation of 10 deg and 0.693 km for 5 deg. To avoid a correction table it has been attempted to perform the correction by means of the effective earth radius fR in stead of R . Because the value ΔH from Equation 8.5 is the difference between the earth curvature corrections (Equation 8.2) with and without ($f = 1$) an atmosphere, it follows

$$\frac{1}{f} = 1 + \frac{2R\Delta H}{D^2 \cos^2 E_0} \quad (8.7)$$

The value f decreases from 1.47 for small H , to 1.15 at the 30 km level. The well-known $f = 4/3$ correction applies only near the 10 km level. Finally the height dependence of f was approximated by

$$f = 1 + 0.43 \exp(-H/26) \quad (8.8)$$

This equation is valid for a standard atmosphere. Separate corrections for warmer or colder atmospheres are not meaningful considering the typical angular accuracy of about 0.1 deg of tracking radars. The same computations have been performed for optical theodolite measurements. Then the correction factor is $f = 1 + 0.22 \exp(-H/48)$.

8.5 Vertical echo profile (attenuation correction)

In contrast with RHI scans the available elevations are not fixed but depend on the scanning schedule (in a 15 min. period). We assume that above polar pixels a series of (attenuation corrected) Z_i -values ($i = 1, n$) in 0.5 dB resolution is available. The set of elevation values E_i has also to be known. The attenuation correction (dB/km) is based on a two-way attenuation

$$A = c \cdot R^d \quad (8.9)$$

where R is computed from the relation $Z = aR^b$ with R in mm/h. The parameters $a\dots d$ have values of e.g. 205, 1.7, 0.0045 and 0.12.

Equation 8.9 is applied iteratively along a radial by adding up the A's from individual polar pixels. First a pixel value is corrected for the attenuation by the intervening pixels and this new pixel value is used to compute the attenuation of the next pixel. And so on. The maximum possible correction for any pixel is a threshold.

NOTE: The default value of this parameter is ridiculously low (1 dB). Also the units are dBZ/km according to the documentation. It would indeed have been better to threshold the result of Equation 8.9 in stead of its accumulations, but that is not how it is implemented.

8.6 Corrections for the shape of the radar beam

The beam is not a thin line, but the energy distribution is more or less Gaussian with an effective angular width of 1 deg. Moreover, there is additional energy at about 2 deg from the axis: the side lobes.

Compared with the main beam the side lobe is down P_{sid} (one way). The radome may reduce P_{sid} . Some 2 degrees above any echo being P_{sid} above noise an upward extension due to the side lobe may occur. The side lobe correction of the profile is as follows

- In a loop $i = 1, n$ the maximum Z_m of the series Z_i is determined.
- If the maximum is below a top detection threshold P_{det} , no top is reported, and a new column is treated.
- If $Z_m < P_{det} + P_{sid}$ there will be no side lobe echo, and else we proceed with the beam width correction.

- If Z_m is strong enough to cause side lobe effects, we search for $i = m, n$ the first elevation h where $Z_h < Z_m - P_{sid}$. Next we search for $i = h, n$ for the elevation j where the echo gradient between $j + 1$ and j is larger than between j and $j - 1$. Then for $j = j + 1, n$ the Z -values are recalculated by continuing the gradient between j and $j - 1$.
- For $i = m + 1$ to n the values Z_i are replaced by Z'_i , where

$$Z'_i - Z_i = C_1 \cdot (-dZ/dE)^{C_2} \quad (8.10)$$

where dZ/dE is the (original) gradient between $i - 1$ and i . This is an empirical relation derived from numerical simulations with model tops and model beams. A Fortran source (see Appendix D) performing this simulation and checking the result of applying C_1 and C_2 , is available. In the 1989 radar computers preprocessed 0.5 dB values of correction by Equation 8.10 were stored in a table.

Since 1966 beamwidth corrections were based on numerical simulations of the observation of realistic vertical echo profiles with radar beams. The actual vertical distribution of the gain of the radar beam can be obtained from measurements. This was described in Chapter 2 on the radar beam. Formula 2.1 of that Chapter is used here

$$F = \exp[-b_0 x^2] + \exp[-b_1(x - a_1)^2 - 0.23d_1] + \exp[-b_2(x - a_2)^2 - 0.23d_2] \quad (8.11)$$

where x is the off-axis angle in deg. We use e.g. $a_1=2.63$, $d_1=63$, $a_2=4.5$, $d_2=67$, $b_0=5$, $b_1=16$, and $b_2=5$. The vertical Z -profile used is

$$G = \exp [2.3I \cdot (1 - \exp[A(H - 9.85)])] \quad (8.12)$$

where H is height and A is a parameter that allows to choose between sharp tops (e.g. $A=1.4$) or diffuse tops ($A=0.14$ or so). The horizontal distribution of the echo is supposed to be homogeneous. For many elevations of the beam axis and many points of the beam $F \cdot G$ is evaluated. The resulting vertical profile is compared with 8.12. The necessary correction depends strongly on the measured vertical gradient. As mentioned, the Fortran source for this simulation can be found in Appendix D. The numerical experiments were performed for 3 values of A and for showers at ranges between 50 and 150 km. C_1 and C_2 are found by plotting corrections for a typical average range, e.g. 120 km, on double logarithmic paper as a function of dZ/dE . The resulting C_1 and C_2 depend strongly on the coefficients in 8.11 and may change with

radar, beamwidth and radome. Especially the radome influence may change suddenly due to rain or snow, or gradually due to pollution.

The parameters C_1 , C_2 , P_{sid} and P_{det} have now values 0.00025, 3.6, 25 dB and 7 dBZ, They are logged in the fileheader under codes P14, P15, P24 and P25. Finally the actual echo elevation is found at the (interpolated if necessary) elevation where the corrected echo profile reaches the value P_{det} . The top height is calculated with Equation 8.1.

8.7 Selecting cloud tops for annotation in PPI displays

Once the complete ETH product is available, it is transmitted to the CRIS, where the following actions take place:

- selection of high tops for annotation of (old) remote displays
- conversion to KNMI-PIF file for display at the MWS
- creation of combined product from more radars for MWS display.

The second and third item are treated in the next section, the first is documented in the following algorithm for selecting individual tops from ETH-product.

The first selection of high tops consists of pixels with higher value than the surrounding ones. Tops below a minimum value (set to 2000 m, default 0) are excluded. The tops inside an inner circle (d_2 , set to 70 km, default 15) or outside an outer circle (d_1 , set to 160 km, default 120) around x_r, y_r are deleted from the series. A number of N tops is remaining.

Next all tops within a 10 km (d_3 , default 10) from a higher top are discarded. An additional selection criterion is needed to discard spurious isolated echoes near the tropopause: a so-called “speckle filter”. For each pixel the surrounding 8 pixels are evaluated. If the central value is a certain amount X higher than the average of the surrounding pixels, that central value is discarded as echo top. The critical difference X is based on the standard deviation of the values of the 8 surrounding pixels with respect to their average:

$$\min(X_1, X_2 \cdot \text{stddev}(\text{surr.8})) \tag{8.13}$$

Default values for the X -parameters are: $X_1=1.8$ km, $X_2=5$.

In the next step the remaining tops are sorted for decreasing height and N is updated. For each of the N remaining tops the quadrant number 1-4 is established. Then the series of quadrant numbers - in order of decreasing top

height - is searched for the first occurrence (highest top) of each quadrant number. Finally the required number M of tops is selected, starting with the first occurrences in each quadrant, then - if necessary - supplemented with the highest remaining tops (independent of quadrant).

The result is a number of tops with pixel coordinates x,y and height. Parameters are: d_1, d_2, d_3 (pixel units, resp. about 150, 50 and 20 km) and M (number of tops searched for) The displayed identification A...D has to be maintained for nearby tops in subsequent pictures. This number tracking has been specified in the KNMI 1987 radar program.

NOTE: The distance parameters proved on first inspection to be internal, any change requiring a new compilation.

NOTE: Initially the height scale was fixed at 100 m per bit value. The maximum height was 25.5 km in stead of about 16 km (label V4 in the extended file header). Preferably the height scale should be read from the input file header.

8.8 CRIS-processing: quality limits and no-data regions

In the CRIS the polar stereographic ETH files are converted to 8 bit KNMI-PIF files, displayable on a MWS. To avoid interpretation errors we mark those parts of the picture where data are not available or unsuitable for use. Finally ETH pictures can be composited to improve the coverage and to save on transmission and user attention. Some measurement errors have been discussed in Section 2. It was argued that at large range the large beam-width and the large spacing between the lowest beams cause large errors.

Moreover, at large range low echoes remain under the horizon: tops lower than 2 km (60 hFt) cannot be observed beyond 150 km due to the earth's curvature. Slightly higher tops are detected by only one beam, so that no echo profile is available. A CRIS parameter R_x (km) has been defined to mark the range where data can become suspect and another range marking the maximum distance allowed. Pixels farther than R_{xx} get the $< NODATA >$ value. The present settings are $R_x=170$ km and $R_{xx}=270$ km.

Another region of "no data" is nearby the radar, where tops are underestimated, because the elevation is not allowed to rise above 12 deg (safety restriction at Den Helder). If the actual tops reach to height H (minimum 1 km), the region within a range

$$R_n = H / \sin(12) = 4.8 \cdot H \quad (8.14)$$

is not used. The R_n is not a fixed value but may vary from about 15 km to 70 km, depending on the situation. It is necessary to evaluate R_n at merging time from actual data. During reading the radar data a histogram is built with the cumulative distribution of echo heights (0-255) for all pixels higher than a certain threshold and within range R_x . After reading the data a significant top height X is determined above which only q-ref per cent of the pixels can be found (30%). If the picture contains less than tt_ref pixels (parameter, set to 100) a default height of 500 m is taken. Finally, for maximum elevation E_x and vertical scale factor v_{sc} :

$$R_n = X \cdot v_{sc} / \sin(E_x) \quad (8.15)$$

8.9 CRIS-processing: merging procedure

For intensity pictures the merging at large range aims at selecting the highest values found by any of the radars. For top measurements at large range the least distant radar is the most accurate. Nearby the radar a more distant radar will be better.

Contrary to pseudoCAPPI compositing, both radars may look at different targets in their ETH pictures. Then a weighted average is not suitable. As an example, the average of a low precipitation top at 3 km and a spurious echo at 13 km would lower the latter to 8 km. The same type of confusion arises if we merge a ground target of one radar with a precipitation top seen by the other. It would be less confusing to present the maximum. However, we still have to avoid the overestimating of precipitation tops between R_x and R_{xx} . Consequently, the following procedure is applied:

- Data beyond R_{xx} are not used.
- Data between R_x and R_{xx} come from the local (= nearest) radar.
- Within R_x from any radar the highest top is chosen.
- Also, inside R_n , the highest top is preferred. This most likely is equivalent to ignoring the local radar.

NOTE: In some summer situations 1 or 3 small zones are within R_n from BOTH De Bilt and Den Helder.

NOTE: If we apply these procedures, the merged echo top field may be discontinuous, especially at a distance R_x from the non-local radar. This could be removed by smoothing (not yet included).

NOTE: the details of the computation are not discussed here. To speed up computing a preprocessed mask decides on the “local” radar and tables inform about the distances between a pixel and the radars. Finally a mask informs the merging process about the contributing pixels of each radar.

NOTE: If desired pixels that are much higher than the average of the surrounding 8 pixels can be scaled down to that average. The algorithm is almost the same as used in the December 1996 CRIS update.

Summing up, the following external parameters are required:

- percentage for estimating critical height q_ref , default 30 (%).
- number of pixels required this estimate tt_ref , default 100.
- maximum elevation E_x (deg), default 12,
- parameters R_x and R_{xx} with defaults 150 and 200 (km)
- parameters required for the pixel filter in Equation 8.13: fixed height difference in units, height difference in standard deviations.

8.10 CRIS processing: navigation, scaling and classification

The labels K1 and K2 give the size of the picture in pixels (e.g. 256 by 256). See for meaning of labels Chapter 5. In the Gematronik header the labels G1-G9 define the projection. The resolution G4,G5 (now 2.5 km) has to be converted to the horizontal scale units (km/pixel) used for scaling R_x, R_{xx} and R_n as follows:

$$h_{sc} = G4 \cdot \left[\frac{\cos(45 - RefLat/2)}{\cos(45 - RadLat/2)} \right]^2 \quad (8.16)$$

where RefLat is read from label G7 and RadLat is the latitude of the radar stored in label F4. The vertical (echo height) scale is found from label V4 which gives the maximum height in km. Eight bit data values can be converted to height in km by multiplying with:

$$v_{sc} = V4/255 \quad (8.17)$$

Note that flightlevel units (hFt) follow from $km/32.9$.

Considering the measurement accuracy a product with 30 hFt resolution (about 1 km) is justified. Given a realistic maximum height of about 14 km

about 16 levels are required (usually not all to be shown in the same picture). Although 4 bits would be enough, the PIF file uses 8 bits per pixel.

Classification is done with the standard CRIS-routine. It can be performed with a linear scale factor and an offset or with a complete table. The necessary parameters are kept in the appropriate CRIS-files Presently V4=14.6 km. a hard table with 30 hFt steps is used to code 0-60 hFt, 60-90 hFt,...450-480 hFt. as 0-14. A no data value is coded as 255, as internationally agreed.

NOTE: The program should check that input label V4 stays the same.

8.11 Interpretation of echo top images

As mentioned in the introduction, the combined use of the echo top and the PPI picture show the three-dimensional structure of precipitation systems to the meteorologist. Details that were up to now hidden in IR satellite pictures, are now available operationally. Examples that could be identified up to now include, anvils, split front, line convection, seeder clouds, etc. As experience grows, more applications will emerge.

For correct interpretation the user should be aware of some non-meteorological phenomena that sometimes show up in ETH pictures. Examples are echoes from aircraft, causing spikes in the picture. Also near-tropopause refractive index inhomogeneities may scatter microwave radiation, causing (fields of) spikes in the picture. Other than the in PPI picture during ETH scans the clutter filter is not active, because significant high-level meteorological echoes can occur above low-level anomalous propagation echoes. Sometimes a lot of ground clutter is visible, mostly originating from the lowest beam. This ground clutter stays close to the ground, at least at moderate range.

As mentioned in Section 3.3 the inexperienced user may be confused by a signal from the rising or setting sun. This is a 2 deg wide “spoke” at a range above 150 km or more.

8.12 References

- KNMI, 1965-1968, Onweders, Optische Verschijnselen, enz. in Nederland, KNMI Publ. 81, LXXVIII - LXXXI (Years 1957-1960)
- J.R.Probert-Jones, 1963, The distortion of cumulonimbus precipitation observed by radar. Techn.Note 13, Dept.of Meteorology, Imperial College, London.

J.Aoyagi, 1963, The quantitative estimation for the heights of radar tops. Proc.10th Weather Radar Conf., Washington DC, 123-133.

R.J.Donaldson,Jr, 1964, A demonstration of antenna beam errors in radar reflectivity patterns. J.Appl.Met.,3, 611-623

B.R.Bean, E.J.Dutton, 1968, Radio Meteorology. Dover Publ.,New York.

R.A.Maddox, et al., 1999, Echo height measurements with the WSR-88D: Use of data from one versus two radars. Weather and Forecasting, 14, p.455-460.

Chapter 9

Miscellaneous information

9.1 Technical information KNMI weather radars

Type: Gematronik Doppler Weather Radar System METEOR 360 AC

	De Bilt	Den Helder
Operational in	1997	1996
Coordinates	52.10269 N 5.17874 E	52.95381 N 4.79089 E
National Grid (km)	140.689/457.072	114.900/551.910
Frequency (MHz)	5667	5810 (lic.5645)
Band width (short, MHz)	1.5	1.5
Max.power(long/short kW)	268/305	264/298
PRF (Hz)	250	250
Max. PRF doppler mode	1200	1200
Pulse length (microsec)	2.023/0.837	2.037/0.855
Height ant.feed (m+NAP)	44.1	51.5
Antenna diameter (m)	4.2	4.2
Bundle width (circ.,deg)	1.04	1.04
Gain (dB)	45.4	45.7
Side lobe reduction (dB)	>28	>28
Polarization	hor	hor
Azimuthal scan (rot/min)	3	3
Elevation (deg)	0.3-12.0	0.3-12.0

NOTE: Coordinates Schiphol radar 52.30503 4.75563 or 111.90 / 479.75 The Schiphol aerial was at a height of 43.4 m +NAP (= above msl)

9.2 Weather radar product sheet

Country: The Netherlands
GTS bulletin header: PANL21 EHDB
GTS centre: Bracknell

Image type: National composite of 2 radars:
- De Bilt at 5.1787 E, 52.1027 N
- Den Helder at 4.7909 E, 52.9538 N

Antenna altitudes: 44 m resp. 51 m above m.s.l.
Frequency: 5.6 GHz (C-band)

Quantity displayed: classified precipitation rate mm/hr
Z-R conversion used: $Z = 200 * R^{1.6}$
Nr.of intensity levels: 8 (mm/h: 0/ 0.1/ 0.3/ 1/ 3/ 10/ 30/ 100/)
(dBZ: 7/ 15/ 23/ 31/ 39/ 47/ 55/)

Type of presentation: CAPPI at about 1 km altitude, but:
- Lowest elevation at far range.
- Area near radar filled by other radar.

Image organisation: Nr. of lines: 256 (0..255)
Nr. of columns: 256 (0..255)

Projection: Polar stereographic on spheroidal earth
Picture parallel to OE meridian
Pixel size 2.5 km at 60N
(Pixel size about 2.4 km in radar area)
Pixel frame aligned at 60N, OE

Position upper left corner of picture:
0.0 pixels E from OE
212.0 pixels S from 60N

Image corners: Lon/Lat: (E =+)
0.00 / 55.32 9.75 / 54.84
0.00 / 49.79 8.34 / 49.39

Timing: Refresh: 5 min is available
Start of scans: HH+00, HH+05, HH+10, HH+15 (=BUFR timestamp)
End of scans: HH+02, etc., followed by compositing
Transmission to GTS: HH+07 approximately
Availability on GTS: 1994
Changes expected: image with 200*200 pixels will be phased out.

Contacts: Exchange coordination: J.P.de Jongh
Phone : 31 30 2206483

E-mail: jonghdej@knmi.nl
Transmission: W.Koetse
Phone : 31 30 2206653
E-mail: koetse@knmi.nl
Information on radars: H.R.A.Wessels
Phone : 31 30 2206456
E-mail: wessels@knmi.nl

Date: 20-10-1995, 06-08-1997, 14-01-1999, 20-2-2001

9.3 KNMI radar chronology

1957 De Bilt : Wind finding radar (until 1986, sometimes combined)
1959 Schiphol : First weather radar (3 cm DECCA)
1962 De Bilt : Weather radar (3 cm Selenia)
1968 Schiphol : Radar replaced (5 cm Selenia)
1978 De Bilt : Radar replaced (5 cm EEC)
1983 Schiphol : New digital radar with local display (5 cm EEC)
1984 De Bilt : Radar digitized and upgraded.
1987 : Composite picture on remote displays
1989 : New radar site computers; automatic echo tops
1993 : New preprocessors; clutter cancellation
1996 D.Helder : Radar installed (5 cm Gematronik)
1997 De Bilt : Radar installed (5 cm Gematronik), Schiphol ends.

9.4 External availability of data

De Bilt, 2000

L.S.

De radars van De Bilt en Den Helder produceren een grote hoeveelheid producten. Sommige worden ge-archiveerd voor gebruik achteraf, ook buiten het KNMI. Aan de meeste wensen van externe gebruikers kan worden voldaan met combinatiebeelden van beide radars waarin elk kwartier de geschatte neerslagintensiteit op zo gering mogelijke hoogte wordt getoond in 6 klassen met grenzen 0.1, 0.3, 1, 3, 10 en 30 mm/h.

Soms wil men echter - bijvoorbeeld voor wetenschappelijk onderzoek - beelden gebruiken met hogere resolutie qua neerslagintensiteit. De oorspronkelijke radarmeting geschiedt met een resolutie van 0.5 dB, zodat regenmetingen met een stapgrootte van 7.5% beschikbaar zijn.

Desgewenst is verstrekking van deze zogenaamde 8-bits beelden mogelijk mits niet ouder dan ca. 6 maanden. Dit betreft beelden van echo's zo dicht mogelijk (1 km of meer) bij de grond. Het zijn geen combinatiebeelden maar beelden van de radar te De Bilt. Eventueel zijn beelden met 5 minuten-interval beschikbaar.

Bestellingen moeten schriftelijk worden gedaan (dus niet per e-mail) en de gewenste periode(n) moeten worden vermeld. Levering uitsluitend per etmaal van 08.00 UT t/m 08.00 UT = 96 kwartierbeelden of 288 5-minuutbeelden. Na verwerking worden de beelden op CD toegestuurd, met een faktuur.

Kosten per dag (alle bedragen excl. BTW):

licentiekosten: 96 beelden X fl. 0,8586 (Eu 0,3896)= fl. 82,43. Voor algemeen (niet commercieel) onderzoek gelden geen licentielosten.

extractiekosten: 96 beelden X fl. 0,2378 (Eu 0,1079)= fl. 22,83 Voor 5-minuutbeelden geldt dubbel tarief.

administratiekosten: fl 28,00 (Eu 12.70).

arbeid/leveringskosten: Die zijn afhankelijk van de hoeveelheid bestelde etmalen. Bij grotere afname stijgt deze post minder dan evenredig. De volgende indicatie is te geven: minimaal een kwartier, voor ca. 10 dagen is een half uur nodig. In het laatste geval zijn de leveringskosten fl 76,50 (Eu 34.71).

KNMI, afd. Klimatologische Dienstverlening,
Postbus 201,
3730 AE De Bilt.

9.5 Description of weather radar data at 0.5 dB resolution

9.5.1 Radar De Bilt

- Position: $L_r=5.1787$ E, $B_r=52.1027$ N;
- Altitude: 44 m above m.s.l.
- Antenna beam width: 1.04 deg
- Radar frequency: 5.6 GHz (C-band)

9.5.2 Output levels

The echo power of calibrated weather radars is converted to units of Z , a property of distributed scatterers (dimension mm^6/m^3) These echo values have been normalised for range, so there is a fixed range-independent relation between the pixel value Z and the rainfall intensity R (mm/h). A frequently used approximation

$$Z = 200R^{1.6} \quad (9.1)$$

Therefore the echo, expressed in logarithmic units (base 10) is

$$\text{dBZ} = 10 \log Z = 16 \log R + 23 \quad (9.2)$$

(examples: 7 dBZ for 0.1 mm/h, 23 dBZ for 1 mm/h, etc.) In the radar output PIF file the data are converted to 8 bit integers (0-255). The scale and offset of the conversion follow from:

$$\text{dBZ} = (\text{value} - 64)/2 \quad (9.3)$$

A rainfall intensity of 0.1 mm/h is represented by the value 78 in a PIF file, 1 mm/h by 110, etc. The lowest value presented is 61, indicating the lowest measurable intensity of about 0.03 mm/h. A data value 0 is used in the PIF file to indicate that no measurement is available, i.e. beyond 320 km from the radar.

9.5.3 KNMI pseudoCAPPI

The antenna scans around a vertical axis. Four complete scans at elevations 0.3, 1.1, 2.0 and 3.0 deg are combined into a single picture. The height H of a radar beam (above the radar level) depends on the elevation and the range D

$$H = D \sin E + \frac{D^2}{2R_a} \quad (9.4)$$

where R_a is the earth radius, multiplied by 1.33, to correct for microwave atmospheric refraction. We take $R_a=1.33 \cdot 6350$ km. In the combined picture we use gradually lower elevations at increasing range. The result is that up to about 100 km the data are measured near 1 km height (CAPPI= constant altitude plan position indicator). At larger range the data come from gradually higher altitude due to the earth's curvature. This pseudoCAPPI picture is built by means of weighted averaging of dBZ values (averaging rainfall would give different results).

The elevations are E_1 , E_2 , E_3 and E_4 . For a certain range and azimuth these elevations contain respectively values P_1 , P_2 , P_3 and P_4 (dBZ). For pseudoCAPPI height H (km) the elevation at distance R (km) is:

$$E = \arcsin \left(\frac{H}{D} - \frac{D}{2R_a} \right) \quad (9.5)$$

The pseudoCAPPI dBZ value P is found as follows:

```

IF E>= E4 THEN P=P4
IF E<E4 AND E>=E3 THEN A=(E-E3)/(E4-E3); P=A*P4 +(1-A)*P3
IF E<E3 AND E>=E2 THEN A=(E-E2)/(E3-E2); P=A*P3 +(1-A)*P2
IF E<E2 AND E>=E1 THEN A=(E-E1)/(E2-E1); P=A*P2 +(1-A)*P1
IF E<E1 THEN P=P1

```

9.5.4 Reprojection

The pseudoCAPPI composition is carried out in a polar coordinate system centered at the radar. The final product is a rectangular 256x256 picture in polar stereographic projection on a spheroidal earth. The picture is parallel to the 0E meridian, and the pixels (size about 2.4 km) are counted positive in E resp. S direction. The upper left corner is at the 0E meridian 212 pixels S from 60N For checking purposes the image corners are presented:

0.0/55.318 9.750/54.840 0.0/49.790 8.342/49.394

Projection Specification:

$R=6378.388$ km	earth equatorial radius (Hayford spheroid, 1910)
$e=0.0819918$	eccentricity of the spheroidal earth (,)
$p=2.5$ km	pixel size at 60N (about 2.4 km near radar)
$L_0=0, B_0=60N$	reference longitude resp. latitude
$i_0=0, j_0=212$	offset pixel count

Functions:

Correction for non-spherical earth

$$f(B) = \frac{1}{\sqrt{1-e^2}} \left[\frac{(1-e) \cdot (1+e \sin B)}{(1+e) \cdot (1-e \sin B)} \right]^{e/2} \quad (9.6)$$

Plotting distance of point with latitude B (deg)

$$r(B) = 2R \cdot f(B) \cdot \tan(45 - B/2) \quad (9.7)$$

Scale (km projection/ km arc length) at latitude B

$$s(B) = \frac{r(B)}{R \cos B} \cdot \sqrt{1 - (e \sin B)^2} \quad (9.8)$$

Conversion from pixel coordinates x,y to Lat,Lon, i.e. B, L ,

$$L = L_0 + \arctan \left(\frac{x + i_0}{y + j_0 + r(B_0)/(p \cdot s(B_0))} \right) \quad (9.9)$$

B is found by iteration, starting at the radar latitude:

$$\text{rplot} = \frac{r(B_0) + (y + j_0) \cdot p \cdot s(B_0)}{\cos(L - L_0)} \quad (9.10)$$

$$B = 90 - 2 \arctan \left(\frac{\text{rplot}}{2R \cdot f(B_r)} \right) \quad (9.11)$$

$$B = 90 - 2 \arctan \left(\frac{\text{rplot}}{2R \cdot f(B)} \right) \quad (9.12)$$

Reverse computation from Lat,Lon to pixel coordinates

$$\text{rpix} = \frac{r(B)}{p \cdot s(B_0)} \quad (9.13)$$

$$x = \text{rpix} \cdot \sin(L - L_0) - i_0 \quad (9.14)$$

$$y = \text{rpix} \cdot \cos(L - L_0) - \frac{r(B_0)}{p \cdot s(B_0)} - j_0 \quad (9.15)$$

9.5.5 PIF file structure

The observing time can be read from the name of the file. The files consist of 257 records with a length of 256 of binary data. The first line consists of header information with no relevance to this particular use.

The following 256 lines contain the picture data, line by line, starting in the most northwestern corner. The position x,y of a pixel can be converted to geographical coordinates, as described in the last section. The decimal value (0-255) can be converted to precipitation intensity, as described in the section on output levels.

9.6 Specification: coding of 200x200 archive (V)ERAS files

- Date/time are in the file name, e.g. YYMMDDHH.MM= 97031223.15
- The file starts with a header of 121 bytes, ending with 03H 03H
- The file contains 200 image lines of 200 pixels,
- The image starts in the upper left (North-West) corner.
- The data from each line are compressed.
- Run-length decoding is as follows:

```
Read byte; Convert to decimal value x
Division x/32 gives value W and remainder R.
If R<>0 H=R
If R=0 READ NEXT BYTE and convert that byte to decimal value H
Fill next part of the image line with H times the value W
Read next byte, etc.
```

NOTE: if more than 15 subsequent pixels have the same value, two bytes are used to code that line segment.

```
Example of one line: 00H  56H  21H  64H  42H  00H  A3H
                    result      86x0      1x1  4x3  2x2      163x0
Example of empty line: 00H  C8H
                    result      200x0
```

Appendix A

Fortran program: rad2obst.f

```
c Program: RAD2OBST.F
c Purpose: Generates 2 tables for radar beams:
c 1. elevation of an object as function of its height & range
c 2. dimensions of obstacles that may be tolerated
c Date: 2001, Feb.23
c Author: HRAW, KNMI
c Notes: --
PROGRAM rad2obst
IMPLICIT none
CHARACTER t11*68, t12*68, t21*68, t22*68, t23*68
REAL py,r,h,hr,hstep,hout,h0,h00,d,d1,dstep,dref,dref0
REAL mult,refh(7),outf(7),b,f,s
INTEGER i,out(21),nstrt,nstop
DATA hr,hstep, dstep, nstrt/0.0515, 0.001, 1.,60/
DATA refh/200,170,140,110,80,50,20/

c
PRINT *, ' Height of de radar antenna in m? >'
READ *, hr
PRINT *, ' Results are stored in <elevout1> & <elevout2>'
hr=hr/1000.
py=ATAN(1.)/45.
r=1.33*6723.1
t11=' d km ' //
* ' ' //
t12='h(m) elev (.01 deg) of target he'//
* 'ight h seen from radar at 51.5 m'
t21='max.hoogte en breedte (m) van obst'//
* 'akels bij radar op 51.5 m '
t22=' afstand (m), max.hoogte | max.br'//
* 'eedte voor obstakels lager dan: '

c first table -----
c b=elevation in .01 deg.,
OPEN (8, FILE='elevout1')
d1=dstep
mult=1.
IF (dstep .LT. 1.) WRITE (t12(4:4),'(a1)') 'h'
IF (dstep .LT. 1.) mult=10.
DO 101, i=1,21
WRITE (t11(3+3*i:5+3*i),'(I3)') NINT(mult*(d1+(i-1)*dstep))
101 CONTINUE
WRITE (t12(63:66),'(F4.1)') 1000.*hr
WRITE (t21(54:57),'(F4.1)') 1000.*hr
```

```

WRITE (8,'(68a)') t11
WRITE (8,'(68a)') t12
nstop=nstrt-54
IF (nstop.LT.0) nstop=0
c
DO 110, h=nstrt*hstep,nstop*hstep,-hstep
DO 109, i=1,21
d=d1+FLOAT(i-1)*dstep
b=-ASIN( ( (r+hr)**2.+d**2.-(r+h)**2. )/d/(r+hr)/2. )
b=100.*b/py
IF (b.LT.-99.) b=-99.
out(i)=NINT(b)
109 CONTINUE
WRITE (8,'(I3,2X,21I3)') NINT(1000.*h), (out(i),i=1,21)
110 CONTINUE
CLOSE (8)
c second table -----
c s= 0.1 * effective beam cross section
c f= 1/(beam-filling by vertical obstacle)
OPEN (9, FILE='elevout2')
WRITE (9,'(68a)') t21
WRITE (9,'(68a)') t22
WRITE (9,'(14X,''brede obst.|'',7(I3,''m '''))')
* (NINT(refh(i)), i=1,7)
h0=INT(hr-1.)
h0=50
dref=0.
DO 210, d=.1, 24., .1
DO 209, h=hr,-0.003, -.0001
b=-ASIN( ( (r+hr)**2.+d**2.-(r+h)**2. )/d/(r+hr)/2. )
b=100.*b/py
c b=NINT(b)
IF (b .LT. -20.) THEN
hout=1000.*h
GOTO 208
ENDIF
209 CONTINUE
208 IF (hout .GE. h0) GOTO 210
dref0=dref
dref=1000.*d
h00=h0
h0=INT(hout)
s=py/10.*(dref0+100.)*.785
DO 221, i=1,7
f=10.4*s/(refh(i)-h0+.001)
IF (f .LT. 1.) f=1.
outf(i)=f*s
IF (refh(i).LT.h0 .OR. outf(i).GT.999.0) outf(i)=999.9
221 CONTINUE
WRITE (9,'(I5,'' - ''',2I5,6X,7F6.1)') NINT(dref0),
* NINT(dref),NINT(h00),(outf(i),i=1,7)
210 CONTINUE
CLOSE (9)
END

```

Appendix B

Fortran program: utlzon5a.f

```
c Program: utlzon5a.f
c Purpose: presents solar positions for any date and location
c Author: H.R.A.Wessels, KNMI De Bilt
c Date: 1991, June 17
c Version: 1999, Jan 24: 10 min. output
c Modified: 2001, Apr 24: added formulae for Epoch 2000
c Note: The accuracy is better than 0.001 deg.
c Reference: D.Sonntag, 1989, Abh. des Met.Dienstes der DDR Nr.143
c Formeln verschiedenen Genauigkeitgrades zur Berechnung
c der Sonnenkoordinaten, pp. 60 etc.
c Reference:Explanatory Suppl.to the Astron.Ephemeris, London 1961
c Reference:J.Meeus, Astronomical formulae for calculators, 1979
c =====
      SUBROUTINE sol19(t,lo,ad,de)
c formulae for Epoch 1900
c solar position <asc.dir>, <decl> and orbit parameters
c t= centuries since 1900 Jan 0,12 ET
c tj=year-1900; tf=fraction of year
c ep=obliquity of the ecliptic
c lo= geocentric mean longitude of sun, mean equinox of date
c ec= numeric eccentricity
      IMPLICIT none
      DOUBLE PRECISION t,tj,tf,lo,dlo1,ad,de, ep,ec,th,ma,omg,py
c
      tj=INT(100.*t)
      tf=100.*t-tj
      py=ATAN(1.)/45.
      ep=23.452294-.0130124*t-.00000164*t*t+.000000502*t*t*t
      ep=ep*py
      lo=279.696678+.0076891*tj+360.0076891*tf+.0003025*t*t
      IF (lo.GT.360.) lo=lo-360.
c neglected are long periodic planetary perturbations
c resp. Venus, Jupiter & Mars, Mars & Venus, finally Mars
      dlo1=(1.882-0.016*t)*SIN(py*57.24+py*150.27*t)
      dlo1=dlo1+6.40*SIN(py*231.19+py*20.2*t)
      dlo1=dlo1+0.266*SIN(py*31.8+py*119.0*t)
      lo=lo+(dlo1+0.202*SIN(py*315.6+py*173.3*t))/3600./3600.
c numerical eccentricity earth orbit
      ec=.01675104-0.0000417992*t-0.0000001254*t*t
c ma= mean anomaly without Mars perturbation term
      ma=358.475845
      ma=ma-.0095025*tj+359.9904975*tf-.00015*t*t-.0000034*t*t*t
```

```

        IF (ma.GT.360.) ma=ma-360.
        ma=ma+dlo1/3600./3600.
        ma=ma*py
c th= geocentric ecliptical length of sun, mean equinox of date
        th=lo+ec*(2-ec*ec/4)/py*SIN(ma)
        th=th+1.25*ec*ec/py*SIN(2*ma) +1.0833*ec*ec*ec/py*SIN(3*ma)
        th=th*py
c neglect 103/96*ec^4*sin(4*m) <0.02", moon <7.25"
c neglect -sin(ep)*tan(b)/cos(th) as lat.sun b<1".3
c apparent length of sun, true equinox of date: appr. nutation:
        omg=259.18-1934.142*t
        1 IF (omg.LT.0.) THEN
            omg=omg+360.
            GOTO 1
        ENDIF
        ep=ep+ 0.00256*COS(omg*py)*py
        th=th-(0.00569+0.00479*SIN(omg*py))*py
c      print *, t,lo,th/py,ma/py,ep/py
c ad=right ascension, de= declination
        IF (COS(th) .EQ. 0) THEN
            ad=py*90.
            GOTO 13
        ENDIF
        ad=ATAN(COS(ep)*TAN(th))
        IF (COS(th) .LT. 0.) ad=ad-180*py
        13 IF (COS(th) .EQ. 0. .AND. SIN(th) .LT. 0.) ad=ad-180.*py
        IF (ad.LT.0.) ad=ad+360.*py
        de=SIN(ep)*SIN(th)
        de=ASIN(de)
        RETURN
        END
c =====
        SUBROUTINE sol20(t,lo,ad,de)
c solar position <asc.dir>, <decl.> and orbit parameters
c t= centuries since 2000 Jan 1,12 ET
c tj=year-2000; tf=fraction of year
c lo= geocentric mean longitude of sun, mean equinox of date
c ep= obliquity of ecliptic
c ec= numeric eccentricity
        IMPLICIT none
        DOUBLE PRECISION t,tj,tf,lo,dlo1,ad,de, ep,ec,th,ma,py,omg
c
        tj=INT(100.*t)
        tf=100.*t-tj
        py=ATAN(1.)/45.
        ep=23.4392811-0.0130042*t-0.0000001641*t*t+0.000000502*t*t*t
        ep=ep*py
        lo=280.4660695+.0077004*tj+360.0077004*tf+0.0003025*t*t
c neglected are long periodic planetary perturbations
c resp. Venus, Jupiter & Mars, Mars & Venus, finally Mars
        dlo1=(1.866-0.016*t)*SIN(py*207.51+py*150.27*t)
        dlo1=dlo1+6.40*SIN(py*251.39+py*20.20*t)
        dlo1=dlo1+0.266*SIN(py*150.8+py*119.0*t)
        lo=lo+(dlo1+0.202*SIN(py*128.9+py*173.3*t))/3600./3600.
c numerical eccentricity
        ec=.016709114-0.0000419051*t-0.000000126*t*t
c ma= mean anomaly without Mars perturbation term
        ma=357.5277233-0.00951344*tj+359.9904866*tf-0.0001603*t*t
        ma=ma-0.000003333*t*t*t
        ma=(ma+dlo1/3600./3600.)*py
c th= geocentric ecliptical length of sun, mean equinox of date
        th=lo+ ec*(2-ec*ec/4)/py *SIN(ma)

```

```

        th=th+ 1.25*ec*ec/py *SIN(2*ma) +1.08333*ec*ec*ec/py*SIN(3*ma)
        th=th*py
c neglect 103/96*ec^4*sin(4*m) <0.02", moon <7.25"
c neglect -sin(ep)*tan(b)/cos(th) because lat.sun b<1".3
c apparent length of sun, true equinox of date: appr. nutation:
    omg=259.18-1934.142*(t+1)
    2 IF (omg.LT.0.) THEN
        omg=omg+360.
        GOTO 2
    ENDIF
    ep=ep+ 0.00256*COS(omg*py)*py
    th=th-(0.005669+0.00479*SIN(omg*py))*py
c ad=right ascension, de= declination
    IF (COS(th) .EQ. 0) THEN
        ad=py*90.
        GOTO 13
    ENDIF
    ad=ATAN(COS(ep)*TAN(th))
    IF (COS(th) .LT. 0.) ad=ad-180*py
13 IF (COS(th) .EQ. 0. .AND. SIN(th) .LT. 0.) ad=ad-180.*py
    IF (ad.LT.0.) ad=ad+360.*py
    de=SIN(ep)*SIN(th)
    de=ASIN(de)
    RETURN
    END
c =====
c Julian daynumber <jd> in year from yy,mm,dd
    SUBROUTINE tjd(jd,yy,mm,dd)
    IMPLICIT none
    DOUBLE PRECISION jd,dd,f
    INTEGER yy,mm,m,a,b,j
c
    m=mm
    j=yy
    IF (mm .LT. 3) THEN
        m=m+12
        j=j-1
    ENDIF
    a=INT(j/100.)
    b=2-a+INT(a/4.)
    IF (J.LE.1582 .AND. mm.LE.10 .AND. dd.LE.15) b=0
    jd=INT(365.25*j)+INT(30.6001*(m+1))+dd+1720994.5+b
    RETURN
    END
c =====
c daynumber yymmdd from Julian daynumber
    SUBROUTINE tday(jd,yy,mm,dd)
    IMPLICIT none
    DOUBLE PRECISION jd,jdz,dd,f
    INTEGER yy,mm,z,a,b,c,d,e
c
    jdjz=jd+.5
    z=INT(jdz)
    f=jdjz-z
    a=z
    IF (z.GE.2299161) THEN
        a=INT((z-1867216.25)/36524.25)
        a=z+1+a-INT(a/4.)
    ENDIF
    b=a+1524
    c=INT((b-122.1)/365.25)
    d=INT(365.25*c)

```

```

e=INT((b-d)/30.6001)
dd=b-d-INT(30.6001*e)+f
mm=e-1
IF (e .GT. 13.5) mm=mm-12
yy=c-4715
IF (mm .GT. 2.5) yy=yy-1
RETURN
END
c =====
PROGRAM main
IMPLICIT none
CHARACTER c(40)*81,c1*81,ct(12)*3
DOUBLE PRECISION py,x,y,y1,jd,jd0,u,u0
DOUBLE PRECISION t,lo,l2,d1,ad,a2,da,de,d2,di,az,dde
DOUBLE PRECISION el,e10,ez,elx,eln,ur,us,h,n,sr0,ss0,dd,dd1
INTEGER i,jj,jj0,mm,mm1,mm0,ij,u2,yy,k,l,inote, epoch
DATA ct/'jan','feb','mar','apr','may','jun',
*      'jul','aug','sep','oct','nov','dec'/
DATA x,y/5.1787, 52.103/
DATA ez/-0.833333/
c
epoch=2000
py=ATAN(1.)/45.
PRINT *, ' This program generates table with positions '
PRINT *, ' azimuth, elevation (or refraction corrected elev.)'
PRINT *, ' of the solar centre for a certain date.'
PRINT *, ' '
PRINT *, ' Enter geographical coordinates of location:'
PRINT *, ' '
101 PRINT *, ' LATITUDE in degrees (-90.0 to +90.0, e.g. 52.0 ): '
READ *, y
IF (y.LT.-90. .OR. y.GT.90.) GOTO 101
102 PRINT *, ' LONGITUDE (-179.9 to +180.0 with East= positive): '
READ *, x
IF (x.LT.-179.99 .OR. x.GT.180.) GOTO 102
103 PRINT *, ' Date in format YYYYMMDD (1900-2099) >>>>> : '
READ *, jj
IF (jj/10000.LT.1900 .OR. jj/10000.GT.2099) GOTO 103
jj0=jj
mm=MOD(jj,10000)/100.
dd=MOD(jj,100)
jj=INT(jj/10000.)
c   print *, jj,mm,dd
CALL tjd(jd,jj,mm,dd)
jd0=jd
c
WRITE (*,'('' Please Wait ..... '')')
y1=y
y=py*y
c
c start time of day concerned
IF (epoch .EQ. 2000) THEN
t=(jd0-2451545)/36525.
CALL sol20(t,lo,ad,de)
ELSE
t=(jd0-2415020)/36525.
CALL sol19(t,lo,ad,de)
ENDIF
l2=lo
a2=ad
d2=de
c now end of day

```

```

t=t+1./36525.
IF (epoch .EQ. 2000) THEN
  CALL sol20(t,lo,ad,de)
ELSE
  CALL sol19(t,lo,ad,de)
ENDIF
IF (ad.LT.a2) ad=ad+360.*py
IF (lo.LT.l2) lo=lo+360.
d1=(lo-l2)/1440.
da=(ad-a2)/1440.
di=(de-d2)/1440.
c
c main loop: 10 min values
u=0
l=0
k=0
DO 299, i=0,1440,10
lo=l2+FLOAT(i)*d1
ad=a2+FLOAT(i)*da
de=d2+FLOAT(i)*di
u0=u
u=INT((i+.0001)/60.)
u2=INT(i-u*60.)
u=u+.01*u2
h=py*(lo-180.+x+FLOAT(i)/4.)-ad
n=COS(h)*SIN(y)-TAN(de)*COS(y)
IF (n.NE.0.) THEN
  az=ATAN(SIN(h)/n)/py
  IF (n.GT.0.) az=az-180.
ENDIF
IF (az.LT.0.) az=az+360.
IF (n.EQ.0.) THEN
  az=90.
  IF (SIN(h).LT.0.) az=270.
ENDIF
e1=SIN(y)*SIN(de)+COS(y)*COS(de)*COS(h)
e1=ASIN(e1)/py
dde=0.
IF (e1.GT.ez) dde= 4.5/283./TAN(PY*(e1+8./(e1+4.23)))
IF (e1 .LT.-2.) GOTO 299
l=l+1
IF (l.GT.21 .OR. (u.GT. 9.55 .AND. u0.LT.9.54)) THEN
  k=k+1
  l=1
ENDIF
c1=c(l)

IF (k.GT.4) GOTO 299
c
  print *,u0,u,u2,l,k
  WRITE (c1(k*16:k*16+15),'(1X,I4,F6.1,F5.1)')
*   INT(100*u+.1),az,e1
  c(l)=c1
299 CONTINUE
  WRITE (*,'(1X)')
  WRITE (*,'(1X,''SOLAR AZIMUTH/ELEVATION AT LONGITUDE'',F8.2,
*   ',LATITUDE'',F7.2,'' FOR DAY'', I9)') x,y/py,jj0
  WRITE (*,'(79A)') ('-',i=1,79)
  DO 410, l=1,21
  WRITE (*,'(A80)') c(l)
410 CONTINUE
c finally check: example Meeus p.79
c   print *,'          226.79147          -17.53682 '
```

```
t=(2443824.5-2415020.0)
t=t/36525.
CALL sol19(t,lo,ad,de)
c   print *, t,ad/py,de/py
t=(2443824.5-2451545.0)
t=t/36525.
CALL sol20(t,lo,ad,de)
c   print *, t,ad/py,de/py
c
END
```

Appendix C

Fortran program: rad7comp.f

```
c Name: RAD7COMP.F by wessels@knmi.nl
c Purpose: Presents/demonstrates formulae for coordinate
c conversions for gridded (radar) data that serve to:
c - create look-up tables azimuth/distance to properly
c position radar data in polar stereographic grid
c - compute lat/lon of the radar pixels in that grid
c - create look-up table to re-arrange radar data
c in a lat/lon grid (i.e.: the lat/lon pixel n,m
c obtains data from polar sterogr.pixel i,j, etc.)
c Date: First version March 1994
c Update: Added conversion lon/lat to UK national grid, May 2001
c Method: Conversion (lat/lon) <-> (pixel i,j) on spheroid
c Finally: Azimuth and distance for pixel.
c The geodetic formulae are described in reference:
c COORDINATE CONVERSIONS FOR PRESENTING AND COMPOSITING
c WEATHER RADAR DATA, H.R.A.Wessels, 1990, KNMI TR-129.
c-----
c LIST OF SUBROUTINES
c polar-stereographic to lat-lon v.v. for ellipsoid earth model
c latlon1(10,b0,re,ea,px,lon,lat,x,y,z)
c pix1(10,b0,re,ea,px,lon,lat,x,y,z)
c polar-stereographic to lat-lon v.v. for spherical earth model
c latnav(10,b0,lcres,px,lon,lat,x,y)
c pixnav(10,b0,lcres,px,lon,lat,x,y)
c lat-lon to national grids (Netherlands also v.v.)
c pixuk(lonu,latu,x,y,ix,iy,irad)
c lbamft(lona,lata,x,y)
c amftlb(lona,lata,x,y)
c radar azimuth /range from polar stereographic (pixel)
c polrect(10,b0,re,ea,px,lonr,latr,xrad,yrad,ypix,ypix,dp,da)
c projection specification of various radar images
c radch(nr,name,10,b0,hsi,vsi,ic,jc,px,lr,br,re,ea,
c loff,coff,lcres)
c-----
c --r= plotting distance of latitude bbd (rad) in polar ster.map
REAL FUNCTION r(bbd,re,ea)
REAL rp,re,ea,r1,bbd,py
IMPLICIT none
c --re,rp= equatorial/polar radius, ea excentricity
py=ATAN(1.)/45.
rp=re
IF (ea .GT. 0.00001) rp=rp*SQRT(1.-ea*ea)
```

```

        r1=2.*re*re/rp
        IF (ea.GT.0.00001) r1=r1*
*      ((1.-ea)*(1.+ea*SIN(bbd))/(1.+ea)/(1.-ea*SIN(bbd)))*(ea/2.)
        r=r1*TAN(py*45.-bbd/2.)
        END
c      --s= scale (km/rad) at latitude bbd (rad) in polar ster.map
        REAL FUNCTION s(bbd,re,ea)
        IMPLICIT none
        REAL rp,re,ea,r1,bbd,r
        s=r(bbd,re,ea)/re/COS(bbd)
        IF (ea.GT.0.00001) s=s*SQRT(1.-(ea*ea* SIN(bbd)* SIN(bbd) ))
        END
c -----
c Name:      Subroutine latlon1
c Purpose:   Conversion polar stereographic pixel coordinates
c           to lat/lon degrees
c Method:    latlon1: trivial (see reference)
c           The radar lat. may be used as a first guess for <lat>
c           Two iteration steps are usually sufficient
c -----
        SUBROUTINE latlon1(l0,b0,re,ea,px,lon,lat,x,y,z)
        IMPLICIT none
        REAL x,y,rd,re,ea,px,lat,b1,b2,lon,l0,b0,bref,py,r,s,z,rz
        INTEGER n
c      -- logitude and plotting distance radar pixel
        py=ATAN(1.)/45.
        lat=lat*py
        rz=r(b0*py,re,ea)/px/s(b0*py,re,ea)
        lon=l0*py+ATAN(x/(y+rz))
        rd=((rz+y)*px*s(b0*py,re,ea)) /COS(lon-l0*py)
c      iteration for latitude b (first guess was in input call)
        n=0
30      n=n+1
        b1=lat
        b2=1.00001*b1
        lat=
*      b1*(1.-1./(1E5*((r(b2,re,ea)-rd)/(r(b1,re,ea)-rd)-1.)))
        IF (ABS(lat-b1) .GT. 1E-7*b1 .AND. n .LT. 20) GOTO 30
c      -- end iterative computation l and b
        lon=lon/py
        lat=lat/py
        RETURN
        END
c -----
c Name:      Subroutine pix1
c Purpose:   Conversion lat/lon (Deg) to polar sterogr. pixel nrs.
c Method:    trivial (see TR-129)
c Note:      This module can help to create a look-up table
c           containing the pixels(i,j) of a pol.ster. input picture
c           that provide the data for a certain pixel(lat,lon)
        SUBROUTINE pix1(l0,b0,re,ea,px,lon,lat,x,y,yp)
        IMPLICIT none
        REAL x,y,dum,r,s,re,rs,ea,px,lat,lon,py,l0,yp,b0,bref
c      -- --
        py=ATAN(1.)/45.
        dum=r(lat*py,re,ea)/px/s(b0*py,re,ea)
        x=dum*SIN(lon*py-l0*py)
        y=dum*COS(lon*py-l0*py)
        yp=y
        y=y-r(b0*py,re,ea)/px/s(b0*py,re,ea)
        RETURN
        END

```

```

c -----
c Name:      Subroutine latnav
      SUBROUTINE latnav(l0,b0,lcres,px,lon,lat,x,y)
      IMPLICIT none
      REAL x,y,lat,lon,lcres,py,p,l0,b0,px
c -----
      py=ATAN(1.)/45.
      lon=l0+(ATAN2( x*lcres,y*lcres ))/py
      lat=90.-2.*ATAN(0.000001*lcres/(1.+SIN(b0*py))*
*      SQRT(x*x+y*y)) /py
      RETURN
      END
c -----
c Name:      Subroutine pixnav
      SUBROUTINE pixnav(l0,b0,lcres,px,lon,lat,x,y)
      IMPLICIT none
      REAL x,y,dum,lat,lon,lcres,l0,b0,py,par(4)
c -----
      py=ATAN(1.)/45.
      dum=1000000./lcres*(1.+SIN(b0*py))*TAN((45.-lat/2.)*py)
      x=dum*SIN((lon-l0)*py)
      y=dum*lcres/lcres*COS((lon-l0)*py)
      RETURN
      END
c -----
c Name:      Subroutine pixuk: pixel# from lon/lat: single UK radar
c Note: Easting and Northing km in UK national grid (Airy ellipsoid)
c      output as x,y. Pixel coordinates for radar irad are ix,iy.
      SUBROUTINE pixuk(lonu,latu,x,y,ix,iy,irad)
      IMPLICIT none
      INTEGER irad,ix,iy
      REAL py,latu,lonu,lat0,lon0,x,y,ru,rpu,ua
      REAL m0,n0,n,e,en,nr,h2,k3,k4,j3,j4,j5,j6,d1
      DATA lat0,lon0,ua/49.,-2.,0.081673372/
c -----
      ru=6377.563396
      py=ATAN(1.)/45.
      rpu=SQRT(ru*ru*(1.-ua*ua))
      en=(ru-rpu)/(ru+rpu)
      ru=0.9996012717*ru
      rpu=0.9996012717*rpu
      latu=py*latu
      k3=latu-lat0*py
      k4=latu+lat0*py
      m0=rpu*( 1.+en+1.25*en*en+1.25*en*en*en)*k3
* - (3.*en+3.*en*en+ 2.375*en*en*en)*SIN(k3)*COS(k4)
* + (1.875*en*en+1.875*en*en*en)*SIN(2.*k3)*COS(2.*k4)
* - 35./24.*en*en*en*SIN(3.*k3)*COS(3.*k4) )
      n0=ru/SQRT(1.-(ua*SIN(latu))**2.)
      nr=n0*(1-ua*ua)/(1.-(ua*SIN(latu))**2.)
      h2=n0/nr-1.
      lonu=lonu*py
      d1=lonu-lon0*py
      j3=m0-100.
      j4=n0/2.*SIN(latu)*COS(latu)
      j5=n0/24.*SIN(latu)*COS(latu)**3. *(5.-TAN(latu)**2. +9.*h2)
      j6=n0/720.*SIN(latu)*COS(latu)**5. *(61.-58.*TAN(latu)**2.
*      +TAN(latu)**4.)
      y=j3 +d1*d1*j4 +d1*d1*d1*d1*j5 +d1*d1*d1*d1*d1*d1*j6
      j3=n0*COS(latu)
      j4=n0/6.*COS(latu)**3. *(n0/nr-TAN(latu)**2.)
      j5=n0/120.*COS(latu)**5. *(5.-18.*TAN(latu)**2. +TAN(latu)**4.

```

```

*                                     +14.*h2-58.*TAN(latu)**2.*h2)
x=400.+dl*j3 +dl*dl*dl*j4 +dl*dl*dl*dl*dl*j5
IF (irad.EQ.7) THEN
  ix=NINT((x-292.5)/5.)
  iy=NINT((407.5-y)/5.)
ELSE
  IF (irad.EQ.8) THEN
    ix=NINT((x-292.5)/5.)
    iy=NINT((587.5-y)/5.)
  ELSE
    ix=0
    iy=0
    print *, 'radar number does not support UK offsets'
  ENDIF
ENDIF
lonu=lonu/py
latu=latu/py
RETURN
END

c -----
c Subroutine: LBAMFT
c Purpose:   Conversion lat/lon (Bessel ellipsoid, deg) to
c            coordinates (km) of the Netherlands
c            'Rijksdriehoeksmeting'.
c Accuracy:  order of 0.1 m
      SUBROUTINE lbamft(lona,lata,x,y)
      IMPLICIT none
      REAL lona,lata,x,y,x2,y2
      x=(lona-5.3876389)*0.36
      y=(lata-52.15616056)*0.36
      x2=190066.98903*x-11830.85831*x*y-114.19754*x*y*y
      x2=x2+0.15774*x*x*x*y-0.04158*x*y*y*y
c      x2=x2-0.00661*x*x*x*x*x
c      y2=309020.3181*y+3638.36193*x*x-157.95222*x*x*y
      y2=y2+72.97141*y*y+59.79734*y*y*y-6.43481*x*x*y*y
      y2=y2+0.09351*x*x*x*x-0.03444*y*y*y*y
c      y2=y2-0.05419*x*x*x*x*y-0.07379*x*x*y*y*y
      x2=(155000.+x2)
      y2=(463000.+y2)
      x=0.001*x2
      y=0.001*y2
      RETURN
      END

c -----
c Subroutine: AMFTLB
c Purpose:   Conversion coordinates (km) of the Netherlands
c            'Rijksdriehoeksmeting' to lat/lon (Bessel, deg)
c Accuracy:  order of 0.1 m
      SUBROUTINE amftlb(lona,lata,x,y)
      IMPLICIT none
      REAL lona,lata,x,x2,y,y2
      x=x/100.-1.55
      y=y/100.-4.63
      x2=5261.3028966*x+105.9780241*x*y+2.4576469*x*y*y
      x2=x2-.8192156*x*x*x+.0560089*x*y*y-.0560092*x*x*x*y
c      x2=x2-0.0025614*x*x*x*y+y+0.001277*x*y*y*y*y
c      x2=x2+0.0002574*x*x*x*x*x-0.0000973*x*x*x*y*y*y
c      x2=x2+0.0000293*x*x*x*x*x*y+0.0000291*x*y*y*y*y*y
      y2=3236.0331637*y-32.5915821*x*x-.2472814*y*y-.8501341*x*x*y
      y2=y2-.0655238*y*y*y+.0052771*x*x*x*x-.0171137*x*x*y*y
c      y2=y2-0.0003859*x*x*y*y*y+0.0003314*x*x*x*x*y

```

```

c      y2=y2+0.0000371*y*y*y*y+0.0000143*x*x*x*x*y*y
c      y2=y2-0.000009*x*x*y*y*y*y
      y2=y2/3600.+52.15616056
      lata=y2
      x2=x2/3600.+5.3876389
      lona=x2
      RETURN
      END
c -----
c Name: Subroutine polrect. to find azimuth and range values that
c       should be used to fill the rectangular pixels of a
c       polar stereographic radar picture
c       This routine can be used to generate look-up tables
c Note: In the 1989 RSC dp/2 and da were stored in 1 resp. 2 bytes
      SUBROUTINE
      * polrect(l0,b0,re,ea,px,lonr,latr,xrad,yrad,ypix,dp,da)
      IMPLICIT none
      REAL py,l0,b0,lonr,latr,xrad,yrad,ypix,px,re,ea,dp,da,s
c
      py=ATAN(1.)/45.
      da=ATAN((ypix-xrad)/(ypix-yrad))
      IF (ypix .GT. yrad) da=da+180.*py
      da=da+(10*py-lonr*py)
      dp=SQRT((ypix-xrad)*(ypix-xrad)+(ypix-yrad)*(ypix-yrad))
      *      *px*s(b0*py,re,ea)/s(latr*py,re,ea)
c      -- extra corrections as in TR-129:
      dp=dp/(1+0.04*TAN(45.*py-latr*py/2.)*COS(da))
      da=da/py+0.00449*dp*TAN(45.*py-latr*py/2.)*SIN(da)
      IF (da .LE. 0) da=da+360.
      RETURN
      END
c -----
c Name: Subroutine radch
c       Projection parameters are specified for
c       radar or composite nrs. ir= 1 ... 12
c Parameters: text, target lon/lat, ref. lon/lat, picture size
c             hor/vert, offset pixels hor/vert, pixel size,
c             earth radius/excentricity, 3 navigation parameters
c Note: Target may e.g. be radar or top left corner.
c       In the latter case the program may be used to find improved
c       values of the offsets and/or px.
      SUBROUTINE radch
      *(nr,name,lr,br,re,ea,l0,b0,hsi,vsi,ic,jc,px,loff,coff,lcres)
      IMPLICIT none
      LOGICAL lexist
      CHARACTER name*2, adum*76
      INTEGER n,nr,hsi,vsi
      REAL lr,br,re,ea,l0,b0,ic,jc,px,loff,coff,lcres
c
      lexist=.FALSE.
      INQUIRE (FILE='rad7comp.tab', EXIST=lexist)
      IF (.NOT. lexist) THEN
        PRINT *, ' NO FILE : rad7comp.tab'
        GOTO 8
      ENDIF
      OPEN (11, FILE='rad7comp.tab',ERR=7)
      READ (11, *) adum
      6 n=n+1
      READ (11, *) name,lr,br,re,ea,l0,b0
      READ (11, *) hsi,vsi,ic,jc,px,loff,coff,lcres
      IF (n.LT.nr) GOTO 6
      7 CLOSE (11)

```

```

      8 RETURN
      END
c -----
c -----
c Program: Main program
c Method: The polar ster.coord. are counted from L0 E, B0 N
c         Estern longitude is positive and      0,0 | 1,0  2,0
c         pixels are counted as in the sketch  ----|-----
c         near the crossing L0 E, B0 N         0,1 | 1,1  2,1
c         The edge of the Netherlands radar picture is at distance
c         ic0=0 resp. jc0 from projection reference lon/lat.
      PROGRAM main
      IMPLICIT none
      CHARACTER ct(12)*2,ct1*2, cvul1(2048)*1,cvul2(512)*1
      INTEGER i,j,k,hsi,vsi,iopt,is,js
      REAL l,lr,br, lat1,lon1,lat2,lon2,fi,fj, px, xr,yr,zr,zdum
      REAL ic,jc,x,y,z,x1,y1,i1,j1, l0,b0,da,dp, re,ea,rq,e0,py,s
      REAL coff,loff,lcres,px0,100,b00,ic0,jc0
      DATA rq,e0,px0,100,b00/6378.388,.0819918,2.5,0.,60./
      DATA ic0,jc0/0.,212./
      DATA ct/
      * 'db','dh','NL','za','em','es','ch','in','FR','DE','UK','EU'/
c
      py=ATAN(1.)/45.
      print *, 'Enter radar number from following list'
      DO 20, i=1,12
      WRITE (*, '(I6, 3X,2A)') i,ct(i)
20 CONTINUE
      PRINT *,' '
      READ *, iopt
      CALL radch
      *(iopt,ct1,lr,br,re,ea,l0,b0,hsi,vsi,ic,jc,px,loff,coff,lcres)
      IF (re .EQ. 0.) GOTO 999
      PRINT *, ' RADAR OR COMPOSITE: ', ct1
      WRITE (*,('' CHECK rad7comp.tab: '' ,7F8.1)')
      * re,ic,jc,px,loff,coff,lcres
      PRINT *,' '

c         IF (iopt.LT.12) GOTO 999
c
c         -- As an example the position of radar or upper left corner.
      CALL pix1(100,b00,rq,e0,px0,lr,br,xr,yr,zr)
      WRITE(*,('' reference lon/lat : '' ,2F10.3)') lr,br
      WRITE(*,('' in NL grid x/y/z : '' ,3F10.3)') xr,yr,zr
      WRITE(*,('' in NL pict. x/y pix: '' ,2F10.3)') xr-ic0,yr-jc0
c The next may be used to search projection parameters if only
c the lat-lon of the image corners are known. Then the off-sets
c produced here can be used to correct entr
      CALL pix1(l0,b0,re,ea,px,lr,br,xr,yr,zr)
      WRITE(*,('' in own grid x/y/z : '' ,3F10.3)') xr,yr,zr
      WRITE(*,('' in picture x/y pix : '' ,2F10.3)') xr-ic,yr-jc
c -----
c
c         -- now picture corner errors as example:
      print *,' '
      print *,' For PICTURE CORNERS offset accurate map on CRIS grid'
c         IF (iopt.EQ.7 .OR. iopt.EQ.8) print *, ' The real corners '//
c         * ' are in the National Grid coordinates'
      WRITE (*,('' nav. parameters (coff,loff,cres):'' ,3F10.3)')
      * coff,loff,lcres
      DO 502, j=0,vsi+1,vsi+1
      fj=jc+j

```

```

DO 501, i=0,hsi+1,hsi+1
fi=ic+i
lat1=br
i1=i
j1=j
z=0.
CALL latlon1(10,b0,re,ea,px,lon1,lat1,fi,fj,z)
CALL pixnav(10,b0,lcrs,px,lon1,lat1,x,y,zdum)
x=x+coff
y=y+loff
IF (i.EQ.0) THEN
  WRITE (*,'(1x,' lon/lat: ',2F7.3,5X,2I4,' ': ',2F8.2)')
* lon1,lat1,i,j,x-i,y-j
  ELSE
  WRITE (*,'(1X,' lon/lat: ',2F7.3,20X,2I4,' ': ',2F8.2)')
* lon1,lat1,i,j,x-i,y-j
  ENDIF
501 CONTINUE
502 CONTINUE
c
  IF (iopt.EQ.3 .OR. iopt.GE.9) GOTO 701
  IF (iopt.LE.2) GOTO 801
c -- create look-up table for resampling foreign data in NL picture
PRINT *, ' '
OPEN (9,FILE='lookup'//ct(iopt)//'.lup', ACCESS='direct',
* FORM='unformatted', RECL=512, ERR=604)
PRINT *, ' WAIT .... while building NL-table.'
DO 605, j=0,255
fj=jc0+j+0.5
DO 603, i=0,255
fi=ic0+i+0.5
CALL latlon1(100,b00,rq,e0,px0,lon1,lat1,fi,fj,z)
c IF (iopt.EQ.7 .OR. iopt.EQ.8) THEN
c CALL pixuk(lon1,lat1,xr,yr,is,js,iopt)
c ELSE
CALL pix1(10,b0,re,ea,px,lon1,lat1,xr,yr,zdum)
is=NINT(xr-ic)
js=NINT(yr-jc)
c ENDIF
IF (is.LT.0 .OR. js.LT.0 .OR. is.GT.hsi .OR. js.GT.vsi) THEN
is=0
js=0
ENDIF
IF ((i.EQ.72 .OR. i.EQ.128) .AND. j.EQ.128)
* PRINT *, ' check x/y target < x/y orig.:', i,j,is,js
cvul1(2*i+1)=CHAR(is)
cvul1(2*i+2)=CHAR(js)
603 CONTINUE
WRITE (9,REC=j+1) (cvul1(k), k=1,512)
605 CONTINUE
604 CLOSE (9)
GOTO 901
c
701 IF (iopt.EQ.12) GOTO 901
c -- create table for resampling foreign composites in EU picture
PRINT *, ' '
PRINT *, ' NOTE: For building large look-up tables use '
PRINT *, ' with RM fortran command: rad7comp /R 2048'
OPEN (9,FILE='lookup'//ct(iopt)//'.lup', ACCESS='direct',
* FORM='unformatted', RECL=2048, ERR=704)
PRINT *, ' WAIT .... while building EU-table.'
ic0=-214.104

```

```

        jc0=-0.269
        px0=4.0
c      start loop:
        DO 705, j=0,511
        fj=jc0+j+0.5
        DO 703, i=0,511
        fi=ic0+i+0.5
        CALL latlon1(100,b00,rq,e0,px0,lon1,lat1,fi,fj,z)
        CALL pix1(10,b0,re,ea,px,lon1,lat1,xr,yr,zdum)
        is=NINT(xr-ic)
        js=NINT(yr-jc)
        IF (is.LT.0 .OR. js.LT.0 .OR. is.GT.hsi .OR. js.GT.vsi) THEN
            is=0
            js=0
            ENDIF
        IF (i.EQ.300 .AND. j.EQ.256)
* PRINT *, ' check x/y target < x/y orig.:', i,j,is,js
        cvul1(4*i+1)=CHAR((is/256))
        cvul1(4*i+2)=CHAR(MOD(is,256))
        cvul1(4*i+3)=CHAR((js/256))
        cvul1(4*i+4)=CHAR(MOD(js,256))
703 CONTINUE
        WRITE (9,REC=j+1) (cvul1(k), k=1,2048)
705 CONTINUE
704 CLOSE (9)
        GOTO 901
c
c
801 IF (iopt.GT.2) GOTO 901
c -- create look-up table for polar-rectangular conversion
        rq=re
        e0=ea
        CALL pix1(10,b0,re,ea,px,lr,br,xr,yr,z)
        OPEN (9,FILE='lazim.lup', ACCESS='direct',
* FORM='unformatted', RECL=2*hsi+2, ERR=812)
        OPEN (10,FILE='dist.lup', ACCESS='direct',
* FORM='unformatted', RECL=hsi+1, ERR=812)
        print *, ' '
        print *, ' WAIT .... while building pol./rect. tables.'
        print *, lr,br,xr,yr
        DO 803, j=0,vsi
        fj=jc+j+0.5
        DO 804, i=0,hsi
        fi=ic+i+0.5
        CALL polrect(10,b0,rq,e0,px,lr,br,xr,yr,fi,fj,dp,da)
        cvul1(2*i-1)=CHAR(MOD(NINT(da),360))
        cvul1(2*i)=CHAR(INT(NINT(da)/360.))
        cvul2(i+1)=CHAR(NINT(dp/2.))
804 CONTINUE
        WRITE (9,REC=j+1) (cvul1(k), k=1,2*hsi+2)
        WRITE (10,REC=j+1) (cvul2(k), k=1,hsi+1)
803 CONTINUE
812 CLOSE (9)
        CLOSE (10)
c
901 print *, ' '
        fj=jc+FLOAT(vsi)/2.+0.5
        fi=ic+FLOAT(hsi)/2.+0.5
        CALL latlon1(10,b0,re,ea,px,lon1,lat1,fi,fj,z)
        fi=FLOAT(hsi)/2.-coff+0.5
        fj=FLOAT(vsi)/2.-loff+0.5
        CALL latnav(10,b0,lcres,px,lon2,lat2,fi,fj,zdum)

```

```
      WRITE (*, '( picture centre exact/(nav-ex.) :',4F10.6)')  
      * lon1,lat1,lon2-lon1,lat2-lat1  
c  
999 END
```


Appendix D

Fortran program: rad8tops.f

```
cProgram: RAD8TOPS.F
cPurpose: evaluating beam correction for radar top measurement
cDate: 2001, Feb.26
cAuthor: HRAW
cNote 1: The radar beam profile is entered as wm .... dbs2
c         in data statement. Also trial values for factor
c         and exponent of correction formula. See description in:
c         'KNMI Radar Methods', Chapters on Radar Beam resp. Tops
cNote 2: The range and echo top gradient are entered manually
c         Typical values are 130 km and 0.4 .....4.1 for diffuse
c         respectively sharp tops
cNote 3: The output columns: elevation (deg), original dBZprofile
c         measured profile after correction (inspect elevation
c         error near top at 7dBZ), original value, gradient,
c         original dBZ measurement error.
c =====
PROGRAM rad8tops
INTEGER i,j,iflag
DOUBLE PRECISION f,gg,t,n,s,sm,z,zr,y,r,el,b,gr,s0,t0,sdum
DOUBLE PRECISION elr,tOr,tOr1,sOr,sOr1, a(0:125,7),elsave
DOUBLE precision wm,ws1,ws2, ans1,ans2, dbs1,dbs2,acorr,pcorr
DATA wm,ws1,ans1,dbs1,ws2,ans2,dbs2, acorr, pcorr/
c * 5., 16., 2.63, 63., 6., 4.5, 67., 0.00148, 2.8/
c * 4.5, 5., 2.95, 57., 6., 4.8, 65., 0.0048, 2.8/
c * 4.5, 5., 2.95, 57., 6., 4.8, 65., 0.000249, 3.6/
c * 2.5, 2.5, 5.3, 63., 3., 8., 67., 0.000363, 3.9/
* 4.5, 5., 2.95, 57., 6., 4.8, 65., 0.000022, 4.5/
c resp. old, GEMATRONIK with radome, 10 cm antenna, etc.
c
DATA r,gr/ 150.0, 1.4/
c
OPEN (8, FILE='topcor.d')
PRINT *, ' r, grad : '
READ *, r,gr
WRITE (8,'(3F7.2)') sm,r,gr
sm=5.
DO 11, el=12.,0.,-0.1
IF (el .GT. 1400./r) GOTO 11
t=0.
n=0.
zr=r*SIN(el/57.)
b=INT(0.12*r)*1.
```

```

c profile of normalised echo intensity (Watt)
  IF (gr*(zr-9.85).GT.-800. .AND. gr*(zr-9.85).LT.800.) THEN
    sdum=(1.-DEXP(gr*(zr-9.85)))
  ELSE
    IF (gr*(zr-9.85).LE.-800.) THEN
      sdum=1.
    ELSE
      sdum=300.
      sdum=(1.-DEXP(sdum))
    ENDIF
  ENDIF
  IF (sdum*sm.GT.-300.) THEN
    sdum=DEXP(2.3*sm*sdum)
  ELSE
    sdum=0.
  ENDIF
c multiply with bundle sensitivity normalised to 1
DO 6, z=zr-b, zr+b, .1
  IF (gr*(z-9.85).GT.-800. .AND. gr*(z-9.85).LT.800.) THEN
    s=(1.-DEXP(gr*(z-9.85)))
  ELSE
    IF (gr*(z-9.85).LE.-800.) THEN
      s=1.
    ELSE
      s=300.
      s=(1.-DEXP(s))
    ENDIF
  ENDIF
  IF (s*sm.GT.-300.) THEN
    s=DEXP(2.3*sm*s)
  ELSE
    s=0.
  ENDIF
c   IF (ABS(z-zr).LT.0.1) sdum=s
DO 5, y=-b, b, .1
c - angular distance from beam axis in degrees
  f=DSQRT((z-zr)*(z-zr)+y*y)*57./r
c - vertical distribution of reflectivity at height z (km)
  print *, z,f,s
c - two-way gain of main beam and side lobes
  gg=0.
  IF (f .LT. 4.) gg=DEXP(-wm*f*f)
c   print *, gg
c   first resp. second sidelobe; 2 versions
  gg=gg+DEXP(-ws1*(f-ans1)*(f-ans1)-0.23*dbs1)
  gg=gg+DEXP(-ws2*(f-ans2)*(f-ans2)-0.23*dbs2)
c   print *,'gg',gg
  t=t+s*gg
  n=n+gg
5 CONTINUE
6 CONTINUE
  elr=el
  sOr1=sOr
  sOr=s0
  tOr1=tOr
  tOr=t0
  IF (t/n/r/r.GT.1.0E-500) THEN
    t0=4.343*DLOG(t/n/r/r)+45.
  ELSE
    t0=-999.999
  ENDIF
c compare with narrow beam with the same axial gain

```

```

IF (sdum.LE.0) THEN
  s0=-999.999
  ELSE
  s0=4.343*DLOG(sdum/r/r)+45.
  ENDIF
IF (el.GE.15.75) GOTO 11
c  WRITE (*,'(F7.2,5F9.3)') elr,s0r,t0r,s0-s0r1,t0-t0r1,t0r-s0r
c  WRITE (8,'(F7.2,5F9.3)') elr,s0r,t0r,s0-s0r1,t0-t0r1,t0r-s0r
print *, elr
a(NINT(10.*elr),1)=s0r
a(NINT(10.*elr),2)=t0r
a(NINT(10.*elr),3)=(t0-t0r1)*5.
a(NINT(10.*elr),4)=t0r
11 CONTINUE
  iflag=e
  DO 110, i=1,120
  IF (iflag.EQ.1 .OR. a(i,2).LT.-300.) GOTO 110
  IF (a(i+1,2).LT.a(i-1,2) .AND.
*   a(i,2)-a(i-1,2) .LT. a(i+1,2)-a(i,2)) THEN
    iflag=1
    elsave=FLOAT(i)/10.
    DO 109, j=i+1,120
    IF (a(j,2).LT.-300.) GOTO 109
    a(j,2)=a(i,2)+(j-i)*(a(i,2)-a(i-1,2))
109  CONTINUE
    ENDIF
110 CONTINUE
    DO 120, j=1,120
    IF (a(j,2).LT.-300.) GOTO 120
    IF (a(j,3).GT.0.) a(j,2)=a(j,2)-acorr*((a(j,3)**pcorr)
120 CONTINUE
    WRITE (8, '( ' elev. dBZ org dBZ cor dBZmeas ' ',
*           ' dBZgrad cor-org ' )')
    DO 200, j=120,0, step -1
    WRITE (*,'(F6.1, 5F9.3)') FLOAT(j)/10., a(j,1),a(j,2),a(j,4),
* a(j,3), a(j,4)-a(j,1)
    WRITE (8,'(F6.1, 5F9.3)') FLOAT(j)/10., a(j,1),a(j,2),a(j,4),
* a(j,3), a(j,4)-a(j,1)
200 CONTINUE
    CLOSE (8)
    WRITE (*, '(F7.2)') elsave
    END

```